

*„Even if all the experts agree,
they may well be mistaken.”*

Bertrand Arthur William Russell

DANKSAGUNG

Die Masterarbeit als Abschluss eines Studiums bildet den letzten Stein eines großen Puzzles, dessen Vollendung sich über Jahre erstreckt. Die Bewältigung der Anstrengungen während dieses Lebensabschnittes sind nur möglich mit den entsprechenden Weggefährten. All jenen, welche mich auf meinem Weg unterstützt haben, möchte ich hiermit danken.

Besonderer Dank geht an Herrn Univ.-Prof. Dr.-Ing. Uwe Schichler, welcher mir bei dieser Masterarbeit zur Seite gestanden ist. Sie haben mich immer mit guten Ideen und fachlicher Kompetenz unterstützt. Selbst wenn die Umstände hin und wieder nicht ganz zufriedenstellend waren, haben Sie stets das Positive hervorgehoben. Danke!

Der Werkstatt des Instituts für Hochspannungstechnik und Systemmanagement und insbesondere Herrn Anton Schriegl und Herrn Matthias Kainz gilt ein großes Dankeschön! Ohne eure handwerkliche und konstruktionstechnische Hilfe wäre diese Arbeit in dieser Qualität nicht möglich gewesen.

Weiterer Dank gebührt Herrn Ao.Univ.-Prof. Dipl.-Ing. Dr.techn. Rudolf Woschitz und Herrn Ao.Univ.-Prof. Dipl.-Ing. Dr.techn. Stephan Pack, welche mir immer mit Ratschlägen zur Seite gestanden sind.

Bedanken möchte ich mich auch bei meinen beiden Schwestern, Franziska Buchner, MSc MA und Mag. iur. Viktoria Buchner und ihren Partnern für die seelische Unterstützung während meiner Studienzeit.

Auch allen Studienkollegen und Freunden möchte ich meinen Dank für jegliche Unterstützung aussprechen.

Besonderen Dank möchte ich meiner Freundin Lydia Mörth, MA aussprechen: Du hast all die Launen im Laufe meines Studiums ertragen und mich immer unterstützt, auch wenn ich durch zeitweiligen Stress nicht einfach auszuhalten war. Danke, dass du für mich da bist!

Darüber hinaus bedanke ich mich bei der gesamten Familie Mörth für gemeinsame, spannende Abende und die Herzlichkeit, welche ihr mir stets entgegenbringt.

Ohne meine Eltern, Dipl.-Ing Wolfgang Buchner und Mag. rer. nat. Ulrike Buchner wäre mein Studium nicht möglich gewesen. Danke, dass ihr mir während meiner schulischen und universitären Ausbildung immer den Rücken in jeglicher Hinsicht freigehalten habt. Ob bei tiefen Gesprächen beim Schnapsbrennen oder die erste Mahlzeit des Tages um 22 Uhr nach einem langen Universitätstag, ihr habt mich immer unterstützt. Danke, dass es euch gibt!

Zu guter Letzt muss hier dem Kaffee gedankt werden. Ohne seine fabelhaft aufputschende Wirkung wäre es nicht möglich gewesen, mein Studium in dieser Weise abzuschließen. Danke!

EIDESSTATTLICHE ERKLÄRUNG

Ich erkläre an Eides statt, dass ich die vorliegende Arbeit selbstständig verfasst, andere als die angegebenen Quellen/Hilfsmittel nicht benutzt, und die den benutzten Quellen wörtlich und inhaltlich entnommenen Stellen als solche kenntlich gemacht habe. Das in TUGRAZonline hochgeladene Textdokument ist mit der vorliegenden Masterarbeit identisch.

Graz, am 14. September 2018

STATUTORY DECLARATION

I declare that I have authored this thesis independently, that I have not used other than the declared sources/resources, and that I have explicitly indicated all material which has been quoted either literally or by content from the sources used. The text document uploaded to TUGRAZonline is identical to the present master's thesis dissertation.

Graz, 14th September 2018

KURZFASSUNG

Durch den vermehrten Einsatz von dezentralisierten, erneuerbaren Energien und der sich damit ergebenden Änderung der verbrauchernahen Energiegestehung hin zu der verteilten Energiegestehung muss die elektrische Energie über weite Strecken bis zum Kunden transportiert werden. Das europäische Hoch- und Höchstspannungsnetz, welches als Verbundnetz konzipiert ist, kommt an die Grenze seiner Transportkapazität. Um dezentrale, erneuerbare Energien effizient einsetzen zu können, bedarf es neuer, kapazitätsstarker Transportleitungen. Die Hochspannungs-Gleichstrom-Übertragung (HGÜ) bietet Vorteile gegenüber der konventionellen Hochspannungs-Wechselstrom-Übertragung (HDÜ) bezüglich der Verluste, der maximalen Leitungslänge und der Regelung. Um in Gebieten, in denen der Freileitungsbau nicht möglich oder erwünscht ist trotzdem Energie transportieren zu können, wird die Kabeltechnologie eingesetzt. Um die Kabeltechnologie möglichst effizient einzusetzen, werden HGÜ-Kabelsysteme verschiedenen Qualitätsprüfungen unterzogen. Diese müssen neben anderen Prüfungen auch einen Präqualifikationstest bestehen, welcher das Kabelsystem als Ganzes, mit Muffen und Endverschlüssen, für den Einsatz qualifiziert. Dieser Präqualifikationstest wird in der Cigré Technischen Broschüre 496 „Recommendations for Testing DC Extruded Cable Systems for Power Transmission at rated Voltages up to 500 kV“ beschrieben.

Im Zuge dieser Diplomarbeit wird die Prüfungsgebung, für die in der Cigré TB 496 beschriebenen Prüfungen erarbeitet, bereitgestellt und erprobt. Der für die abschließende Prüfung mit überlagerten Spannungen benötigte Universal-Spannungsteiler wird ausgelegt, entwickelt und kalibriert. Aus den gewonnenen Erkenntnissen wird ein Konzept für den Bau eines modularen universalen Spannungsteilers erstellt.

Zum Abschluss der Arbeit wird ein adaptierter Präqualifikationstest mit einem Standard-VPE-AC-Mittelspannungskabelsystem, bestehend aus zwei 10 Meter langen Kabelstücken, mit Standard-Kabelendverschlüssen und einer Standard-Kabelmuffe, durchgeführt, um eine eventuelle Nutzung von bereits verlegten AC-Kabeln als DC-Kabel zu ermöglichen. Ein DC-Kabelsystem könnte verwendet werden, um Transportengpässe in urbanen Gebieten zu umgehen, da die übertragbare Leistung bei Verwendung von DC abhängig von der gewählten Nennspannung im Vergleich zur AC-Nutzung steigt.

Schlüsselwörter:

HGÜ, Mittelspannungs-DC-Kabel, Mittelspannungs-AC-Kabel, Präqualifikationstest, Cigré TB 496, Universal Spannungsteiler, überlagerte Spannungsprüfung

ABSTRACT

Because of the growing use of decentralised, renewable energy sources as well as the resulting changes of the consumer near energy generation towards a distributed energy generation, the electrical energy has to be transported over long distances to costumers. The European high and extra-high voltage grid, which is set up as an integrated grid, is driven to the limits of its transport capability. To use decentral, renewable energy sources efficiently, new and high-capacity transport lines are required. The High-Voltage Direct-Current (HVDC) transmission offers advantages compared to the conventional High-Voltage Alternating-Current (HVAC) transmission regarding losses, maximum transmission length and controllability. To bypass areas, where the building of overhead lines is not possible or allowed, cable systems can be installed instead. Beside other tests, HVDC cable systems have to pass also the prequalification test, which qualifies the cable system as a whole, with joints and terminations for usage. This prequalification test is described in the Cigré Technical Brochure 496 “Recommendations for Testing DC Extruded Cable Systems for Power Transmission at rated Voltages up to 500 kV”.

Throughout the work for this thesis, the test environment for the in Cigré TB 496 described test will be developed, built up and tested. For the final superimposed voltage test, an universal divider is required, which will be designed, built and calibrated. With the acquired knowhow, a concept for a modular universal divider will be developed.

The final part of this thesis will be an adapted prequalification test with a standard XLPE AC medium voltage cable system, consisting of two 10 meter long pieces of cable, equipped with standard cable terminations and with a standard cable joint, to make a statement about the conversion of already existing AC MV cable systems to DC cable systems. This way, transportation bottle necks in urban areas can be prevented, because the transmittable power rises, depending on the chosen nominal voltage, when DC is used instead of AC.

Keywords:

HVDC, medium voltage DC cable, medium voltage AC cable, prequalification test, Cigré TB 496, universal voltage divider, superimposed voltage tests

LIST OF CONTENT

1	Introduction	1
2	HVDC Cables.....	3
2.1	Types of HVDC Cables	3
2.1.1	Oil-Filled DC Cables	3
2.1.2	Mass-Impregnated DC Cables.....	3
2.1.3	Extruded DC Cables.....	4
2.2	Effects in HVDC Cables	6
2.2.1	Electric Field Inversion.....	6
2.2.2	Accumulation of Space Charges.....	8
2.2.3	Thermal Runaway	11
3	HVDC Power Transmission: LCC versus VSC	12
4	Prequalification Test according to Cigré TB 496.....	14
4.1	Overview	14
4.2	Long Duration Voltage Test	16
4.2.1	Load Cycle	16
4.2.2	Load Cycle with Polarity Reversal	17
4.2.3	High Load Cycle.....	17
4.2.4	Zero Load Cycle	17
4.3	Superimposed Impulse Test	17
4.4	Required Equipment.....	19
5	Modular Universal Divider	20
5.1	Divider Basics.....	20
5.2	Prototype	21
5.2.1	Specification	21
5.2.2	Selection of Components and Geometry of the High Voltage Part.....	23
5.2.3	Realisation and Troubleshooting.....	25
5.2.3.1	High Voltage Part.....	25
5.2.3.2	Low Voltage Part.....	26
5.2.4	Performance Test of the Prototype Divider	30
5.2.5	Conclusion of the Prototype Voltage Divider.....	32
5.3	Final Design of Universal Divider	36
5.3.1	Dimensioning and Design	36

5.3.2	3D CAD Construction	39
6	Test Setup.....	41
6.1	Description of the Cable System.....	41
6.1.1	Cable.....	41
6.1.2	Termination.....	42
6.1.3	Joint.....	43
6.2	Preliminary Tests	44
6.3	Device under Test.....	44
6.4	Implementation of Heating	45
6.5	DC Generator and its Connection.....	49
6.6	Impulse Generator and its Connection.....	50
7	Adapted Prequalification Test for MV DC Cable	54
7.1	Test Setup and Cycles	54
7.2	Superimposed Voltage Test	57
7.3	Results.....	59
8	Outlook	61
9	Summary	62
10	References	63
	List of Abbreviations.....	66
	List of Figures.....	67
	List of Tables.....	70
	Appendix A Datasheets.....	71
Appendix A.1	Resistors.....	71
Appendix A.2	Capacitors	73
Appendix A.3	Damping Resistors.....	77
	Appendix B Measurements.....	79
Appendix B.1	Prototype calibration DC ₊	79
Appendix B.2	Prototype calibration DC ₋	80
Appendix B.3	Prototype calibration AC _{Peak,+}	81
Appendix B.4	Prototype calibration AC _{Peak,-}	82
Appendix B.5	Prototype calibration LI _{Peak,+}	83
Appendix B.6	Prototype calibration LI _{Peak,-}	83
Appendix B.7	Prototype calibration LI _{Timecomp}	84
	Appendix C Construction Drawings	85

1 INTRODUCTION

Through the growing use of decentralized and renewable energy sources and international power exchange new challenges are approaching the transmission grid of tomorrow.

In the past, conventional powerplants were built near consumers to have short energy transmission lengths. Over the years, the electrical energy consumption grew world-wide. In 1960 the annual worldwide electrical energy generation was about 2.500 TWh. The increased use of electrical energy in the society and the growing population led in 2015 to an annual electrical energy generation of about 20.000 TWh. To satisfy the need of electrical energy in the future, additional powerplants will be needed. The ecological and sustainable thinking of the society and the global warming led to higher usage of renewable energy sources. However, renewable powerplants have to be built where the density of available energy is high. A wind park makes no sense in an area where no wind occurs. This leads to geographical separation of power generation and usage. Therefore, energy has to be transmitted over long distances [1, 2, 3].

Nowadays, transmission grids are based on alternating current (AC), which comes along with some restrictions. Through the need of reactive power, the maximum transmission length is limited. In addition to that, dielectric losses as well as the skin effect influence the efficiency of power transmission. Due to these restrictions, the use of direct current (DC) is beneficial in terms of efficiency and transmission length. Power transmission with High Voltage Direct Current (HVDC) will help to overcome challenges related to shortage of transmission capacity [3, 4, 5].

Nowadays, HVDC transmission is used to overcome long transmission distances, to couple asynchronous grids, such as continental Europe with Great Britain, as well as for back-to-back short coupling in combination with land cables or sea cables. Furthermore, it is used to connect offshore wind parks with the main grid [5].

In 2011 the Merkel government decided to shut down all nuclear powerplants in the course of the German energy revolution. Also, the incident at the nuclear power plant of Fukushima, Japan in 2011 strengthened this decision. Furthermore, the European climate and energy 20/20/20 targets focus on the expansion of renewable energy sources in order to reduce the greenhouse gas emissions. This leads to the necessity of additional transmission lines in Europe [5, 6, 7].

Referred to the planned HVDC transmission lines, the German government decided to build new transmission lines as earth cable systems instead of overhead lines to get higher acceptance of the affected population. This choice speeds up the construction time of new transmission lines [6, 8]. Further projects like ALEGrO or A-NORD from the German grid operator Amprion or SuedLink from TenneT will use HVDC cables [9, 10].

Additionally, the transmission capacity of already existing AC cable systems can be enhanced by using them as DC links as illustrated in Figure 1-1. Especially in cities, where ground works for installing new cable systems is not desired from an infrastructural point of view, this approach is beneficial [11].

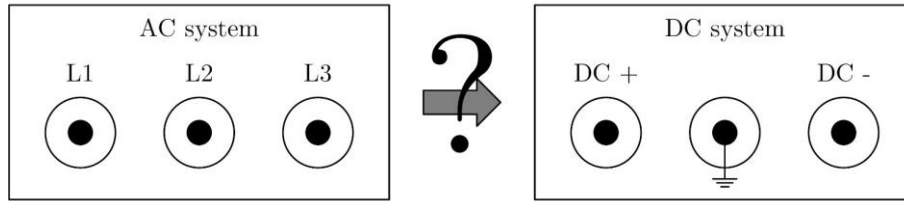


Figure 1-1: Transformation of AC system to DC system

To overcome the above addressed problems at the transmission grid of tomorrow, a prequalification test (PQ) of HVDC cables is the second step after the development of a cable for a successful implementation in the grid. A PQ test is used to prequalify a cable system for the usage. Further tests are required like a type test or a sample test, which will not be dealt with in this thesis.

In this thesis the test environment for PQ tests at the Institute of High Voltage and System Management at Graz University of Technology will be developed according to the Cigré Technical Brochure 496 (TB 496). Additionally, a modular high voltage divider for impulse voltages up to 300 kV will be designed and built to measure the voltage during a PQ test. After that, a shortened PQ test will be performed with a standard 12/20 kV medium voltage (MV) AC crosslinked polyethylene (XLPE) cable as a DC cable following TB 496 to check the built up test environment for its function and to strengthen the concept of using a standard AC XLPE MV cable as DC cable.

2 HVDC CABLES

2.1 TYPES OF HVDC CABLES

2.1.1 OIL-FILLED DC CABLES

The main insulation of oil-filled DC cables as shown in Figure 2-1 is made of paper impregnated with insulating oil.

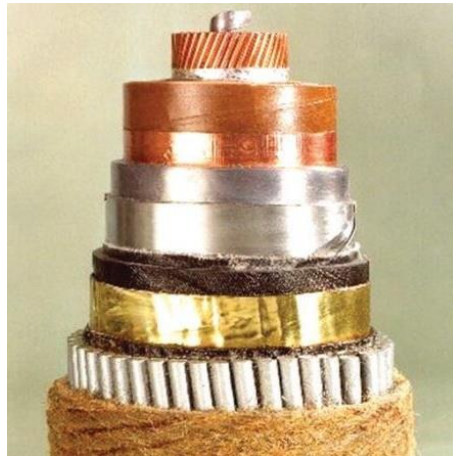


Figure 2-1: Oil-filled HVDC cable [12]

Oil-filled DC cables can be differed in two types: cables filled with low-viscosity oil and cables filled with high-viscosity oil. The oil pressure of low-viscosity oil-filled cables has to be maintained over the whole cable length in order to maintain the insulation integrity of the cable system. This is done via pressurised oil containers at joints or cable terminations, which lead to a maximum possible cable length of 30 - 60 km. Cables filled with high-viscosity oil on the other hand do not need such reservoirs due to the lack of fluidity of oil. Theoretically, their applicable length is unlimited.

Nowadays, oil-filled DC cables have a maximum voltage rating of 600 kV. Due to environmental impacts at oil leakages or at recycling, oil-filled cables are less used nowadays [5, 13].

2.1.2 MASS-IMPREGNATED DC CABLES

The insulation body of mass-impregnated DC cables is also made of paper, similar to oil-filled cables. The difference compared to oil-filled cables is, that mass-impregnated cables do not have any free oil. Instead the paper is impregnated under vacuum with high viscosity oil. This process is used in order to reduce the possibility of formation of voids filled with gas. Due to the lack of free fluid oil, the length of the cable is theoretically unlimited.

Another advantage of using this type of cable is the avoidance of oil leakages. Moreover, no oil reservoirs are required to maintain the pressure and therefore the insulation integrity [5]. Mass-impregnated DC cables are available for voltages up to 500 kV. The maximum conductor temperature $T_{C, \max}$ is limited to 55 °C. Through adding polypropylene laminated paper (PPLP) to the insulation, mass-impregnated cables can be further improved. Compared to conventional mass-impregnated cables, the electric stress can be up to 60 % higher and the maximum conductor temperature $T_{C, \max}$ can reach up to 85 °C [5, 13].

2.1.3 EXTRUDED DC CABLES

The insulation of extruded DC cables consists of cross-linked polyethylene (XLPE), which is a polymeric thermoset material. A polymer is a high molecular material consisting of small low molecular components stringed to each other. Depending on the applied additives the physical properties can be varied in wide range. Polypropylene (PP) is also used as insulation material, which is not dealt with in this thesis [13, 14].

In Figure 2-2 the main structure of extruded cables is shown: inner conductor, inner semi-conducting layer, insulation, outer semiconducting layer, swelling tape, copper screen, separation crepe, armour and sheath.

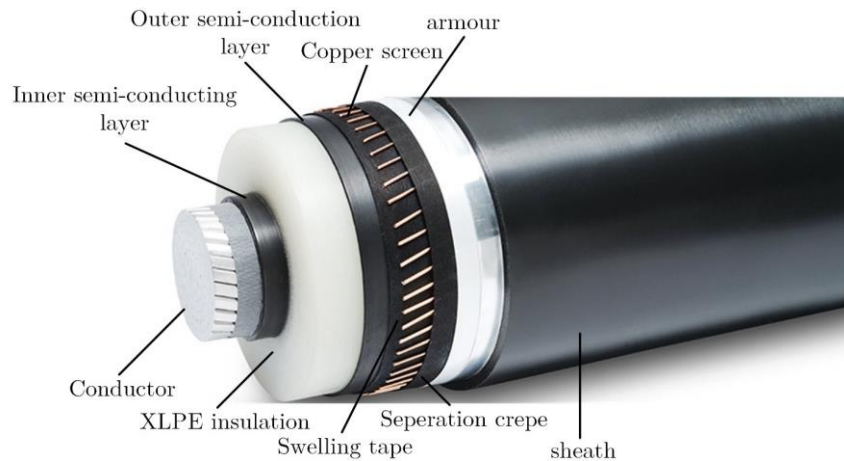


Figure 2-2: Typical extruded MVAC cable [15]

The term extruded cable refers to the way of production of polymer-insulated cables. During the process of extrusion a synthetic material is heated up and pushed in prefabricated shapes under high pressure. The inner semi-conducting layer, the insulation and the outer semi-conducting layer are extruded to the conductor directly after each other in one process, which is called the triple extrusion. Two procedures of extrusion are common: the high- and the low-pressure procedure. The high-pressure procedure leads to low-density polyethylene, whereas the low-pressure procedure leads to high-density polyethylene. Polymer particles

are heated and mixed to gain a homogenous viscous mass, which is pushed through extrusion nozzles to surround the conductor evenly [3, 14]. A schematic drawing of a triple extrusion is shown in Figure 2-3.

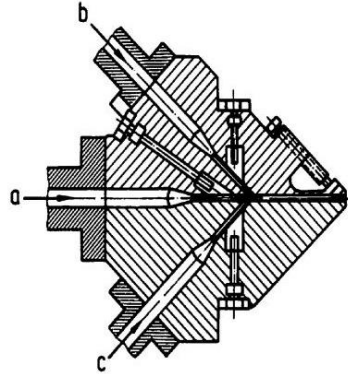


Figure 2-3: Schematic drawing of a triple extrusion [14]

After the extrusion of the polyethylene and the semi-conducting layers the cross-linking procedure is performed to make XLPE out of the extruded polyethylene. In this procedure, the cable core surrounded with the two semiconducting layers as well as the insulation, is put in the vulcanisation pipe, where under high pressure and high temperatures, the cross-linking of the single polymers takes place. In the last step of the cable production the swelling tape, the copper screen and the sheath are added to the pre-fabricated cable [3, 14].

Due to the high possible conductor temperature $T_{C, \max}$ of 90 °C, an extruded DC cable is capable of transporting more energy than normal mass-impregnated DC cables. As there is no oil included in the insulation system, there is no risk of environmental impacts due to oil leakage. Another environmental advantage is the fact that extruded cables are recyclable. Additionally, the installation process of terminations and joints is much easier compared to other types of cables. These factors paved the way for the high usage of these cables within the last years [5].

Nowadays, system voltages for extruded DC cables go up to 500 kV [16]. The Danish cable manufacturer NKT for example designed and produced a HVDC cable with a system voltage of up to 640 kV [17]. For giving some context: extruded AC cables are available up to 500 kV [3].

Generally, extruded DC cables have similar properties as AC cables. However, under DC stress, attention has to be paid to the material behaviour. Furthermore, the electric field distribution under AC is capacitive, whereas the field distribution under DC is resistive.

Under DC space charges can accumulate (chapter 2.2.2). Such space charges can lead to field distortions, which can further lead to additional electrical stress if the polarity of the voltage is changed. Additionally, a gradient in the conductivity can be recognised due to a

radial temperature gradient caused by ohmic losses in the conductor. This leads to the so-called field inversion (chapter 2.2.1) [3, 4].

If not stated otherwise, all later mentions according to cables are related to extruded DC cables.

To understand the challenges related to the design and operation of DC cables, the three major characteristics are discussed in the following chapters. The mentioned effects do not occur when operating extruded AC cables.

2.2 EFFECTS IN HVDC CABLES

2.2.1 ELECTRIC FIELD INVERSION

The electric field distribution in the insulation system of an AC cable is described by the formula of a cylindrical capacitor (Eq. 1) where r_i is the inner and r_o is the outer radius.

$$E(r) = \frac{U}{r \cdot \ln\left(\frac{r_o}{r_i}\right)} \quad (1)$$

If the insulation system is homogeneous, meaning no different dielectric materials are used, which leads to a constant ϵ_r , the electric field distribution under AC depends only on the geometry, not on the material parameters.

By applying a DC voltage, this simple circumstance changes to a complex relation between temperature distribution and applied voltage. Both influences the conductivity, which determines the radial field distribution.

According to [4] and [18] the electric field distribution $E(r)$ of a cable under DC is given by Equation 2:

$$E(r) = \frac{\delta \cdot U_0 \cdot \left(\frac{r}{r_o}\right)^{\delta-1}}{r_o \cdot \left(1 - \left(\frac{r_i}{r_o}\right)^\delta\right)} \quad (2)$$

with δ given by Equation 3:

$$\delta = \frac{\frac{\alpha \cdot \Delta T}{\ln\left(\frac{r_o}{r_i}\right)} + \frac{\beta \cdot U_0}{r_o - r_i}}{1 + \frac{\beta \cdot U_0}{r_o - r_i}} \quad (3)$$

In the equations above, U_0 is the applied DC voltage, r_i and r_o are the inner respectively outer diameter of the insulation and ΔT is the temperature gradient over the insulation. α and β are material parameters. According to Mazzanti the temperature coefficient of electrical resistivity $\alpha = 0,084 \text{ 1/}^\circ\text{C}$ and the electric stress coefficient of electrical resistivity $\beta = 0,0645 \text{ m/MV}$ [18]. These parameters can be determined for different insulation material probes. In this thesis the mentioned values are used for the demonstration of the differences between AC and DC field distributions.

A current flowing through a conductor causes a voltage drop, since a piece of conductor has a non-zero resistance. The current flowing through the resistance generates heat, which results in losses in the transmission line. These losses heat up the insulation from the inside, whereas the sheath is cooled from the surrounding medium. This leads to a temperature gradient over the thickness of the insulation.

As shown in Figure 2-4, a significantly higher electric stress can be observed when a temperature gradient is present due to the losses (orange curve). Furthermore, the point of the highest electric field is shifted to the outer radius, which is as above, the so-called field inversion.

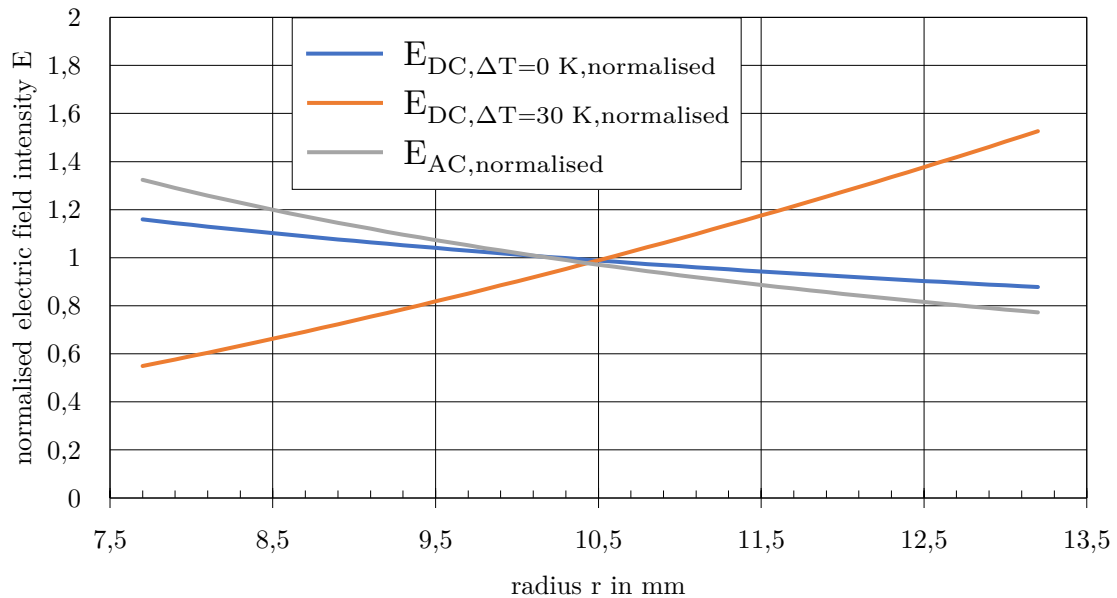


Figure 2-4: Electric field density E over the radius r

At the same voltage, the maximum electric field strength in the insulation under DC is about 36 % higher than under AC. The slight difference between the curves for DC without a temperature gradient and AC has its origin in the dependence on the electric field strength of the conductivity of the XLPE.

2.2.2 ACCUMULATION OF SPACE CHARGES

Space charges in the insulation are seen as the major factor for fast aging of HVDC cables. They are typically caused by two factors: charge injection (conductor/insulation interface) or charging of impurities like cross-linking by-products and other defects. Space charges can only accumulate if trapped. The energetical trap depth depends on factors like temperature, electric field and material parameters [5, 13, 19].

If space charges are accumulated due to charge injection, space charges aggregate unipolar at the electrodes (negative charges on the negative electrode and positive charges on the positive electrode), which is called homocharge (Figure 2-5a). This leads to a distortion of the electric field over the insulation. Near the electrodes, the electric field decreases, whereas in the middle the electric field increases, in comparison to a uniform electric field [5, 13].

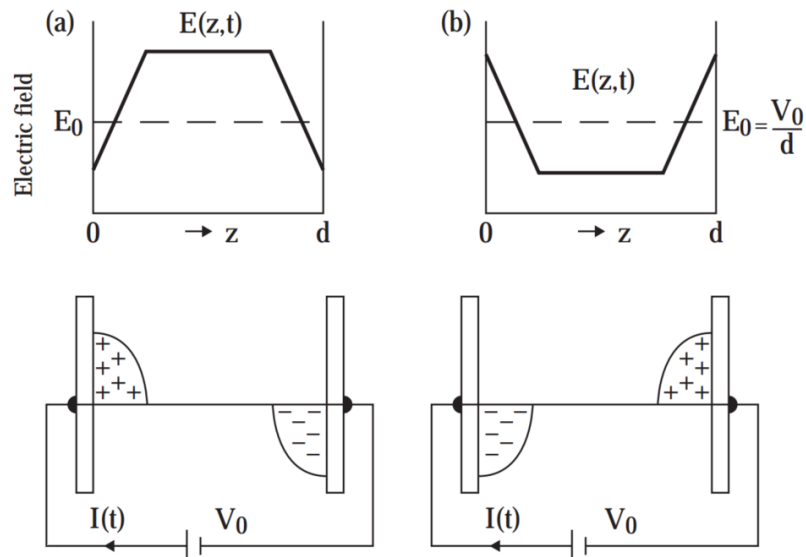


Figure 2-5: Electric field distribution [13]

a) homocharge b) heterocharge

If space charges occur due to charging of imperfections, heterocharges occur (positive charges at negative electrode and vice versa), which leads to a lower electric field in the middle and a higher electric field at the electrodes (Figure 2-5b) [5, 13].

Due to the high resistivity of the insulation trapped charges cannot degrade rapidly. If a polarity reversal occurs, in order to reverse the direction of the power flow (chapter 3), the electric field is intensified due to the present space charges. This can lead to an exceeding of the local electric field strength, which can initiate a failure of the insulation system [13].

Several research projects deal with the development of HVDC XLPE cables. Through adding nano particles, such as MgO, SiO₂ or soot, major improvements in the area of accumulation respectively reduction of space charges can be achieved [3, 16, 20].

The accumulation of space charges can be measured with multiple destructive and non-destructive methods. Destructive methods are the dust figure method as well as the field probe method. Destructive methods are generally the older methods, which were used in the past [5, 13].

There are two main types of non-destructive methods used [5, 13]:

- Thermal step method (TSM)
- Pulse electroacoustic method (PEA)

In the following, the pulse electroacoustic method will be described further.

Assuming, a probe of homogeneous dielectric material with infinite resistance where space charges are located. This probe of a defined thickness is put between two plane electrodes, where pressure pulses can be applied with one electrode. Applying a mechanical pulse causes charges, which are attached to the atomic lattice, to shift. Furthermore, the local relative permittivity ϵ_r is changed due to different local concentrations of charges. Under the circumstance of an open circuited probe a voltage can be measured between the two electrodes. If the probe is on the other hand operated short circuited, a current can be measured. The course of the measured signal provides information about the space charge distribution in the probe [13].

The pulse electroacoustic method (PEA) uses the Coulomb force law. An electrical impulse is applied to the probe. The applied DC voltage charges imperfections and injects charges in the insulation material. If these space charges are hit by an impulse wave, they react with an acoustic wave, which propagates through the probe. These acoustic waves can be measured with a piezoelectric device. In comparison to the pressure wave propagation method, where the pressure wave is generated externally, the pressure wave is here generated by the present space charges. The amplitude of the applied impulse depends on the thickness of the sample and can reach 4 kV with a pulse width of 5 - 200 ns. As the impulse wave hits the space charges located in the test object, the space charges move slightly and cause an acoustic wave [13, 21].

A space charge measurement on a specimen without space charges, results in a curve as shown in Figure 2-6.

The peaks in the plot have its origin in the charges accumulated on the surfaces of the electrodes. They can be used to determine the start and the end of the probe [22].

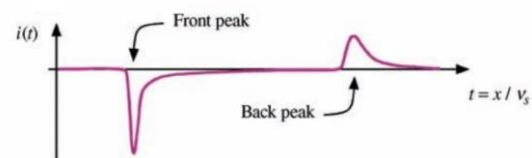


Figure 2-6: Typical signal of PEA space charge measurement without space charges [13]

Considering a probe with space charges a typical measurement signal is distorted. Several peaks and transitions, as shown in Figure 2-7, occur in the measurement signal. The peaks from the electrodes are still visible allowing also at charged specimen the determination of its boundaries.

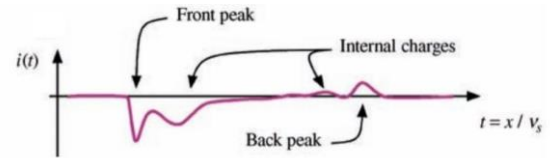


Figure 2-7: Typical signal of PEA space charge measurement with space charges [13]

The advantage of PEA compared to other measuring methods is the separation of the high voltage part and the sensitive low voltage measuring part as shown in Figure 2-8.

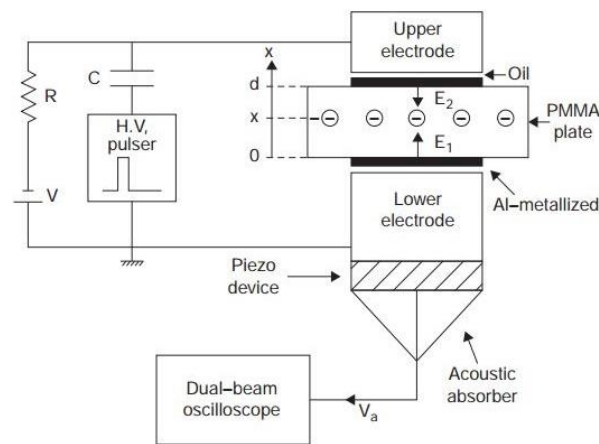


Figure 2-8: Block diagram of the pulsed electroacoustic (PEA) method [13]

The PEA method can as well be used with coaxial cable samples. Therefore, the earth screen has to be removed at the measurement point to expose the outer semiconducting layer. On this section the PEA cell, containing the piezo electric sensor, is placed. To achieve a proper acoustic coupling, the cable probe is fixed to the PEA cell with a spring-loaded bar. The geometry of the PEA cell can either be flat or round. A round sensor surface can provide a better acoustic coupling, whereby a flat sensor can be used for different diameters. Figure 2-9 shows a schematic measurement setup for PEA measurements of a cable.

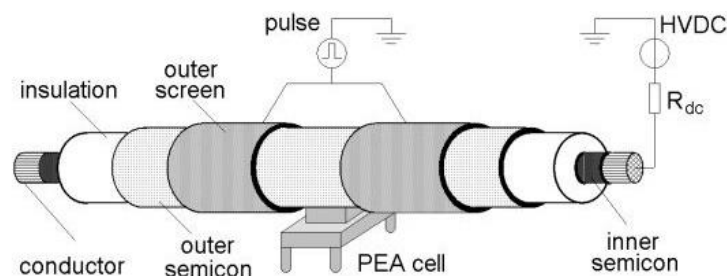


Figure 2-9: Measurement setup for PEA with a cable [21]

To investigate the influence of the temperature gradient on the insulation, a setup can be used as described in [22].

Through the evaluation of measurements over the time as shown in Figure 2-10, the process of space charge accumulation can be investigated and statements regarding the behaviour of XLPE under long duration voltage exposure can be made.

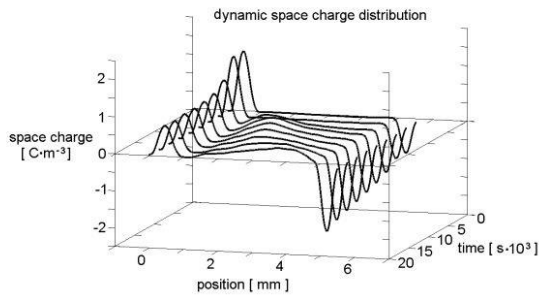


Figure 2-10: Dynamic space charge distribution over time [21]

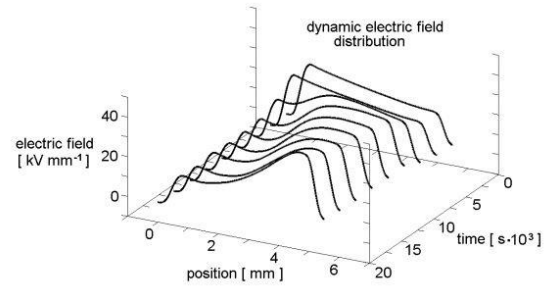


Figure 2-11: Electric field distribution over time due to space charges [21]

With the results of these measurements a development of the distribution of the electrical field can be derived as shown in Figure 2-11. Further information can be found in literature [13, 21].

2.2.3 THERMAL RUNAWAY

Due to the non-infinite resistance of the insulation material a leakage current flows from the inner conductor to the copper screen. This current is determined by the applied voltage and the resistivity of the insulation, which is, as mentioned above, highly dependent on the temperature. If these leakage currents are too high, the insulation material is heated up and dielectric heating takes place. The resistance of the insulation material decreases due to the increased temperature resulting in an increased leakage current heating the insulation further up. This is called the thermal runaway and can take place in single spots or the whole insulation volume [12].

At modern XLPE insulated DC cables the risk of a thermal runaway has decreased due to new technologies and materials used in the insulation. Modern XLPE insulated DC cables can be operated with a conductor temperature $T_{C, \max}$ up to 90 °C [18, 23].

3 HVDC POWER TRANSMISSION: LCC VERSUS VSC

Most of the electric power systems are built on AC. To convert the electric power from a three phase AC system to a DC system a converter is required. Semiconducting elements like diodes, thyristors and transistors are used to build such converters.

Nowadays, two technologies are common: the line commutated converter (LCC) or HVDC classic and the voltage source converter (VSC), named HVDC Plus at SIEMENS or HVDC light at ABB.

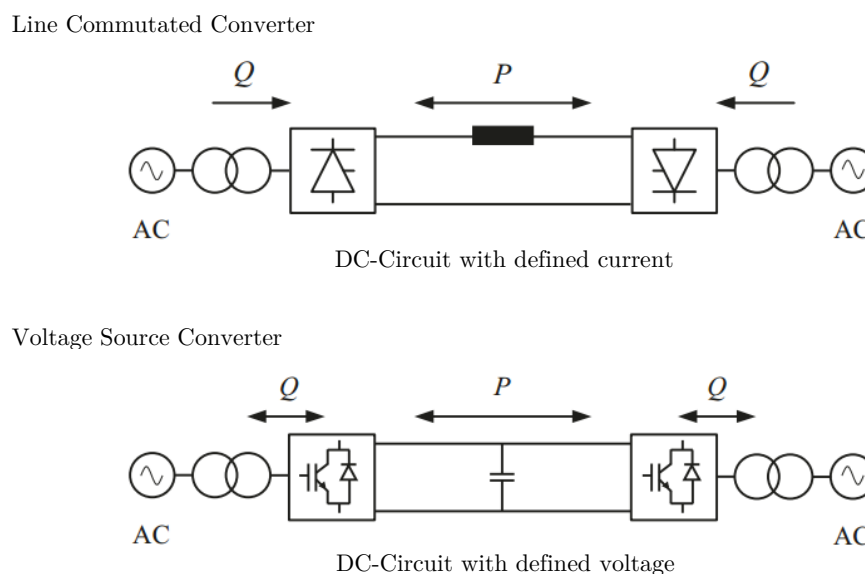


Figure 3-1: Line Commutated Converter versus Voltage Source Converter [24]

LCC, which is the older technology, is based on thyristor technology. Generally spoken, a thyristor is an electrically controllable switch. The state of a thyristor is initially a blocking state. To change it from blocking state to conducting state a gate impulse has to be applied. Additionally, the voltage drop over the thyristor has to be positive. If the current through the thyristor reaches zero, it changes its state automatically from conducting to blocking. The direction of the power flow is controlled by changing the polarity of the voltage. To couple two AC grids, two converters are needed, one to convert the voltage from AC to DC and one to convert the DC voltage back to AC voltage. The two converters are only able to work properly if the AC grid provides enough reactive power. Therefore, in most cases, the converter station is combined with capacity banks to provide and compensate the required reactive power. The transmission line is a direct current intermediate circuit [24].

VSC is based on insulated-gate bipolar transistor (IGBT) technology. IGBTs can be switched on and off by appropriate gate signals. The direction of power flow is controlled

by changing the direction of the current. Therefore, the voltage has always the same polarity. In the case of VSC the transmission line is a direct voltage intermediate circuit [24].

Depending on the used technology, the DC voltage is superimposed with an AC ripple and transients, which originates in the switching events.

Table 3-1 provides further information on the differences between the VSC and the LCC technology:

	LCC	VSC
maximum transmission length	theoretically unlimited, practically limited by voltage drop	
space requirement converter station	~ 25 m ² /MW	~ 10 m ² /MW
reactive power requirement	50 – 60 % of converter power	controllable
voltage regulation	slowly by tap changer of transformer	fast (response time < 100 ms)
power flow reversal	polarity reversal	direction of direct current
filter units	huge requirements on AC filter	small or no requirements
grid connection requirements	strong AC grid	no particularly requirements
black start capability	no	yes, with additional equipment

Table 3-1: Basic information: LCC and VSC [24]

4 Prequalification Test according to CIGRÉ TB 496

4.1 OVERVIEW

A prequalification test (PQ) is meant to demonstrate the long-term performance of a cable system. A cable system consists of the cable itself, joints and terminations. Unless there are no major changes in the cable system, a PQ test has to be done only once to prequalify the system for usage. Major changes refer to change of material, manufacturing process, general design and designated voltage level [25].

According to TB 496, a cable system for a PQ test has to be constructed as shown in Figure 4-1 depending on the cable accessory included.

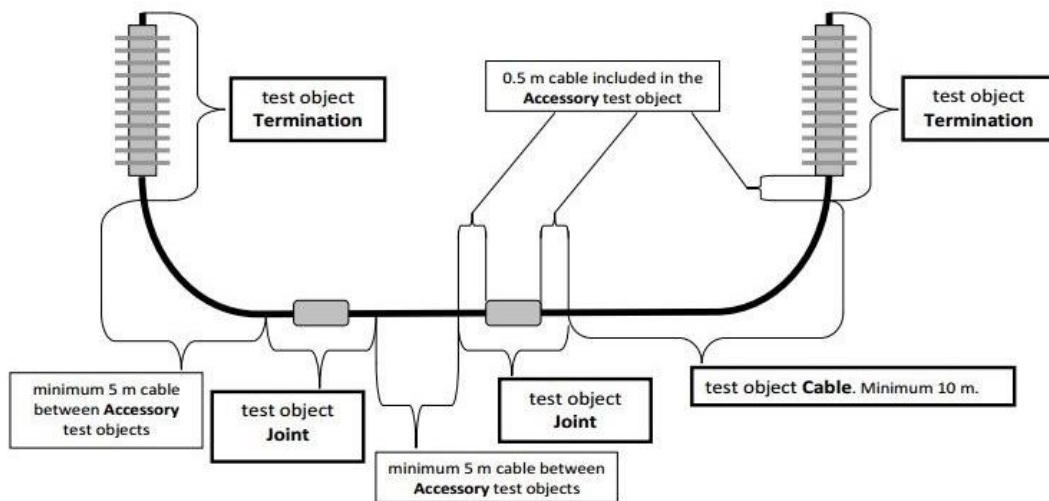


Figure 4-1: Example of a test loop according to TB 496 [25]

The TB 496 gives recommendations for the testing procedures for PQ tests of extruded DC cables, as well as for development tests, type tests, routine tests, sample tests and after installations tests.

PQ tests have been performed with AC cables in the past. Therefore, procedures are very well-known and appropriate standards exist. Due to the low usage of DC transmission in the past, no such standards exist for PQ tests of DC cables, except the TB 496 and the previous document TB 219 (“Recommendations for Testing DC Extruded Cable Systems for Power Transmission at a rated Voltage up to 250 kV”), which are, as mentioned above, just recommendations.

A PQ test according to TB 496 consists of different parts:

- Load cycle (LC)
- Load cycle with polarity reversal (LC + PR)
- High load cycle (HL)
- Zero load cycle (ZL)
- Superimposed impulse test (S/IMP)

If a certain HVDC system uses LCC technology, the transmission system (cable or overhead line) must overcome polarity reversals in order to change the direction of power flow (described in chapter 3). This is necessary in grid operation, which is the reason for the two different sequences of the PQ test (shown in Table 4-1 and Table 4-2) according to the recommendations in the TB 496.

	LC	LC	LC + PR	HL	HL	ZL	LC	LC	LC + PR	S/IMP
Number of cycles or days	30 cycles	30 cycles	20 cycles	40 days	40 days	120 days	30 cycles	30 cycles	20 cycles	-
Test voltage	+	-		+	-	-	+	-		$U_{P2,0} = 1,2 \times U_0$ $U_{P1} = 2,1 \times U_0^*$
	U_{TP1}	U_{TP1}	U_{TP2}	U_{TP1}	U_{TP1}	U_{TP1}	U_{TP1}	U_{TP1}	U_{TP2}	

Table 4-1: PQ test sequence for LCC [25]

* if required

	LC	LC	HL	HL	ZL	LC	LC	S/IMP
Number of cycles or days	40 cycles	40 cycles	40 days	40 days	120 days	40 cycles	40 cycles	-
Test voltage	+	-	+	-	-	+	-	$U_{P2,0} = 1,2 \times U_0$ $U_{P1} = 2,1 \times U_0^*$
	U_{TP1}							

Table 4-2: PQ test sequence for VSC [25]

* if required

Following voltages related to the cycles of the PQ test are defined in the TB 496 [25]:

- U_0 : “is the rated DC voltage between conductor and core screen for which the cable system is designed.”
- U_{TP1} : “is the DC voltage during prequalification test (load cycle test), type test (polarity reversal test) and test after installation. For the scope of this recommendation $U_{TP1} = 1,45 \times U_0$.”
- U_{TP2} : “is the DC voltage during the prequalification polarity reversal test. For the scope of this recommendation $U_{TP2} = 1,25 \times U_0$.”
- $U_{P2,0}$: Voltage amplitude of the applied switching impulse measured from the zero-line as shown in Figure 4-2 top. For the scope of the PQ test $U_{P2,0} = 1,2 \times U_0$.
- U_{P1} : Voltage amplitude of the applied lightning impulse measured from the zero-line as shown in Figure 4-2 bottom. For the scope of the PQ test $U_{P1} = 2,1 \times U_0$.

At the end of a PQ test, a superimposed impulse test is mandatory. The PQ test shall not be evaluated due to the impulse level, rather the S/IMP test shall confirm the integrity of the insulation system of the tested cable system [25].

The following chapter deals with the different types of cycles used in a PQ test according to Cigré TB 496. All types of cycles are addressed to issues related to the usage of a cable system in the grid.

4.2 LONG DURATION VOLTAGE TEST

4.2.1 LOAD CYCLE

During a load cycle the applied voltage must be $U_{TP1} = 1,45 \times U_0$. The voltage is either positive or negative depending on the actual cycle. As the term indicates, the cable is stressed by a load current. The TB 496 recommends conductor heating as heating method to recreate a situation resembling the reality. The current used for heating can either be AC or DC. This thermal treatment is applied for at least 8 hours, whereby the maximum conductor temperature $T_{C, \max}$ has to be constant for at least two hours before finishing the heating period. The same applies to the temperature drop ΔT_{\max} across the insulation. If these conditions are not possible, the duration of the heating period has to be enlarged by the required additional time in order to reach the requirements mentioned above. After the heating period the cable has to cool off for at least 16 hours naturally to reach the initial temperature conditions. Therefore, the duration of a complete cycle is at least 24 hours.

Between two blocks of different polarities a resting period of 24 hours with heating but without voltage is highly recommended [25].

The temperature conditions mentioned above originate in the problem of field inversion described in chapter 2.2.1.

4.2.2 LOAD CYCLE WITH POLARITY REVERSAL

A load cycle with polarity reversal contains the same thermal conditions as mentioned in chapter 4.2.1. The applied voltage has to be $U_{TP2} = 1,25 \times U_0$. During a cycle, the polarity of the voltage is changed three times. The switching events have to be evenly distributed over the length of the cycle, whereas a PR has to be done in less than two minutes. It is recommended to place the first PR as soon as the heating mechanism is turned off. As mentioned above, a load cycle with polarity reversal is only performed, if the cable is designed and intended to be used with LCC topology [25].

4.2.3 HIGH LOAD CYCLE

A high load cycle is performed under the same thermal conditions as mentioned in chapter 4.2.1. In this case the heating mechanism is not turned off after 8 hours, but $T_{C, \max}$ and ΔT_{\max} are held for the rest of the high load cycle. The applied voltage is $U_{TP1} = 1,45 \times U_0$ and is either positive or negative. Between two blocks of different polarities a resting period of 24 hours with heating but without voltage is highly recommended [25].

4.2.4 ZERO LOAD CYCLE

A zero load cycle does not include any heating but constant negative voltage $U_{TP1} = 1,45 \times U_0$ for 120 days [25].

4.3 SUPERIMPOSED IMPULSE TEST

After finishing the long duration voltage test, the integrity of the insulation system is checked with a superimposed impulse test. In such a test a defined DC voltage is superimposed with a defined impulse voltage, either switching or lightning impulse. The TB 496 refers to the execution of superimposed voltage tests to a Cigré report in the Electra 189, listed as [26] in the literature. Furthermore, the superimposed voltage test and the according setup are described in the IEC standard 60060–1 [27]. During this test, a defined DC voltage is superimposed with an impulse voltage [25].

The test setup to generate such superimposed voltages comes along with several challenges, which will be further dealt with in chapters 4.4 and 6 [25].

According to Cigré TB 496 a test with superimposed switching impulses is mandatory. A test with superimposed lightning impulses only has to be carried out if required by the customer. In Figure 4-2 a rough overview of the test voltages is given [25].

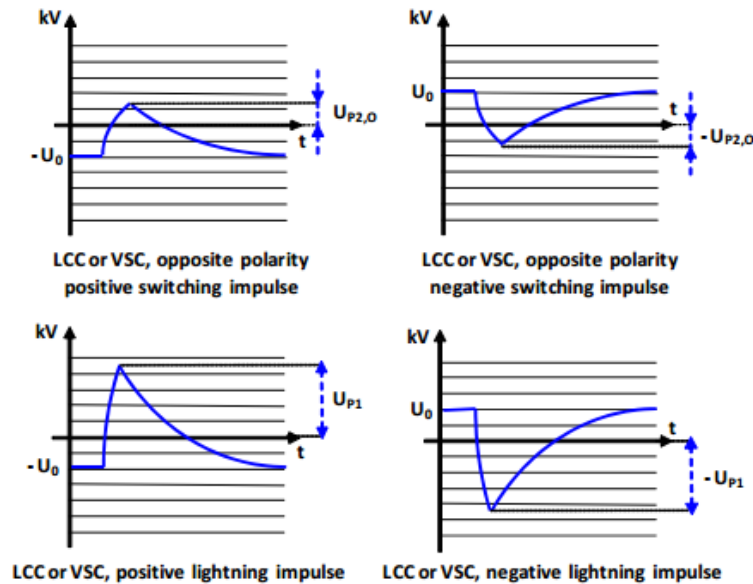


Figure 4-2: Superimposed test voltages according to Cigré TB 496 [25]

The tested cable system has to withstand 10 positive and 10 negative superimposed switching impulses and, if required, 10 positive and 10 negative superimposed lightning impulses. The required impulse voltage levels are as follows [25]:

- S/IMP switching impulse: $U_{P2,0} = 1,2 \times U_0$
- S/IMP lightning impulse: $U_{P1} = 2,1 \times U_0$

Before each S/IMP test the cable system must be conditioned. Conductor heating must be applied as described in chapter 4.2.1 to reach the temperature conditions for at least 10 hours. Also the voltage U_0 of the required polarity has to be applied for at least 10 hours. After this conditioning period 10 superimposed impulses shall be applied. Two consecutive impulses have to be separated by a resting interval of at least two minutes. To proceed with the superimposed voltage test of the opposite polarity the cable system has to be deenergised in order to apply the heating current and conditioning voltage for the second part of the S/IMP test. The second conditioning period is equal to the first. The only difference is the change of voltage polarity [25, 26].

The time parameters for the impulse voltages are given in [26]:

- S/IMP switching impulse:
 - Time to crest (T_{CR}) = $250 \mu\text{s} \pm 20 \%$
 - Time to half value (T_2) = $2500 \mu\text{s} \pm 60 \%$
- S/IMP lightning impulse:
 - Time to crest (T_1) = $1 - 5 \mu\text{s}$
 - Time to half value (T_2) = $50 \mu\text{s} \pm 10 \%$

4.4 REQUIRED EQUIPMENT

To perform a prequalification test according to Cigré TB 496 the DC generator and the impulse generator must be combined in one test setup to superimpose these two voltage forms. Therefore, additional equipment is required to protect the two voltage sources.

To protect the DC generator from the high frequent HV impulses a blocking impedance is needed. As well, the impulse generator has to be protected against the DC voltage. Therefore, a coupling capacitor or a spark gap can be used [28]. Both possibilities have their advantages and disadvantages, which are discussed in chapter 6.6 [29, 30].

To measure the actual voltage on the tested cable system a universal high voltage divider is needed [30]. A divider of such a kind has been built as part of this thesis.

Furthermore, to achieve the required temperature parameters, a system is needed to deliver an adequate heating current. In Figure 4-3 a rough overview of the used test setup is given.

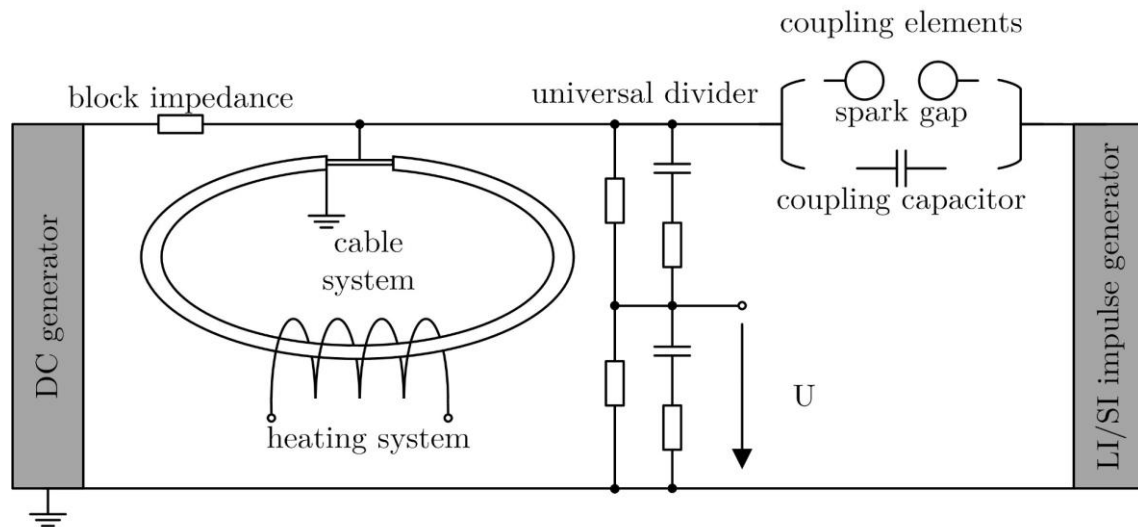


Figure 4-3: Scheme of the test setup

5 MODULAR UNIVERSAL DIVIDER

5.1 DIVIDER BASICS

The measurement of high voltages provides special requirements on the used equipment. Common devices to measure voltages such as multi-meters or oscilloscopes are only capable of a limited input voltage range. Therefore, to measure high voltages, these high voltages have to be broken down by appropriate devices. Such devices are called high voltage divider. The divided signal is directly proportional by the scale factor to the original high voltage. However, the shape of the measured signal has to be equal compared to the high voltage signal. As shown in Figure 5-1 there are several types of high voltage dividers for different purposes to ensure the proper reproduction of the measured signal [3].

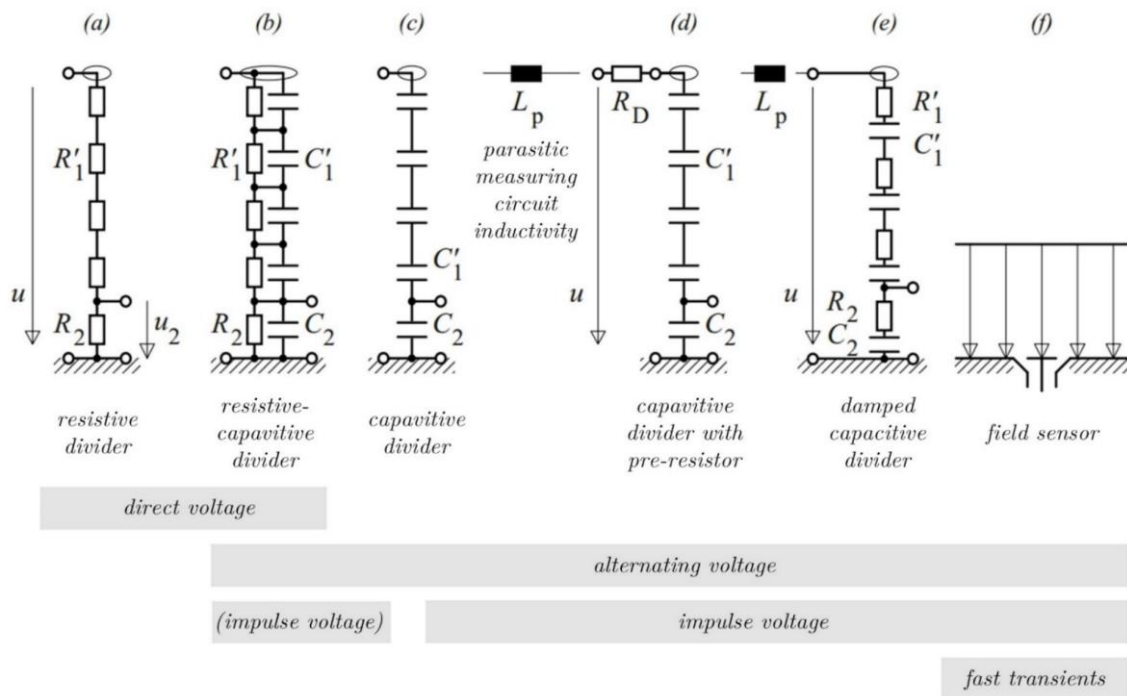


Figure 5-1: Different types of high voltage dividers [3]

A resistive divider (Figure 5-1a) is mostly used for DC voltages. Due to the combination of high resistive values and not negligible earth capacities, the divider has a low pass behaviour and is not appropriate for measuring AC (50 Hz) or even voltages with higher frequencies [3, 31].

A capacitive divider (Figure 5-1c) is suitable for measuring AC voltages. Unlike the resistive divider, the electric field distribution is capacitive. This is the reason, why such dividers are useless with DC as the field distribution is undefined. The inductivities combined with the capacities of the high voltage divider build up a LC network, which oscillates with several

MHz. Without any further adoption such a divider is not useable for measuring impulse voltages. This problem can be solved by using appropriate damping resistors within the capacitive divider, which finally leads to the damped capacitive divider (Figure 5-1e) or the Zaengl divider as it is called in German speaking regions [3, 32].

To get an universal high voltage divider a combination of a resistive divider and a damped capacitive divider was chosen to achieve both, accurate DC and impulse measurement.

Assuming two impedances (\underline{Z}_1 and \underline{Z}_2) of different values connected in series as shown in Figure 5-2. The overall impedance of this circuit is $\underline{Z} = \underline{Z}_1 + \underline{Z}_2$. According to the ohmic law the current flowing through this arrangement is $\underline{I} = \underline{U}/\underline{Z} = \underline{U}/(\underline{Z}_1 + \underline{Z}_2)$. This current flows through both impedances causing different voltage drops. The voltage on \underline{Z}_1 is thereby $\underline{U}_1 = \underline{Z}_1 \cdot \underline{I}$ and the voltage on \underline{Z}_2 is $\underline{U}_2 = \underline{Z}_2 \cdot \underline{I}$. Due to the Kirchhoff's voltage law the applied voltage \underline{U} equals the sum of \underline{U}_1 and \underline{U}_2 . In this relation the equation of \underline{U}_1 can be used to eliminate the term resulting in the equation $\underline{U} = \underline{Z}_1 \cdot \underline{I} + \underline{U}_2$. Using the equation for the current from above leads to the relation $\underline{U} = \underline{Z}_1 \cdot \underline{U}/(\underline{Z}_1 + \underline{Z}_2) + \underline{U}_2$. Proper rearrangement of this equation delivers the relation $\underline{U} = \underline{U}_2 \cdot (\underline{Z}_1 + \underline{Z}_2)/\underline{Z}_2$, which describes the behaviour of the divider in a simple way.

The term $(\underline{Z}_1 + \underline{Z}_2)/\underline{Z}_2$ is the scale factor \underline{F} and describes the relation between the high voltage and the measured voltage. This scale factor is not implicitly frequency independent as the mentioned impedances can contain inductivities. Additionally, the influence of earth capacities has to be considered.

5.2 PROTOTYPE

5.2.1 SPECIFICATION

For the universal high voltage divider, specifications according to Table 5-1 were defined. The different voltage levels originate in the fact, that this divider is tending to be modular. These specifications were selected to match the values of U_{TP1} and U_{P1} of cables of common HVDC voltage levels.

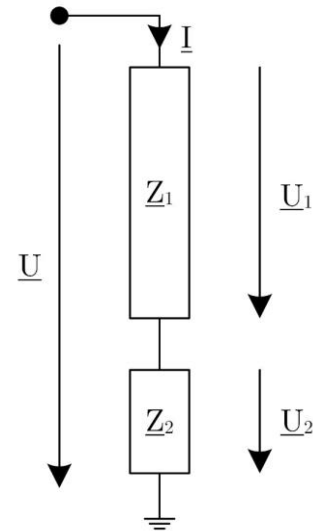


Figure 5-2: Voltage divider with two impedances

voltage form	rated voltage
-	kV
DC	180
SI	200
LI	300

Table 5-1: Specifications of universal high voltage divider

In Figure 5-3 a simplified circuit of a universal voltage divider is shown, where R_1 , R_{D1} and C_1 represent the high voltage part and R_2 , R_{D2} and C_2 the low voltage part. Z is the termination resistance and Z_W is the wave impedance of the cable to the oscilloscope. Furthermore, $R_{in,Oszi}$ is the input resistance of the oscilloscope. Inductivities from the components or earth capacities are neglected in this figure.

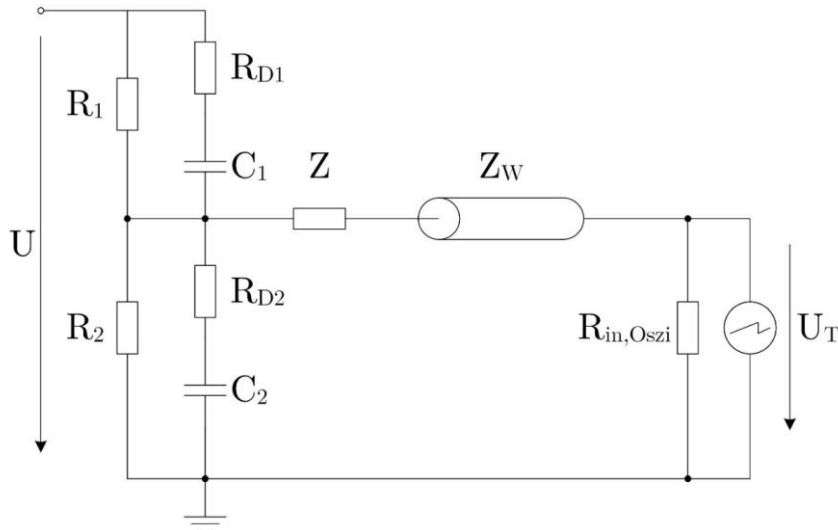


Figure 5-3: Simplified circuit of a universal voltage divider

To achieve a frequency independent scale factor and an adjusted high voltage divider, the time constants of the damped capacitive high- and low-voltage part have to be the same as K uchler [3] and Meisner [33] described with the relation shown in Equation 4.

$$\tau_1 = \tau_2 \rightarrow R_{D1} \cdot C_1 = R_{D2} \cdot C_2 \quad (4)$$

In addition to this relation, the desired scale factor \underline{F} is determined by the ratio of the impedances of the high- and low-voltage part as described in chapter 5.1. In Equation 5 this relation is shown adapted to the simplified circuit shown in Figure 5-3.

$$\underline{F} = \frac{R_1 \parallel \left(\frac{1}{j \cdot 2\pi \cdot f \cdot C_1} + R_1 \right) + R_2 \parallel \left(\frac{1}{j \cdot 2\pi \cdot f \cdot C_2} + R_2 \right)}{R_2 \parallel \left(\frac{1}{j \cdot 2\pi \cdot f \cdot C_2} + R_2 \right)} \quad (5)$$

Equation 5 only contains the values of the components used to build this divider. All parasitic influences like inductivities from the setup or the components as well as earth capacities are neglected in this relation.

Parasitic earth capacities can be considered according to Figure 5-4 in a simplified equivalent circuit or according to Figure 5-5 in an iterative equivalent circuit.

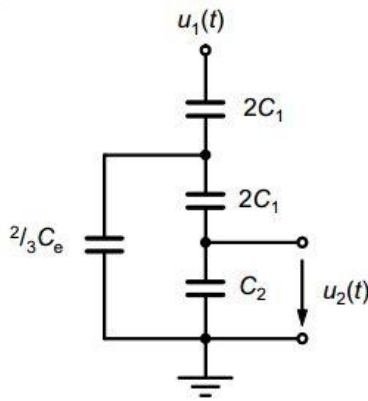


Figure 5-4: Simplified equivalent circuit of capacitive divider with concentrated earth capacity [32]

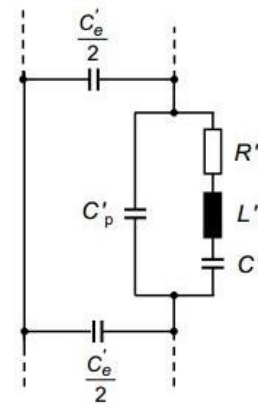


Figure 5-5: Iterative equivalent circuit element of damped capacitive divider with earth capacity and inductivity [32]

Parasitic inductivities due to components or setup can be considered in the simplified equivalent circuit as two series elements, one in the upper part and one in the lower part of Figure 5-4 as well as proportionally divided as series elements in the iterative equivalent circuit as shown in Figure 5-5.

The height of one module was specified to be 1,5 m. To keep the load of the test circuit low, the resistance was set to 2,5 G Ω and the capacity to 202,6 pF.

5.2.2 SELECTION OF COMPONENTS AND GEOMETRY OF THE HIGH VOLTAGE PART

To measure high frequent signals, it is important to have as little inductivities within the divider as possible. Some simulations were carried out to check the possibility to arrange the passive components in a meander like way to reduce the inductivity. As a result, it can be said that it is very difficult to keep the electrical field strength under 10 kV/cm in order to prevent the occurrence of corona discharges. For this reason, a helix-like setup was chosen

for the prototype. A helical design is easy to realise but comes along with the disadvantage of inductivity. Since the inductivity of a solenoid is proportional to its cross-section, the diameter of the divider was kept low. A diameter of 100 mm was the result of the mechanical setup to give enough space for soldering the components to each other.

Table 5-2 shows the components used for the high voltage part of the universal voltage divider prototype. It is important to mention, that the costs played a major role in the selection of the components. If costs were not considered, the choice of better components would have been beneficial in terms of an increased precision and performance. For example, resistors with a lower voltage coefficient can be used which results in a lower non-linearity for DC voltages.

component name	component value	number of components	value of module
resistor R_1 OHMITE MOX-750232505FE	25 M Ω	100	2,5 G Ω
capacitor C_1 CORNELL DUBILIER 940C20S47K-F	47 nF	232	202,6 pF
damping resistor R_{D1} OHMITE TFSD100RJE	100 Ω	12	1200 Ω

Table 5-2: Selected components for the universal voltage divider prototype

The used capacitors have an overall inductivity of about $L_{CP} = 5 \mu\text{H}$. The mentioned geometrical dimensions result in an overall earth capacity according to Equation 6 of 30 pF [32].

$$C_e = \frac{2 \cdot \pi \cdot \varepsilon_0 \cdot l}{\ln\left(\frac{2}{\sqrt{3}} \cdot \frac{l}{d}\right)} = 29,3 \text{ pF} \quad (6)$$

$$\text{with } l = 1,5 \text{ m } d = 0,1 \text{ m}$$

According to [32], the optimum damping resistor is about 3 to 4 times the wave impedance of the divider:

$$R_{opt} = (3 \dots 4) \sqrt{\frac{L}{C_e}} = 1224 \Omega \quad (7)$$

$$\text{with } L = 5 \mu\text{H and } C_e = 30 \text{ pF}$$

This damping resistor was realised by 12 discrete resistors evenly distributed over the length of the divider.

5.2.3 REALISATION AND TROUBLESHOOTING

5.2.3.1 HIGH VOLTAGE PART

There are many possible ways of designing a high voltage divider. The Physikalisch-Technische Bundesanstalt (PTB) for example built a high voltage divider with four arms: two shield arms to guarantee a homogeneous electric field inside and to prevent the divider from the influence of proximity effects, one capacitive arm for signals of higher frequencies and one resistive one for the DC component [34].

Due to time and cost efficiency the author decided to use one damped capacitive arm and one resistive arm for the built prototype. In Figure 5-6 pictures of the final prototype are shown.

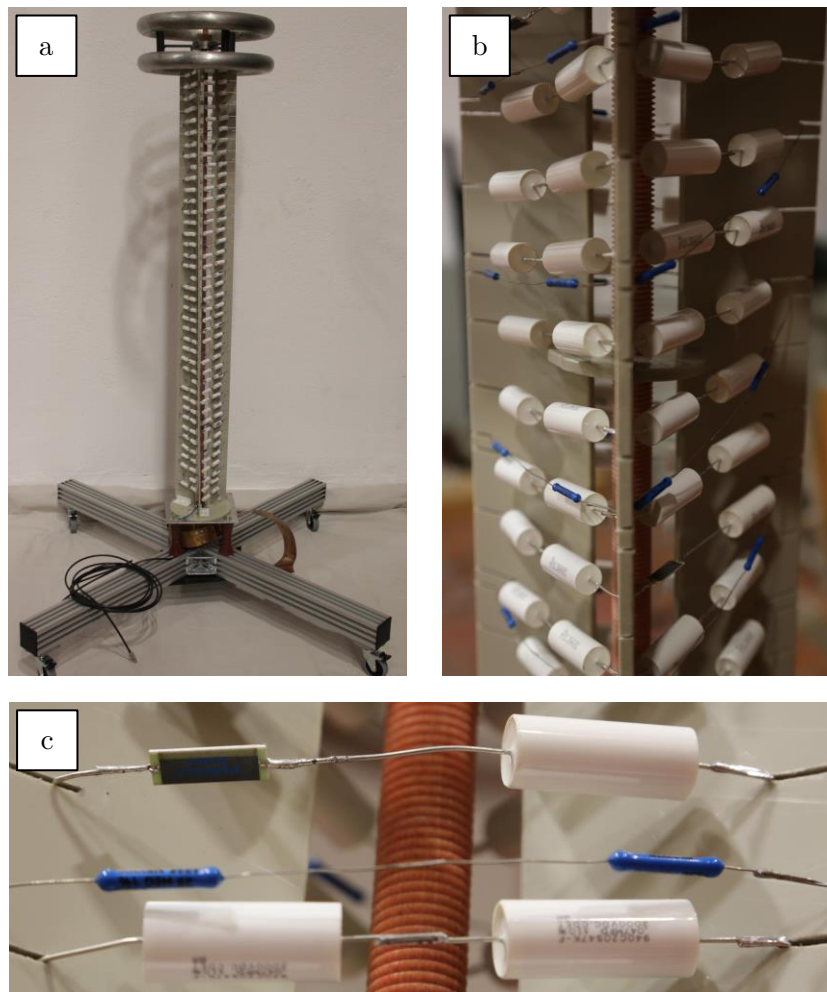


Figure 5-6: Overview and detail pictures of the prototype
a) Prototype overview b) Geometry c) Components

The choice of the geometry, which is like a triangle when seen from above, was in the first place a good idea due to the simplicity of the mechanical set up combined with the three pillars used for the framework. Later, the geometry turned out to be a big disadvantage with regards to the partial discharge behaviour. The pointy turns (Figure 5-6b) in each layer of the divider deliver a good starting point for corona discharges. For the final universal divider this circumstance will be eliminated through a much rounder geometry.

5.2.3.2 LOW VOLTAGE PART

Version A of the low voltage part was designed to reach a scale factor of $F = 10001$. The impedance was built in a concentric way to achieve a proper current distribution. This way, the inductivity of the low voltage part can theoretically be minimised. As shown in Figure 5-7, rather thin wires were used to make the concentric rings, which led to a higher inductivity. Furthermore, a piece of 50Ω cable was used to connect the high and the low voltage part. Through the coaxial cable the wave impedance changed at the connection point between the high- and low voltage part immediately to 50Ω . This caused reflections resulting in high frequency components in the measured signal. These three unlucky chosen decisions led to a high overshoot and unwanted oscillations of measured lightning impulse voltages as shown in Figure 5-8.

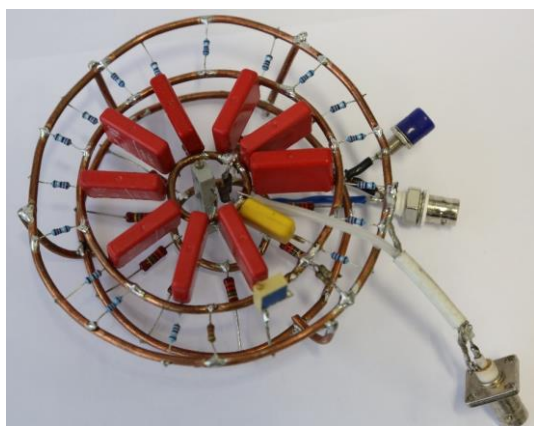


Figure 5-7: Version A of low voltage part

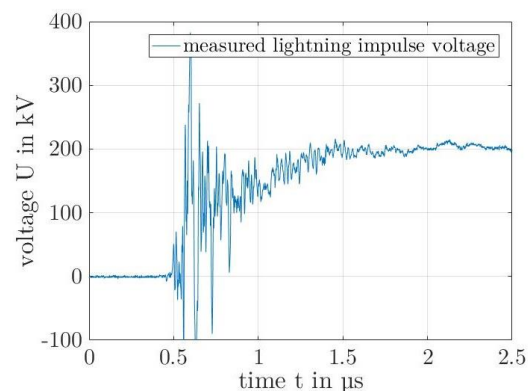


Figure 5-8: Measured lightning impulse voltage with low voltage part A

Schwab argued in his textbook (chapter 2.3.4, [31]): “*During reading the previous chapter, the impression may have occurred, that the major difficulties at building a capacitive high voltage divider exist in appropriate dimensioning of the high voltage part. At a closer look though, a capacitive divider is just as good as its low voltage part.*”

This statement led to version B of the low voltage part, where the scale factor was reduced to $F = 4001$. Furthermore, wide concentric rings of copper were used instead of the rather thin copper wires used in version A. The components were soldered in pre-drilled holes evenly distributed over the whole circumference. Additionally, version B was equipped with a shield case made of copper parts riveted together. The connection between the high- and low voltage part was established via a 6 mm² thick insulated copper wire, a banana plug on the low voltage part and a banana socket on the bottom of the high voltage part. Also, a wide terminal out of copper was soldered on the bottom side of the low voltage part to enable the establishment of a proper and low inductive earth connection with a wide copper band. Reflections and oscillations originating from the earthing system can be minimised this way. The low voltage part version B is shown in Figure 5-9 to Figure 5-11.



Figure 5-9: Low voltage part B: outer view

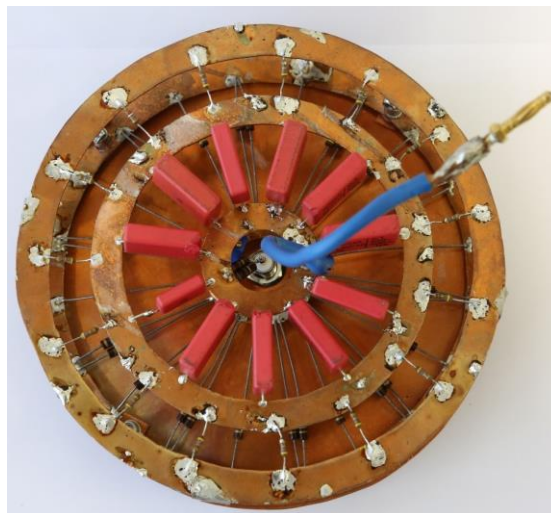


Figure 5-10: Low voltage part B: inner view, top

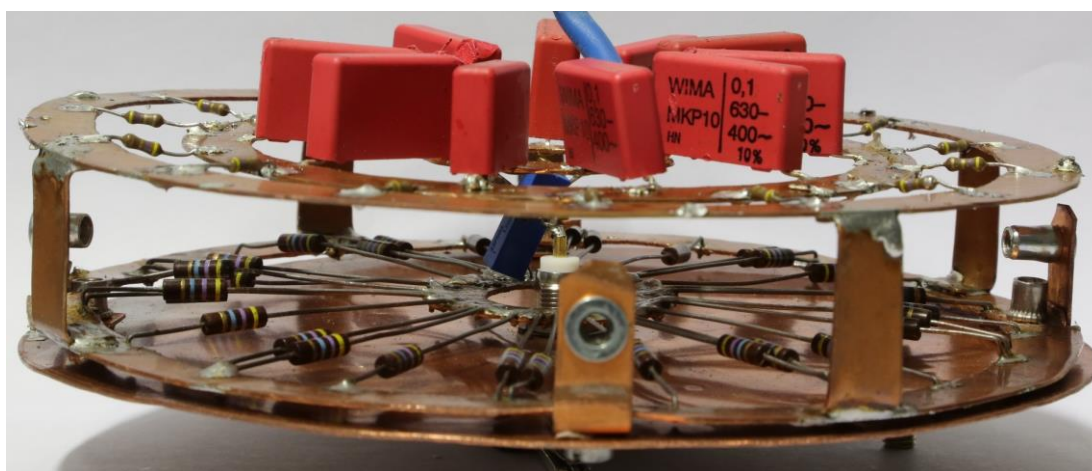


Figure 5-11: Low voltage part B: inner view, front

To achieve a scale factor of $F = 4001$, following values are required in the low voltage part:

- $R_2 = 625 \text{ k}\Omega$
- $C_2 = 810,3 \text{ nF}$
- $R_{D2} = 0,3 \text{ }\Omega$

These values were achieved by the parallel arrangement of many discrete elements. The capacity C_2 was made by the parallel arrangement of eight 100 nF capacitor, two $4,7 \text{ nF}$ capacitors and one 1 nF capacitor. The damping resistor R_{D2} was made by the parallel arrangement of 14 $4,7 \text{ }\Omega$ resistors and one potentiometer which was replaced by an adequate resistor of $2,9 \text{ }\Omega$ after the adjustment, which is explained later on. For R_2 another value than mentioned above is needed, which is explained later as well.

The termination resistor Z was needed to terminate the $50 \text{ }\Omega$ coaxial cable used for the connection to the oscilloscope. Otherwise oscillations along the cable occur at higher frequencies. Furthermore, at higher cable lengths a termination on the oscilloscope side of the connection cable with a resistor and a capacity in series was suggested by [32].

The input resistance $R_{in,Osz}$ of the used oscilloscope (YOKOGAWA DLM2054) is $1 \text{ M}\Omega$. Through the parallel connection, established by the measurement cable, of R_2 and $R_{in,Osz}$ the sum resistance of the low voltage part gets lower and distorts the scale factor under DC voltages. Therefore, R_2 has to be designed, so that the parallel connection of R_2 and $R_{in,Osz}$ equals $625 \text{ k}\Omega$. To achieve this value, R_2 has to be $1,666667 \text{ M}\Omega$. Therefore, 30 $47 \text{ M}\Omega$ resistors were used in a parallel arrangement with a potentiometer in series to adjust the scale factor. This potentiometer was later removed by an adequate resistor.

If a measurement device is used with an input resistance not equal to $R_{in,Osz} = 1 \text{ M}\Omega$, the scale factor is not accurate anymore and a new low voltage part has to be built and calibrated or a converter network has to be added to correct the input resistance of the new measurement device to the value required. Needless to say that such an arrangement has to be calibrated again to include the whole measurement chain in the calibration as such a converter network is in this case part of the measurement chain. As a next step after the major improvements, a lightning impulse was measured with the prototype. By comparing Figure 5-8 and Figure 5-12, the improvement in the impulse response can be seen easily. The remaining oscillations in Figure 5-12 have its origin in the used impulse voltage generator and the required big setup to connect the divider with the impulse generator. This theory was checked with a transportable impulse generator (HILO) which delivers impulse voltages up to 24 kV . The measured lightning impulse was very smooth as shown in Figure 5-13.

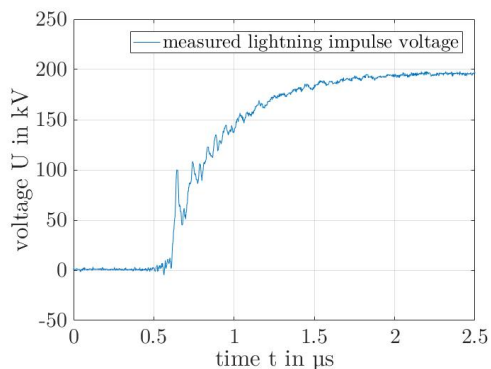


Figure 5-12: Measured lightning impulse voltage with low voltage part B

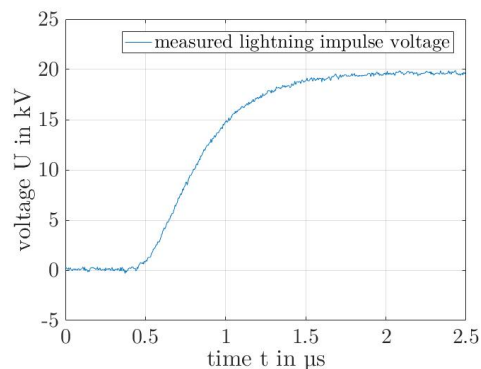


Figure 5-13: Measured lightning impulse voltage (impulse from HILO)

At the end of this test phase a negative step voltage was applied to the high voltage divider in order to check the step response. The used step generator (DR. STRAUSS KAL 1000) charges the calibration object to an adjustable voltage of up to 1000 V. With the trigger the output of the step generator is short circuited causing the discharge of the test object. The result is a negative step. In Figure 5-14 the measured step response of the high voltage divider is shown. Due to not negligible inductivities coming from the helical setup of the high voltage part oscillations occurred with a frequency of 12 - 33 MHz at the step test.

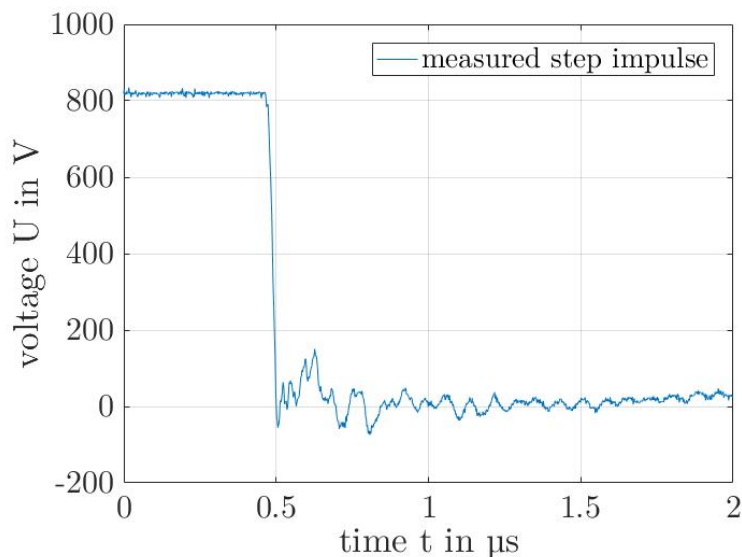


Figure 5-14: Step response of high voltage divider

A helical arrangement of 40 windings, a height of 1,5 meters and a diameter of 100 mm, as these measurements describe the built prototype, has an inductivity of about $L_P = 10 \mu\text{H}$ as calculated in Equation 8 [35].

$$L_P = \frac{N^2 \cdot \mu_0 \cdot A}{l} = 10,5 \mu\text{H} \quad (8)$$

$$\text{with } N = 40, \mu_0 = 4\pi \cdot 10^{-7} \frac{\text{N}}{\text{A}^2}, A = r^2\pi, r = 0,05 \text{ m and } l = 1,5 \text{ m}$$

If this additional inductivity is considered for the calculation of the damping resistor, the built-in resistors are too small. According to Equation 7, the required damping resistor with an inductivity of $15 \mu\text{H}$ is at least 2100Ω .

According to [31] the basic frequency of an oscillation is calculated by Equation 9:

$$f = \frac{1}{2 \cdot \sqrt{L \cdot C_e}} \approx 23 \text{ MHz} \quad (9)$$

$$\text{with } L = 15 \mu\text{H and } C_e = 30 \text{ pF}$$

The result of this calculation also represents the oscillations measured during the step response test. Nevertheless, the response time of the divider of about 40 ns can be described as very fast. To adjust the divider factor, one adjustable resistor was built in the resistive branch of the low voltage divider and one in the damping part of the damped capacitive branch of the low voltage part. To adjust the divider, a step of the step generator described above was used. The adjustable resistor of the resistive branch was used to match the DC scale factor to the scale factor specified by the capacitive ratio between high and low voltage part. The adjustable resistor in the damping resistor part of the damped capacitive branch was used to adjust the damping behaviour to achieve step responses as smooth and sharp as possible.

5.2.4 PERFORMANCE TEST OF THE PROTOTYPE DIVIDER

The prototype phase was completed with a calibration measurement for DC, AC and lightning impulse according to IEC 60060-2 respectively IEC 60060-1. The aim of the calibration was to determine the exact scale factor for each voltage form (AC, DC and impulse) and the corresponding measurement uncertainty.

As calibration method “Calibration of measuring system by comparison with a reference measuring system” over the whole voltage range was used. Because the prototype voltage

divider can be compared over the whole range with the reference measuring system, a separate linearity test was not necessary. To carry out the calibration the measured value of a reference system was compared with the measured voltage of the prototype to get the scale factor. This was done at several voltage levels equally distributed over the specified voltage ranges as listed in Table 5-1.

At each voltage level ten observations were made to minimise fluctuations due to read off errors. Afterwards, the scale factor F_g of each observation was determined and the mean value of the scale factor over each voltage level $F_g = 1/n \sum_{i=1}^n F_{i,g}$ was calculated. While n is the number of observations and the index g represents the different voltage levels. Also, the standard deviation $s_g = 1/F_g \sqrt{1/(n-1) \cdot \sum_{i=1}^n (F_{i,g} - F_g)^2}$ and the relative measurement uncertainty $u_g = s_g/\sqrt{n}$ were calculated for each observation. The scale factor F of the divider was then computed as mean value of the scale factors F_g over all voltage levels. Furthermore, a type A standard deviation $u_A = \max(u_g)$ and a type B standard uncertainty $u_{B0} = 1/\sqrt{3} \cdot \max |F_g/F - 1|$ were calculated. Type A uncertainties were calculated as a statistical analysis from a series of observations, type B uncertainties are uncertainties not calculated by statistical methods.

To take account of thermal effects, the short-term stability was also investigated. Therefore, the maximum voltage was applied for 30 minutes. The whole investigation was monitored with an infrared camera (FLIR E60). A small temperature rise of 3 K was observed during the short-term stability test. The derived scale factors at the beginning and the end were compared in order to get a type B estimated value u_{B4} . These values were then combined to gain the uncertainty of the calibration [36].

The DC calibration was done by positive and negative polarity by comparing arithmetic mean values. At AC, the peak values of both, negative and positive halfwaves, were compared.

For the lightning impulse calibration, not only the amplitude at both polarities, but also the time parameters were observed. Therefore, according to IEC 60060 two different steep impulses were measured, a fast one with $T_1 = 0,7 \mu\text{s}$ and $T_2 = 43 \mu\text{s}$ and a slower one with $T_1 = 1,5 \mu\text{s}$ and $T_2 = 45 \mu\text{s}$.

The reference measuring system for calibration consisted of the according voltage divider, the measurement cable and the measurement unit. Both, LI and DC reference dividers are ohmic voltage dividers, whereas the AC reference divider is a capacitive one. In case of AC and DC calibration, the measurement unit was a MU18, for LI calibration a DR. STRAUSS measurement system was used.

In Figure 5-15 to Figure 5-17 the calibration setups for DC, AC and LI are shown.



Figure 5-15: Calibration setup DC



Figure 5-16: Calibration setup AC



Figure 5-17: Calibration setup LI

5.2.5 CONCLUSION OF THE PROTOTYPE VOLTAGE DIVIDER

The calibration of the prototype, according IEC 60060, delivered following scale factors with the corresponding measurement uncertainties:

voltage form	scale factor F	uncertainty
DC ₊	4033,44	1,66 %
DC ₋	4045,80	2,90 %
AC _{Peak,+}	3946,14	1,29 %
AC _{Peak,-}	3983,21	1,24 %
LI _{Peak,+}	4031,16	1,76 %
LI _{Peak,-}	4017,24	1,60 %
T ₁	0,7 - 1,5 μs	9,56 %
T ₂	43,0 - 45,0 μs	5,42 %

Table 5-3: Scale factors and measurement uncertainties of prototype voltage divider

In Table 5-4 to Table 5-7, the scale factors for each voltage level are given.

voltage	F_g	s_g	u_g	$\Delta F_g/F$
kV	-	%	%	%
20	4000,06	0,129	0,041	-0,83
40	4003,05	0,162	0,051	-0,75
60	4018,43	0,085	0,027	-0,37
80	4027,89	0,108	0,034	-0,14
100	4023,31	0,085	0,027	-0,25
120	4040,18	0,076	0,024	0,17
140	4046,22	0,079	0,025	0,32
160	4050,23	0,060	0,019	0,42
180	4060,34	0,287	0,091	0,67
200	4064,73	0,063	0,020	0,78

Table 5-4: Scale factors and uncertainties
for DC₊

voltage	F_g	s_g	u_g	$\Delta F_g/F$
kV	-	%	%	%
20	3980,04	0,178	0,056	-1,63
40	3982,67	0,170	0,054	-1,56
60	4002,12	0,105	0,033	-1,08
80	4021,49	0,056	0,018	-0,60
100	4025,56	0,091	0,029	-0,50
120	4033,61	0,060	0,019	-0,30
140	4062,64	0,194	0,061	0,42
160	4090,49	0,103	0,032	1,10
180	4129,32	0,128	0,041	2,06
200	4130,04	0,045	0,014	2,08

Table 5-5: Scale factors and uncertainties
for DC.

voltage	F_g	s_g	u_g	$\Delta F_g/F$
kV	-	%	%	%
20	3941,13	0,188	0,059	-0,13
40	3956,76	0,048	0,015	0,27
60	3942,81	0,045	0,014	-0,08
80	3946,09	0,064	0,020	0,00
100	3941,77	0,067	0,021	-0,11
120	3947,84	0,103	0,032	0,04
140	3938,72	0,046	0,014	-0,19
160	3944,47	0,105	0,033	-0,04
180	3945,58	0,065	0,021	-0,01
200	3956,25	0,055	0,017	0,26

Table 5-6: Scale factors and uncertainties
for AC_{Peak,+}

voltage	F_g	s_g	u_g	$\Delta F_g/F$
kV	-	%	%	%
20	3981,55	0,082	0,026	-0,04
40	3979,81	0,099	0,031	-0,09
60	3991,78	0,054	0,017	0,21
80	3982,01	0,061	0,019	-0,03
100	3982,35	0,158	0,050	-0,02
120	3986,49	0,185	0,059	0,08
140	3979,81	0,136	0,043	-0,09
160	3975,78	0,109	0,034	-0,19
180	3983,61	0,093	0,029	0,01
200	3988,93	0,038	0,012	0,14

Table 5-7: Scale factors and uncertainties
for AC_{Peak,-}

voltage	F_g	s_g	u_g	$\Delta F_g/F$
kV	%	0	%	-
50	4011,28	0,174	0,055	-0,49
100	4006,34	0,226	0,071	-0,62
150	4029,66	0,168	0,053	-0,04
200	4036,29	0,186	0,059	0,13
250	4038,87	0,238	0,075	0,19
300	4034,32	0,241	0,076	0,08

Table 5-8: Scale factors and uncertainties
for LI_{Peak,+}

voltage	F_g	s_g	u_g	$\Delta F_g/F$
kV	%	0	%	-
50	4000,73	0,248	0,078	-0,41
100	4012,17	0,137	0,043	-0,13
150	4019,86	0,217	0,069	0,07
200	4032,86	0,243	0,077	0,39
250	4024,00	0,237	0,075	0,17
300	4022,85	0,238	0,075	0,14

Table 5-9: Scale factors and uncertainties
for LI_{Peak,-}

In Figure 5-18 to Figure 5-20 the relative changes of the scale factor over the voltage for DC, AC and LI are shown.

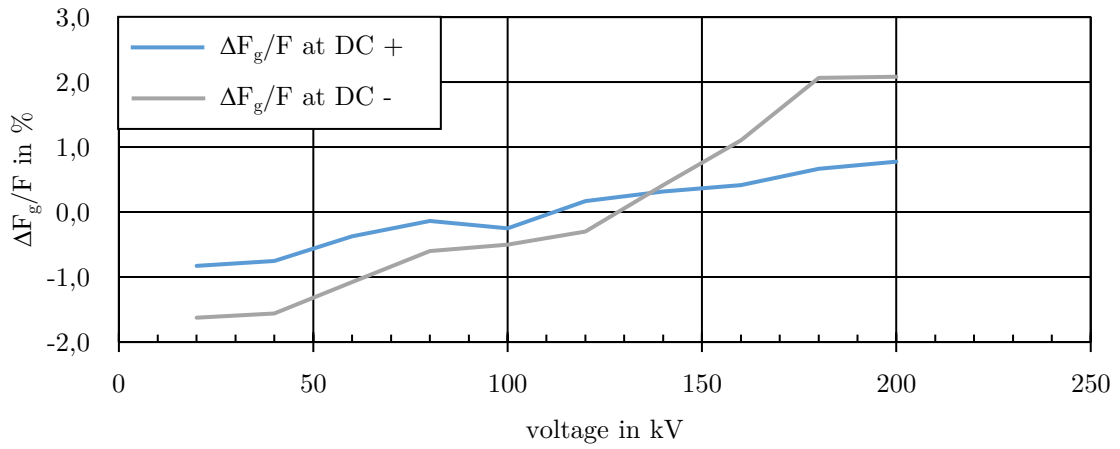


Figure 5-18: Relative change of scale factor over the voltage, DC

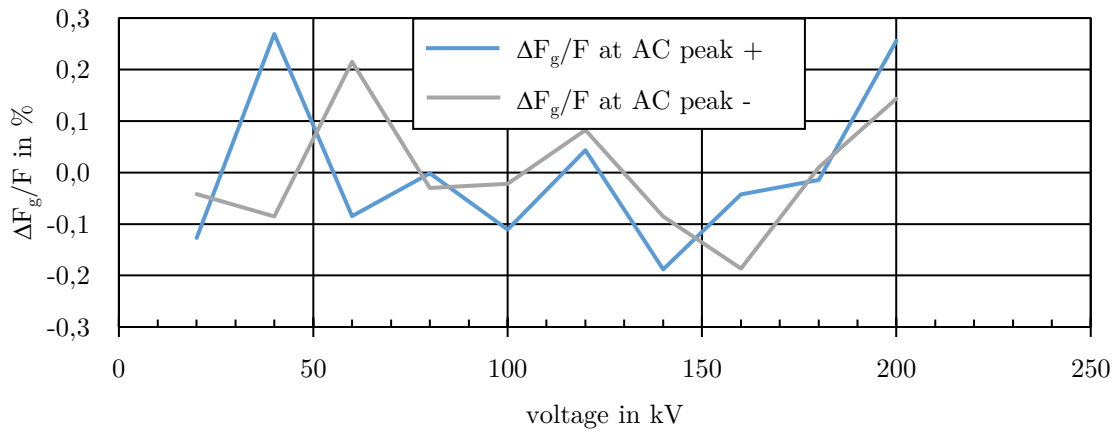


Figure 5-19: Relative change of scale factor over the voltage, AC

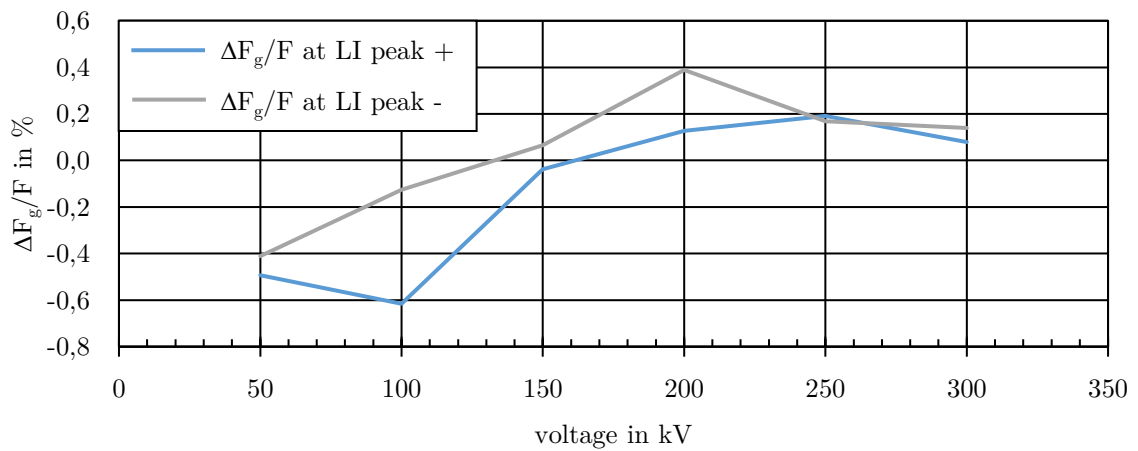


Figure 5-20: Relative change of scale factor over the voltage, LI

The used reference measurement systems have a relative measurement uncertainty $u_{\text{ref}} = 0,6 \%$ for DC, $0,65 \%$ for AC and $0,75 \%$ for LI.

For measuring DC only the resistive branch is relevant. For this branch, 100 resistors were used, each with a voltage coefficient of 2 ppm/V. If 200 kV are applied to the divider, the voltage drop over each resistor is 2 kV, which means a change of the resistive value of 0,4 %. Furthermore, corona discharges have been observed at the top five windings of the divider at 120 kV. Corona discharges lead to leakage currents, which cannot be detected by the measurement system [31, 37]. Therefore, if the measured voltage at the low voltage part, which gets lower due to the lower current, is compared with the voltage applied, the scale factor gets higher the higher the applied voltage gets. This explains the high nonlinearity at DC calibration.

In Figure 5-18 an edge occurs at a DC voltage of 120 kV. As mentioned above, corona discharges were observed at this voltage and above, which explains the faster rise of the scale factor from this voltage level upwards.

The inception voltage at negative voltages is lower compared to positive voltages. This is called the polarity effect [3]. This explains why the curve of the voltage with positive polarity in Figure 5-18 does not start to rise faster at 120 kV compared to the curve of the voltage with negative polarity.

The rise of the scale factor at high AC voltages, as shown in Figure 5-19, can as well be explained by occurring corona discharges. By comparing Figure 5-18 and Figure 5-19 the missing nonlinearity due to the voltage coefficient of the resistive branch is noticeable. This happens as the impedance of the damped capacitive branch under AC is significantly smaller than the impedance of the resistive one. It is not clear, why the above-mentioned polarity effect cannot be observed in the curves of the AC calibration for the positive and negative halfwave.

Due to the small current of 0,08 mA at 200 kV through the divider, the temperature rises only by 3 K in the resistors during the short-term stability test. With a temperature coefficient of 25 ppm/°C as shown in Appendix A.1, the overall change in resistance is about 75 ppm, or 0,0075 %. If this small dependence is considered as too much, a compensation by using the same resistors in the high and low voltage part is possible [31].

The results of the LI calibration are shown in Figure 5-20. The rise of the scale factor is seen as a combination of all effects mentioned before. Furthermore, a difference between the scale factor of DC, AC and LI can be observed. This has to be investigated in further researches where a proper way of adjusting an universal divider will be worked out.

5.3 FINAL DESIGN OF UNIVERSAL DIVIDER

5.3.1 DIMENSIONING AND DESIGN

To get a better dynamic behaviour and to reduce the oscillations within the divider, the damped capacitive branch will be divided into two helices. The first will be wound clockwise, the second one anticlockwise. In that arrangement, the fluxes of the two helices will cancel out each other in the common inner area as shown in Figure 5-21.

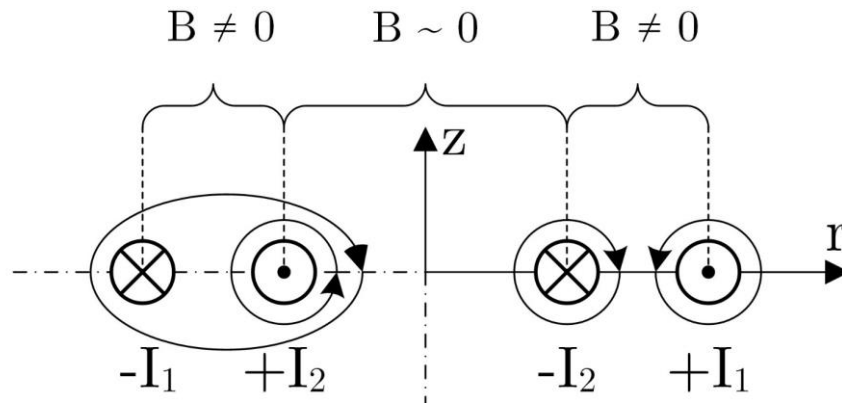


Figure 5-21: Magnetic flux situation by using double helix design

Between the two windings, the magnetic flux cannot be considered as zero. The inductivity of the divider can be minimised, but not eliminated in this way. Also, the inductivity of the capacitors themselves get lower due to the two parallel branches. This will result in a better step response with less overshoot respectively less oscillations.

- To prove this concept a finite element method (FEM) simulation with MagNet was set up. In Figure 5-22 and Figure 5-23 two concentrically arranged coils are modelled. In Figure 5-22 only the outer coil ($l = 1,45 \text{ m}$, $r = 49,5 \text{ mm}$, $N = 40$) is under current with a resulting inductivity of $9,52 \text{ } \mu\text{H}$. In Figure 5-23 only the inner coil ($l = 1,45 \text{ m}$, $r = 32,5 \text{ mm}$, $N = 40$) is under current with a resulting inductivity of $4,28 \text{ } \mu\text{H}$. Both, Figure 5-22 and Figure 5-23 as well as Figure 5-24 show the simulated magnetic flux density field. The diameter of the inner coil is determined by the length of the capacitors and additional space between each component for soldering. The dimension of the outer coil is determined by the diameter of the inner coil and the diameter of the capacitors.

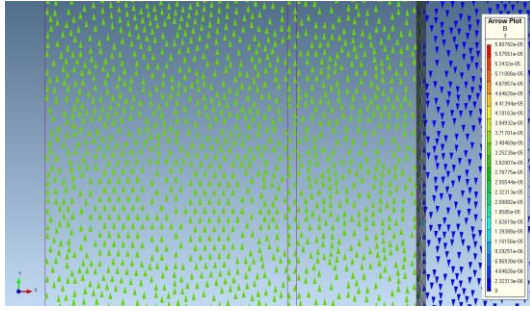


Figure 5-22: FEM simulation, outer coil under current

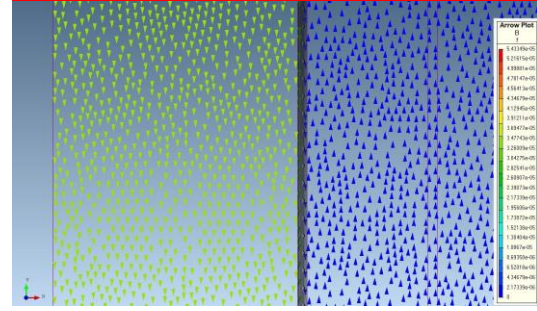


Figure 5-23: FEM simulation, inner coil under current

- If the current from the inner coil flows out of the drawing plane and the current of the outer coil flows into the drawing plane, the flux in the inner part of the coils is nearly cancelled out as it is shown in Figure 5-24. In this case, the resulting inductivity is 5,56 μH . Through the two parallel branches of capacitors as mentioned above, the additional inductivity of the capacitors is then only 2,5 μH resulting in an overall inductivity of 8,06 μH . Under these circumstances, the resulting damping resistor according to Equation 7 would be 1810 Ω with a factor of 3,5. This means that in every branch a damping resistance of 3220 Ω must be present.

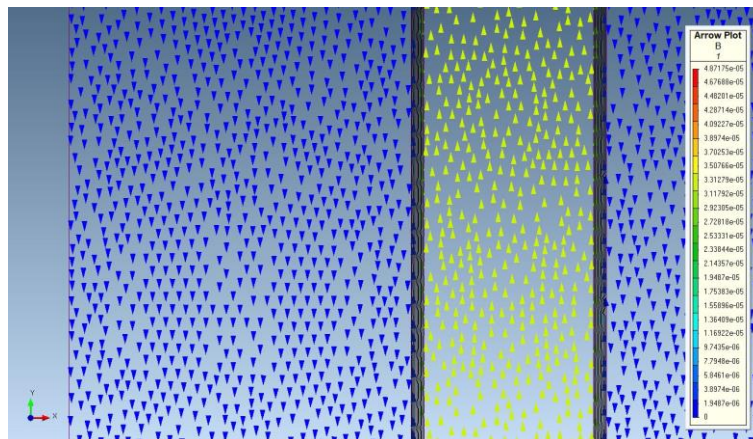


Figure 5-24: FEM simulation, both coils under current

- In reaction to the nonlinearity caused by the corona discharges, the components are applied on a construction with six pillars to get a much rounder shape. Furthermore, to guarantee the constant behaviour independent of humidity and dust, a sealed housing was designed, which will be filled with nitrogen.
- To reduce the influence of leakage currents due to discharges or other creepage currents, the impedance of the resistive branch will be reduced to reach a current of 0,5 to 2 mA, as it is suggested in [37]. For a voltage of 200 kV this will result in an overall resistance

of 100 – 400 M Ω . Furthermore, resistors with a lower voltage coefficient will be used in a higher amount to reduce the voltage drop per resistor and therefore the impact of the voltage coefficient.

- To reach the requirement of the modularity, a complex flange design was developed to enable the gas filling, as mentioned above.
- To cancel out the influence of proximity effects and to create a homogenous electric field around the universal divider, shield arms arranged in opposite helices, as [34] describes it can be added. Therefore, the flanges have to be adapted with a special feed-through to separate the shield branch from the measurement branches. However, this configuration won't be dealt with in this thesis.
- During the tests of the universal divider, it was recognised, that the used scale factor of 1:4001 is not practical in combination with the above mentioned YOKOGAWA oscilloscope, if the rated voltage is set to 200 kV AC. The mentioned voltage has a peak to peak value of $U_{pp} = 2 \cdot \sqrt{2} \cdot 200 \text{ kV} = 566 \text{ kV}$. If the oscilloscope is set to maximum V/div (10 V/div) the highest fully observable voltage is 80 V due to the limitation of 8 divisions on the Y-axis. With a scale factor of 1:4001 this is equal to a maximum peak to peak value of 320 kV or 113 kV RMS. To see the whole sine on the oscilloscope, a scale factor of at least 1:8000 is required.

5.3.2 3D CAD CONSTRUCTION

In this chapter the mechanical design of the divider will be explained. All not mentioned dimensions can be seen in Appendix C. In Figure 5-25 an overview of the designed divider module is shown. The height of one module is 1650 mm at rated voltages as given in Table 5-1. The first module can be placed on an isolated plane. Between this plane and ground the low voltage part will be installed. Furthermore, to gain good aspects in terms of transportability, the isolated plane will be mounted on a carrier cross equipped with wheels.

As described above, the framework was constructed out of six pillars with three spacers equally distributed over the whole height, which is shown in Appendix C. Polycarbonate will be used as material for the supporting framework because of the material's strength and transparency. In Figure 5-26 a sectional view of the bottom respectively top flange is shown. The complex design is owed to the circumstance of the gas-filled divider, as already described in chapter 5.3.1. To do some maintenance work, it is required to access the inner parts without damaging the housing. By removing the lock screws in Figure 5-26, the top flange with the complete housing can be lifted off. To guarantee the tightness, O-rings were implemented on both, top and bottom end. The gas inlet is equipped with a valve and a pressure gauge to enable the gas filling.

The connection between the flange and the component framework termination is established via four screwed-in banana plugs. Two modules can be combined by a screw-nut combination through the recess in Figure 5-26, bottom right.

To guarantee the mechanical stability when using three or more modules, it is recommended to insert struts after two modules. Furthermore, the component framework should be made of a tougher material in order to prevent damages to the structure due to tension or shearing forces.

The connection between housing tube and flange, as well as the connection between component framework termination and pillars will be established by special adhesive.

All components will be placed centrally in the holes of the framework pillars. The connection wires are cut in length, bent in a circular way and soldered under high temperatures to achieve spike and corona free connections.



Figure 5-25: Universal divider design

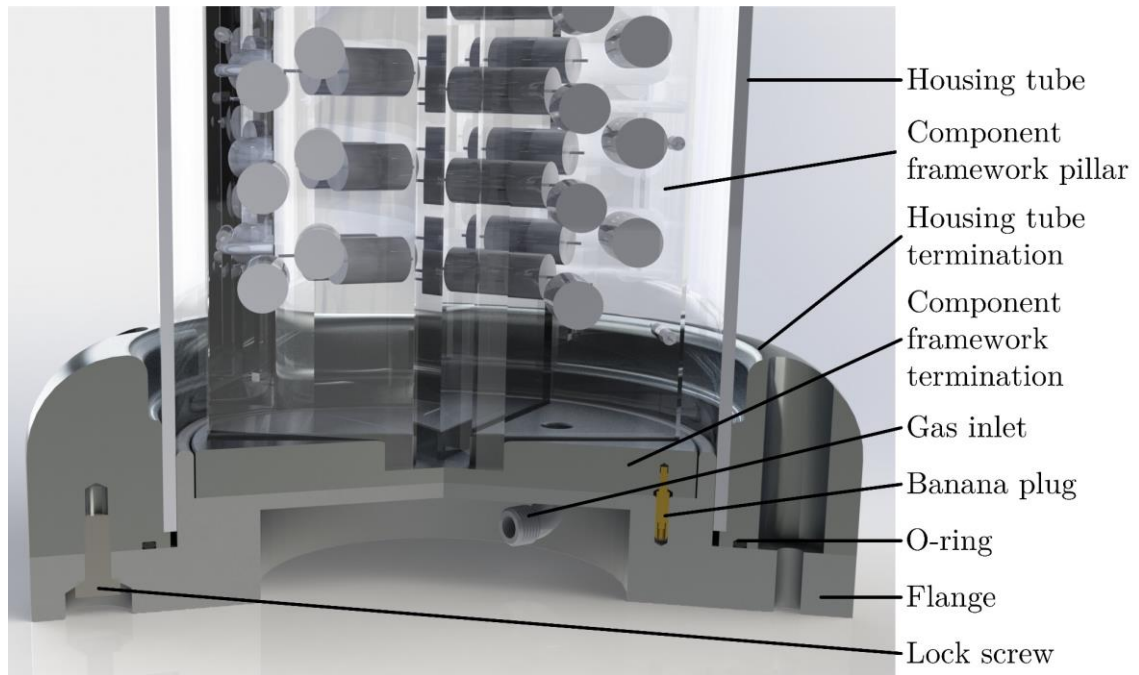


Figure 5-26: Sectional view of bottom of the universal divider

The big radii on the outside and the smooth transitions on the inside of the housing tube termination deliver a corona free flange.

The framework and the housing tube do not have to be made of polycarbonate. This material was chosen due to its transparency to make the inner parts visible. Another excellent choice would be glass-reinforced plastic (GRP). Attention has to be paid to high-quality GRP with focus on voids to prevent inner partial discharges.

6 TEST SETUP

6.1 DESCRIPTION OF THE CABLE SYSTEM

6.1.1 CABLE

The cable used in this thesis was a standard 12/20 kV 150 mm² XLPE AC cable, stored indoor for about five years at common conditions, as it is used in urban medium voltage grids. The structure of the cable, as described in chapter 2, is as follows:

- Conductor: 150 mm² aluminium
- Inner semi-conducting layer
- XLPE insulation: 5,5 mm thickness
- Outer semi-conducting layer
- Semi-conducting swelling tape
- Screen: Copper wires, 25 mm² copper
- Sheath: Polyethylene

In Figure 6-1, a cross-section and a picture of the used cable are shown.

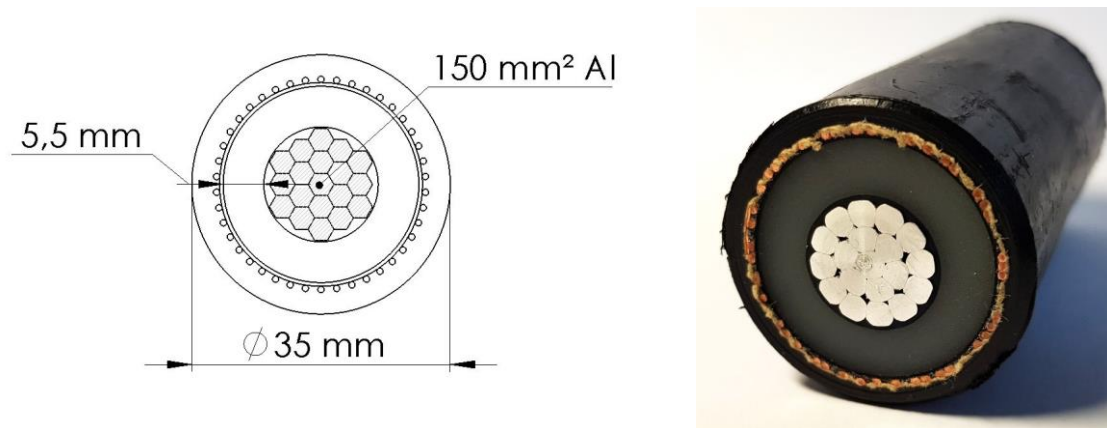


Figure 6-1: Cross-section of used cable

The minimal bending radius of 0,53 m defined by the manufacturer was respected and fulfilled during all manipulations and tasks of the test setup.

6.1.2 TERMINATION

A cable cannot be simply connected to switchgear, transformers, converters or wall bushings. The electric field between the inner conductor and the outer earth screen has to be degraded in a defined way. Otherwise, flashovers will occur at the end of the cable at nominal voltages due to high electric field intensities as shown in Figure 6-2.

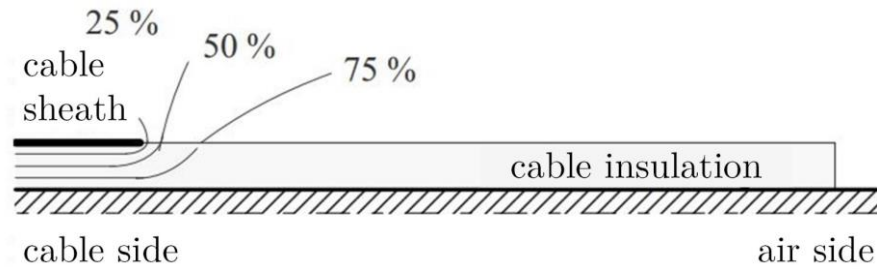


Figure 6-2: Electrical field distribution at end of a cable, uncontrolled [3]

One way of electric field control is the geometric one. The outer semi-conducting layer is extended by the termination and widened with a big radius as shown in Figure 6-3.

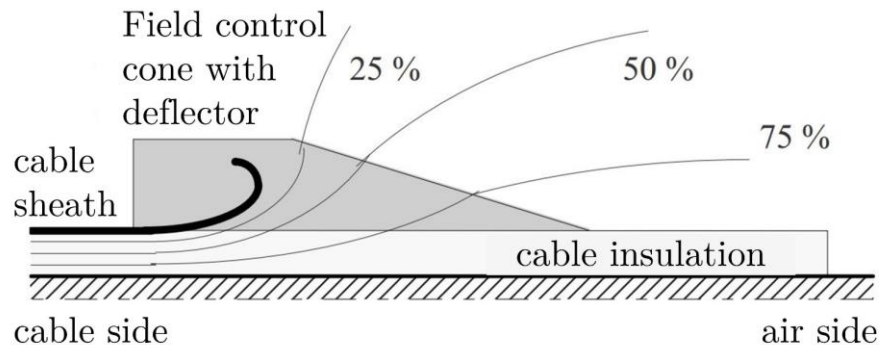


Figure 6-3: Electrical field distribution at end of a cable with geometrical field control [3]

For this thesis, a standard 12/20 kV AC cable termination was used. The geometrical field control part is integrated in the termination and consists of conducting silicone. It is located in the back end of the termination and connects, when properly installed, with the outer semi-conducting layer of the cable.

As the later on described preliminary tests showed, one cable termination is not enough to withstand the desired voltage levels of the lightning impulses. Therefore, one termination was put over another one without the field control part as shown in Figure 6-4 to enlarge the creepage distance from the inner conductor to the earth screen.



Figure 6-4: Installed double standard 12/20 kV AC cable termination

6.1.3 JOINT

Cables cannot be delivered in infinite lengths. The usual length depends on the diameter of the cable and thus the conductor cross-section and the insulation thickness. To connect two pieces of cables to each other, so-called joints are necessary to provide a safe and reliable connection over years.

The used joint is a standard 12/20 kV AC cable joint as shown in Figure 6-5. For installation the two cables were spliced with a screw connector. To connect the semi-conducting layers of the cable, an electrical field control is established via a semi-conducting shrinking tube. This shrinking tube has to degrade the whole voltage due to its position directly between the two semi-conduction layers and the conductor. In the following step, the insulation body with the outer semi-conduction layer was applied via shrinking. After establishing a screen with a copper band and connecting the screens of the two cables, a protection shrinking tube was applied.



Figure 6-5: Installed standard 12/20 kV AC cable joint

6.2 PRELIMINARY TESTS

Preliminary tests were performed to examine the system limits of the device under test (DUT). In Table 6-1 the performed preliminary tests are shown. During the preliminary tests, two DUT were used.

test number	DUT number	description of DUT	test and results
1	1	two 5 meter long cables, one as reference circuit with thermal elements, one with 30 cm removed sheath, shield and outer semi-conducting layer	aged with 500 A ($T_C = 90\text{ }^\circ\text{C}$) and 80 kV of each polarity for 800 hours
2	1	as described in test number 1, furthermore the sheath was removed in steps up to 150 cm	flashover at - 170 kV LI
3	1	as described in test number 1, furthermore the cable ends were equipped with field control cone	flashover at - 170 kV LI
4	2	two 10 meter long cables, both with single terminations, one with joint, tests were made at $T_C = 20\text{ }^\circ\text{C}$ and $T_C = 90\text{ }^\circ\text{C}$	flashover at - 150 kV LI
5	2	as described in test number 4, but with two terminations each (one with, the other one without field control)	withstand LI up to $\pm 170\text{ kV}$
6	2	as described in test number 4	S/IMP test with different voltages. Breakdown of joint at + 80 kV DC/ - 170 kV LI

Table 6-1: Preliminary tests

The results and experiences gained during the preliminary tests led to the decision of the choice of a DC system voltage of $U_{DC} = 55\text{ kV}$.

6.3 DEVICE UNDER TEST

Shekhar et al. suggested that existing AC cables can be used as DC links to enhance the grid capacity [11]. Therefore, a 12/20 kV 150 mm² XLPE AC cable as described in chapter 6.1 was used as a DC cable.

The tested cable system consists of two 10 meters long cable segments, each terminated by two cable terminations as a consequence of the preliminary tests described in chapter 6.2 to withstand the later performed superimposed impulse test. According to the results of the preliminary tests, the system voltage for the DC cable was set to $U_{DC} = 55 \text{ kV}$.

The first termination was used with the field control, the second termination was used without field control to enlarge the creepage distance as described in chapter 6.1.2. Furthermore, one segment was equipped with a cable joint as mentioned in chapter 6.1.3.

6.4 IMPLEMENTATION OF HEATING

As shown in Figure 6-6 a loop was established with the two cable segments. To reach the required temperature conditions (chapter 4.2.1) an appropriate current was driven through the test loop by using a current transformer. The used transformer is a current converter for measuring purposes of the type TS 13.3 with a maximum primary voltage of 380 V manufactured by trafomodern.



Figure 6-6: PQ test setup

To reach an appropriate heating current, the cable was put through the current transformer two times considering the minimal bending radius. The current transformer was supplied via a variable transformer with additional safety and control equipment, as shown in Figure 6-7.

To satisfy security issues, the heating circuit was equipped with a current relay to stop the current supply in case of faults leading to a rise of the current. This was done by implementing the current relay in the safety circuit. Furthermore, the current transformer was supplied over a contactor, which was controlled by a timer. The used timer enabled the definition of the load cycles.

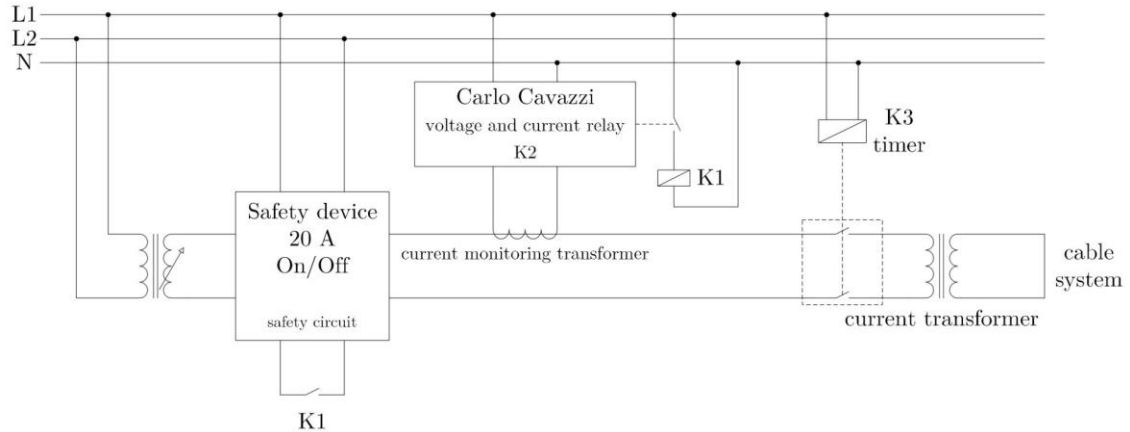


Figure 6-7: Current circuit with safety circuit

Through preliminary tests, a correlation was found between the conductor temperature T_C and the sheath temperature T_S as shown in Figure 6-8. If the conductor temperature T_C is $90\text{ }^\circ\text{C}$, the sheath temperature is $63\text{ }^\circ\text{C}$ at an ambient temperature of $25\text{ }^\circ\text{C}$. It has to be mentioned that this correlation is not valid by different ambient temperatures.

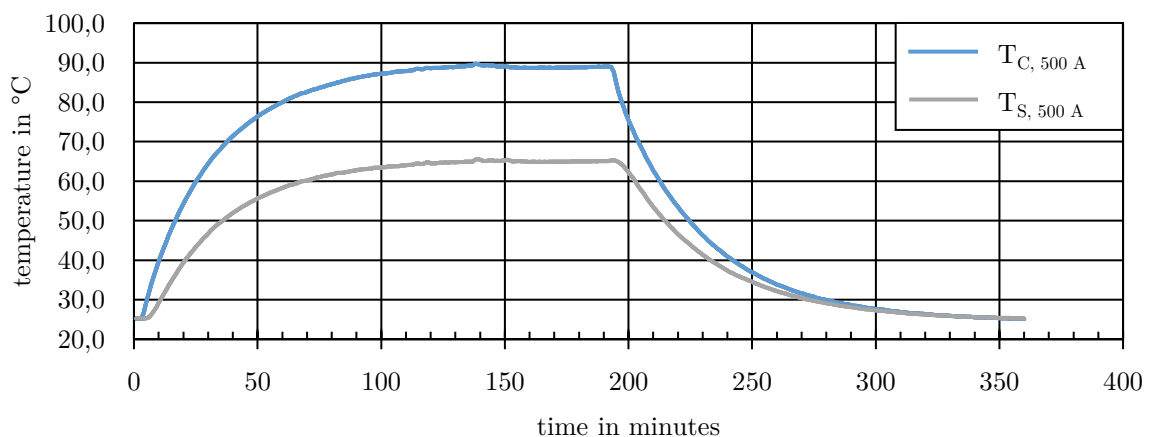


Figure 6-8: Temperature development over the time, $I = 500\text{ A}$

This measurement was carried out with a datalogger (YOKOGAWA Daqstation DX1006) and type K thermal elements. The thermal element on the sheath was applied to the surface

with an adhesive tape, the thermal element in the conductor was put in a pre-drilled hole as shown in Figure 6-9. The hole for the conductor thermal element was drilled deeper due to the fact, that the thermal element had a shrinking tube as coating to insulate it electrically. Furthermore, this thermal element was glued in with epoxy resin.

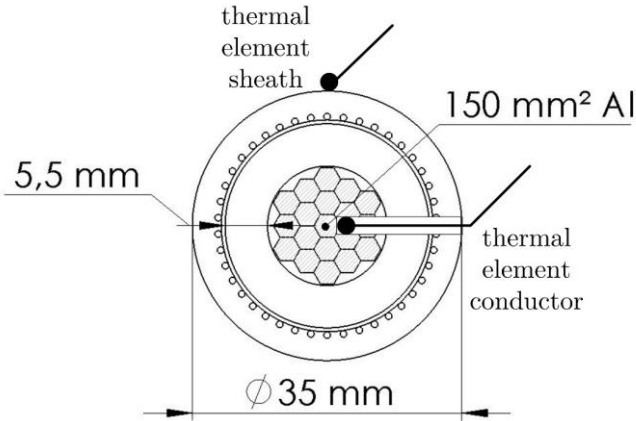


Figure 6-9: Position of the thermal elements in the cable

Due to the relation between conductor and sheath temperature a simplification was made and the temperature was only measured on the surface of the DUT. Otherwise an identical reference circuit with an identical heating current would be required to measure the conductor temperature. The conductor temperature can only be measured by drilling a hole for the thermal element, which destroys the insulation integrity of the cable system leading to the loss of the capability of maintaining the voltage.

Three thermal elements of the type K were placed on the cable system, one on each cable sheath and one on the cable joint, in order to measure the temperature during the PQ test.

The IEC 60287 standard describes the way to calculate the nominal current of a given cable at given environmental conditions and laying method with respect to the conductor temperature [38, 39]. Calculations according to this standard led to the result, that the required current to reach 90 °C of conductor temperature with an ambient temperature of 25 °C is 498 A if the cable is laid in air (Eq. 10).

$$I = \sqrt{\frac{\Delta T}{R \cdot (T_1 + T_2 + T_4)}} \quad (10)$$

ΔT is the temperature difference between ambient temperature and conductor temperature T_C . The AC resistance of the conductor at maximum temperature $T_{C,\max}$ is represented by R . T_1 and T_2 are thermal resistances related to the interior of the cable and T_4 is the thermal resistance between the cable surface and the surrounding medium [38].

Proximity effects, dielectric losses, circulation currents and eddy currents can be neglected or do not occur with DC voltage. It has to be mentioned here, that if the cable is used as DC cable, also DC flows through the cable instead of AC, which is used as heating method throughout the tests performed for this thesis. This leads to a higher allowed current due to the lack of skin effect.

With the parameters in Table 6-2 the thermal resistances were calculated.

parameter	value	unit	description
$\rho_{T,XLPE}$	3,5	Km/W	thermal resistivity XLPE
$\rho_{T,PE}$	3,5	Km/W	thermal resistivity PE
$\rho_{E,Al,20\text{ }^{\circ}C}$	2,83E-08	Ωm	electric resistivity aluminium
$\rho_{E,Cu,20\text{ }^{\circ}C}$	1,72E-08	Ωm	electric resistivity copper
$\alpha_{20\text{ }^{\circ}C,Al}$	4,03E-03	1/K	temperature coefficient aluminium
$\alpha_{20\text{ }^{\circ}C,Cu}$	3,93E-03	1/K	temperature coefficient copper
A	150	mm ²	cross section of conductor
t ₁	5,5	mm	thickness of insulation
t ₂	3	mm	thickness of sheath
D _S	28,5	mm	outer diameter shield
D _C	13,82	mm	outer diameter of conductor
D _E	34,5	m	outer diameter cable

Table 6-2: Parameters for current calculation according to IEC 60287

In terms of completeness the results of this calculation with different conductor temperatures T_C are shown in Table 6-3.

current I	conductor temperature T_C
A	$^{\circ}C$
498	90
460	80
417	70
367	60
308	50

Table 6-3: Calculated rated currents for different conductor temperatures T_C

Through the iterative measurement process as described above, a current of 500 A was determined for a conductor temperature of 90 °C (Figure 6-8). In datasheets of different manufacturers values of about 432 A can be found for the cable installation in free air in flat formation. This value is smaller due to the heating effect of potential neighbour cables. All in all, the calculated value according to IEC 60287 and the gained value of the iterative process match together.

6.5 DC GENERATOR AND ITS CONNECTION

The used DC generator (High Volt GPM 30/800) is capable of 800 kV DC of each polarity with an output current of 30 mA. To protect the DC generator against high voltage impulses due to the superimposed voltage test a water resistor was built [40].

To achieve a good impulse absorption, the resistor was chosen to have a resistance of 3 MΩ. Furthermore, an incoming impulse of 200 kV was not allowed to creep along the water resistor, which led to an overall length of 3 meters. As container a transparent hose with an inner diameter of 12,7 mm was chosen. With Equation 11 the required conductivity of the water can be calculated to achieve the desired resistance with given geometrical measurements.

$$\sigma_{H_2O} = \frac{1}{\left(\frac{R}{l} \cdot \frac{D^2 \cdot \pi}{4}\right)} = 7,8 \frac{mS}{m} = 78 \frac{\mu S}{cm} \quad (11)$$

$$\text{with } R = 3 \text{ M}\Omega, l = 3 \text{ m}, D = 0,0127 \text{ m}$$

Two sorts of water, tap water ($\sigma \approx 350 \mu S/cm$) and purified water ($\sigma \approx 0,1 \mu S/cm$) were mixed together to gain the desired conductivity. The hose was filled under water in order to prevent bubbles from being trapped in the water resistor, which can lead to failure of the resistor. Two conical shaped plugs were put into each end of the hose and fixed with a hose clamp to provide a connection and to keep the water inside as shown in Figure 6-10.



Figure 6-10: Water resistor, conical shaped plug

Electrolytical processes built up an oxide layer on the two plugs made of aluminium, which caused the dark colour. If the DUT breaks down, a not neglectable current flows through the water resistor in which H_2O is split into oxyhydrogen (H_2 and O_2). This mixture is highly explosive causing the water resistor to detonate in presence of a spark at one of the plugs. This circumstance was known beforehand, but accepted as the DC generator has an additional impedance, which protects it in case of a breakdown.

Another possibility would be a protection resistor made by discrete elements, which was not dealt with in this thesis due to an exceeding range of work.

6.6 IMPULSE GENERATOR AND ITS CONNECTION

To generate appropriate impulses, a four-staged impulse generator as shown in Figure 6-11 was used. The following list shows the elements of this impulse generator.

- impulse capacity C_S' : 134,4 nF/stage
- damping resistor R_D' : 75 Ω /stage
- discharging resistor R_E' : LI: 470 Ω /stage
SI: 34,6 k Ω /stage
- charging voltage U_C' : 200 kV/stage

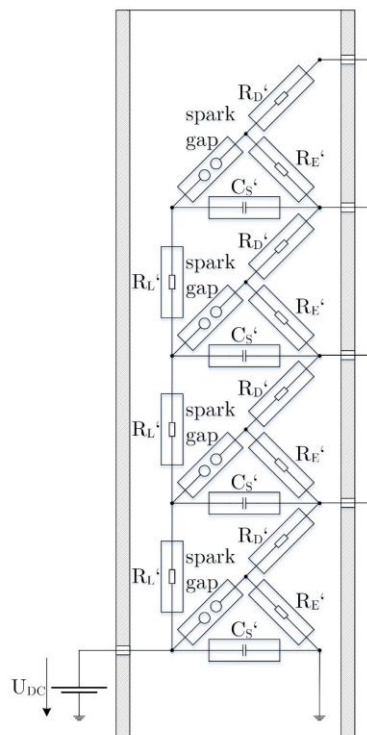


Figure 6-11: Schematic drawing of impulse generator, electric elements as shown with housing

To protect the impulse generator against uncontrolled charging with DC a coupling element is needed, which blocks the DC voltage. There are two possibilities to achieve this: a spark gap or a blocking capacity [30, 41].

Complications by using a spark gap may occur [28, 30, 42]. However, these complications mostly show up at unipolar superimposed voltages (DC+ and LI/SI+ and vice versa). Due to the fact, that the TB 496 only requires bipolar superimposed voltages (DC+ and LI/SI- and vice versa) the spark gap was investigated for possible use in this thesis.

As Prasser, Pischler and Schichler and respectively Voß and Gamlin furthermore argued, the use of a spark gap has some disadvantages [28, 29, 30]. First of all, the spark gap has to withstand the applied DC voltage, which leads to a breakdown voltage $U_{BD} = U_{DC} + \Delta U$, where ΔU represents the safety margin to ensure the withstand voltage U_{DC} . To make the spark gap conducting, a voltage equal or higher than the breakdown voltage of the spark gap is required. This leads to some restrictions regarding the amplitude of the superimposed impulse. At bipolar superimposed voltages, the minimum voltage to fire the spark gap is therefore ΔU . If unipolar superimposed voltages must be generated, the minimum required impulse voltage rises to $2 \cdot U_{DC} + \Delta U$. By using a switching impulse, the spark gap might extinguish due to slow voltage changes. This leads to edges in the tail [28, 30].

Another possibly occurring problem when using the spark gap as coupling element is shown in Figure 6-12. The blue curve represents the voltage directly at the test object, the green curve represents the voltage on the impulse generator.

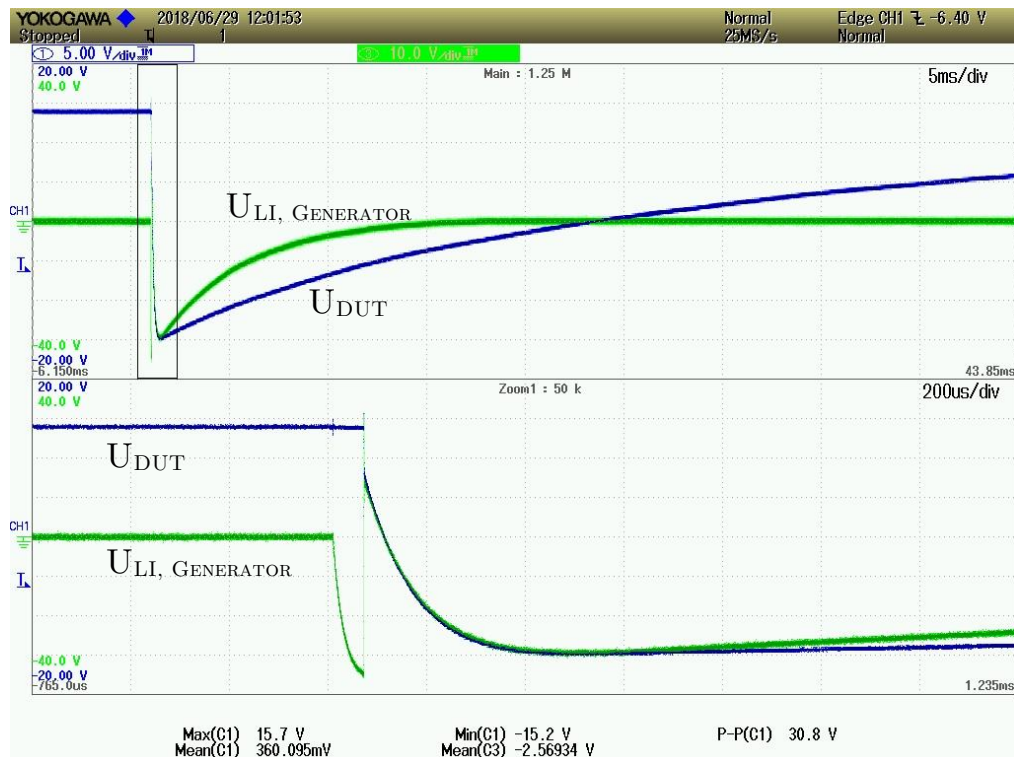


Figure 6-12: Problem when using spark gap as coupling element (bottom: zoomed)

It can be observed, that the impulse at the DUT and at the impulse generator have different time constants in the tail. The reason for this is, that the spark extinguishes right after the crest and the two systems (system 1: DC, universal divider and DUT, system 2: impulse generator) are not connected to each other anymore. In the further course the two systems discharge separately, which leads to two different T_2 .

Furthermore, the wave form can be distorted. A very well-known phenomenon is the so-called front chopping, where the spark gap does not fire in the first moment and the impulse is transmitted capacitively [28]. This as well is shown at the bottom in Figure 6-12, where the voltage at the impulse generator rises until the spark gap connects the two systems. When the flashover happens, the voltage on the DUT is immediately pulled down before following the impulse.

A coupling capacitor on the other hand changes the efficiency of the impulse generator, as the coupling capacitor and the DUT represent a capacitive voltage divider. Thereby the applied impulse has to be higher compared to the case when using a spark gap. Additionally, the capacitor has to withstand the full DC voltage [30].

Due to the previously described problems with the use of spark gaps, all further tests for this thesis were made with a coupling capacitor as blocking element. Capacitors in this dimension are not common. Therefore, as Voß and Gamlin suggested in [30], the impulse capacitor of the third stage of the impulse generator was used to establish the connection between the DUT and the impulse generator as shown in Figure 6-13 on the left hand side.



Figure 6-13: Overview of complete test setup

The internal cross-section for this configuration is shown in Figure 6-14.

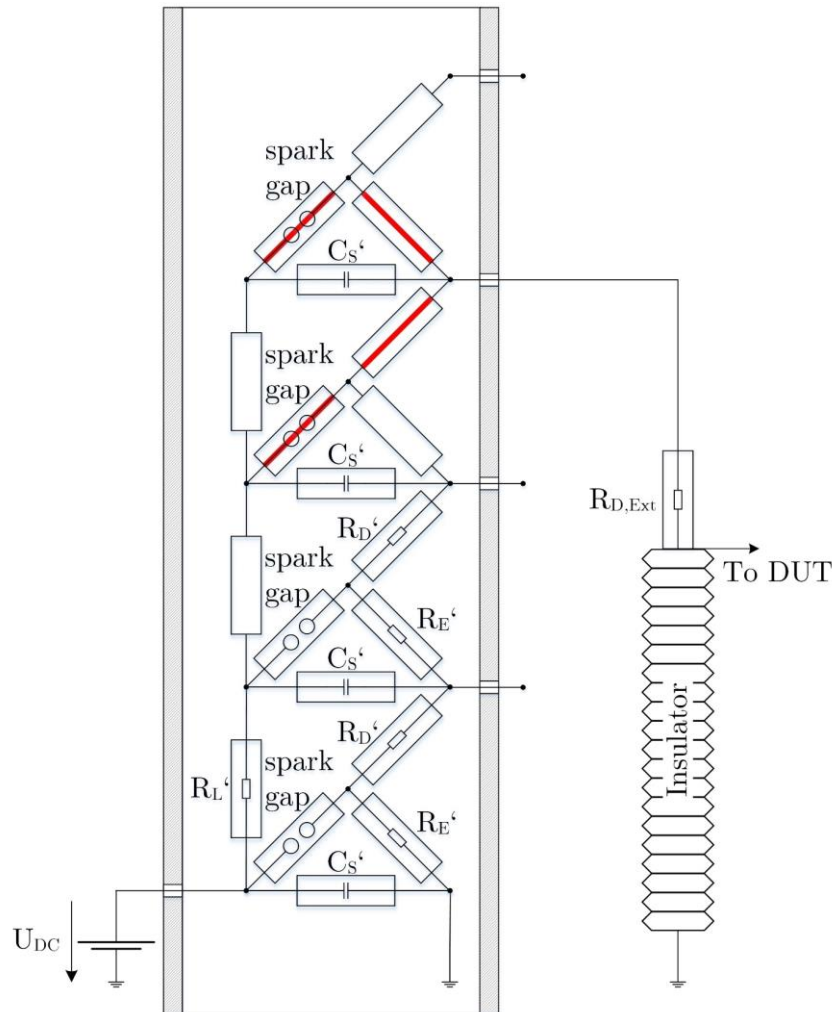


Figure 6-14: Schematic drawing of impulse generator, electric elements as shown with housing, modified configuration

All resistors corresponding to the third and fourth stage (damping, discharging and charging resistors) of the impulse generator were removed. For reasons of safety, the impulse capacity of the fourth stage was short-circuited via the spark gap and the terminals of the discharging resistor of the corresponding stage.

An impulse generated by the first and second stage reaches the impulse capacity of the third stage. From there on both, the spark gap and the terminals of the damping resistors of the third stage are short-circuited, which conducts the impulse to the output terminal of the third stage.

In this configuration, the impulse capacity of the third stage was used as coupling element between the DC and the impulse generator. To achieve the required time parameters, an external resistor, placed on an insulator, with a value of $R_{D,Ext} = 20 \text{ k}\Omega$ was necessary.

7 ADAPTED PREQUALIFICATION TEST FOR MV DC CABLE

7.1 TEST SETUP AND CYCLES

As mentioned above, the aim of this thesis was to provide the test setup and the required equipment to perform a prequalification test, not to perform a full PQ test. Therefore, the most stressful cycles for a cable system were chosen for a shortened PQ test.

As device under test, a representative 12/20 kV AC cable system, consisting of two 10 meter long cables, both with two cable terminations, one with a cable joint (system A), one without a joint (system B), was used and considered as a 55 kV DC cable.

As described in chapter 4.2, one load cycle (LC), according to TB 496, has to be at least 24 hours (8 hours heating, 16 hours cooling), except the thermal constant of the tested cable is that high, that the required temperature cannot be reached within the mentioned six hours. In this case, the cycle time has to be extended. Due to the fact that the thermal constant of the used cable system is about 30 minutes as shown in Figure 6-8, the duration of the heating period during load cycles (LC) was set to four hours followed by 8 hours for cooling.

The conductor temperature T_C of the cable system was defined with $T_C = 70\text{ }^\circ\text{C}$. This temperature was chosen to approach the values defined in the TB 496. Preliminary tests and calculations according to IEC 60287 delivered the required current to reach conductor temperature $T_C = 70\text{ }^\circ\text{C}$ is 425 A. At an ambient temperature of $20\text{ }^\circ\text{C}$ this current corresponds to a sheath temperature of $T_S = 52\text{ }^\circ\text{C}$ as shown in Figure 7-1.

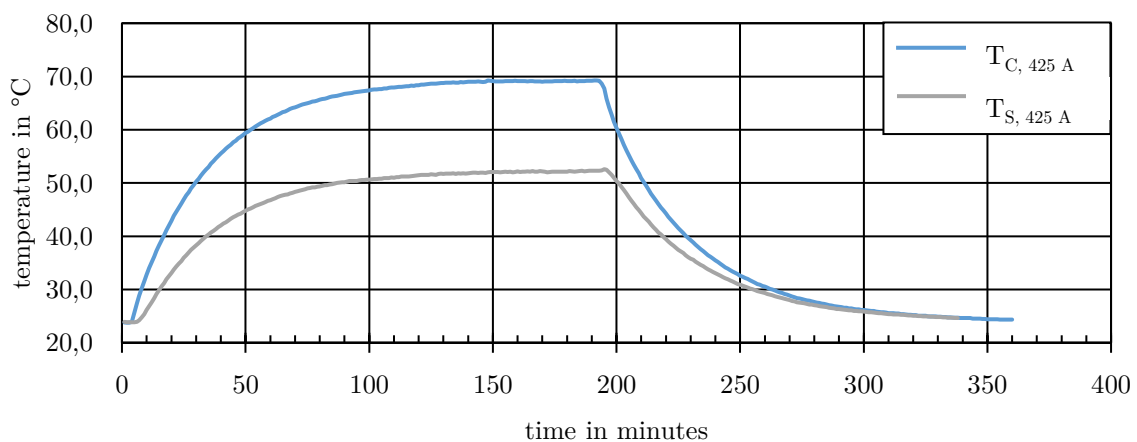


Figure 7-1: Temperature development over the time, $I = 425\text{ A}$

For the adapted PQ test 30 positive load cycles were completed, where ten cycles were performed with 8 hours of heating and 16 hours of natural cooling and 20 cycles with 4 hours of heating and 8 hours of cooling.

In Figure 7-2 the temperature development at all measurement points during a short LC is shown. System A was equipped with two thermal elements, one on the joint and one on the cable sheath. At a closer look, a difference in the time constants of the surface temperatures of the cable and the joint can be observed. Due to the thickness of the joint, this thermal system is slower than the cable itself. Consequently, the chosen time of heating (4 hours) is slightly too short for the joint.

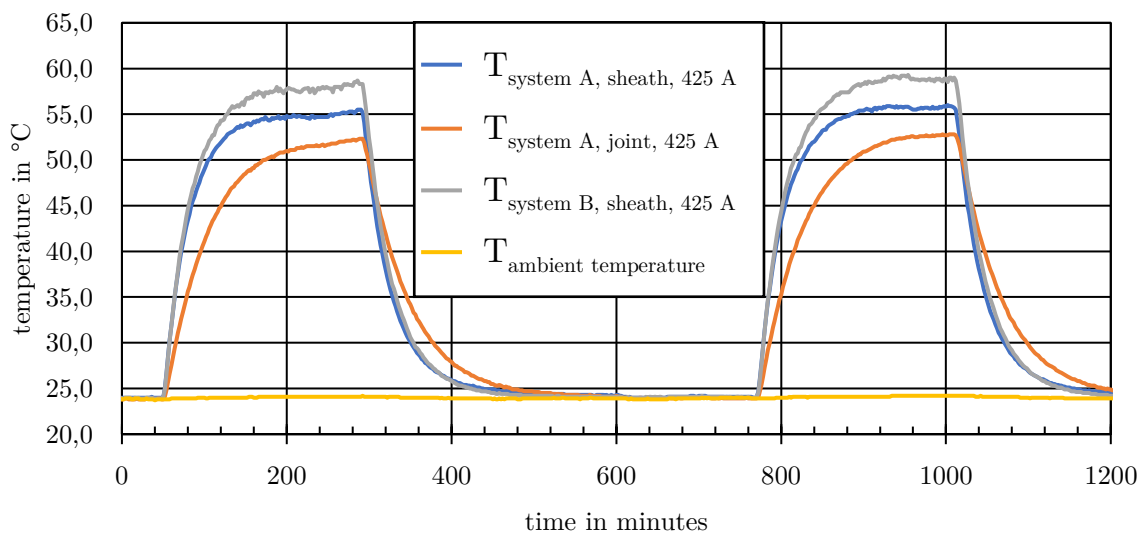


Figure 7-2: Temperature development over time during short Load Cycle (LC)

As shown in Figure 6-5, the cable joint has a significantly larger diameter than the cable itself. As a consequence, the surface area and therefore the cooling performance of the joint is better compared to the cable itself. This is the reason why the surface of the installed cable joint can never reach the surface temperature of the cable.

System B, consisting of a 10 meter long cable and two terminations was only observed by one thermal element. To monitor the test environment, the ambient temperature was also recorded. With this information, anomalies in the recorded temperatures of the cable have been explained, for example an open door of the test laboratory.

Due to the assumption, that the cable system is seen as a 55 kV DC System, the voltage for the load cycles (LC) was set to $U_{TP1} = + 80$ kV according to chapter 4.2.1.

In Figure 7-3 the voltage and the related current during the positive LC are shown.

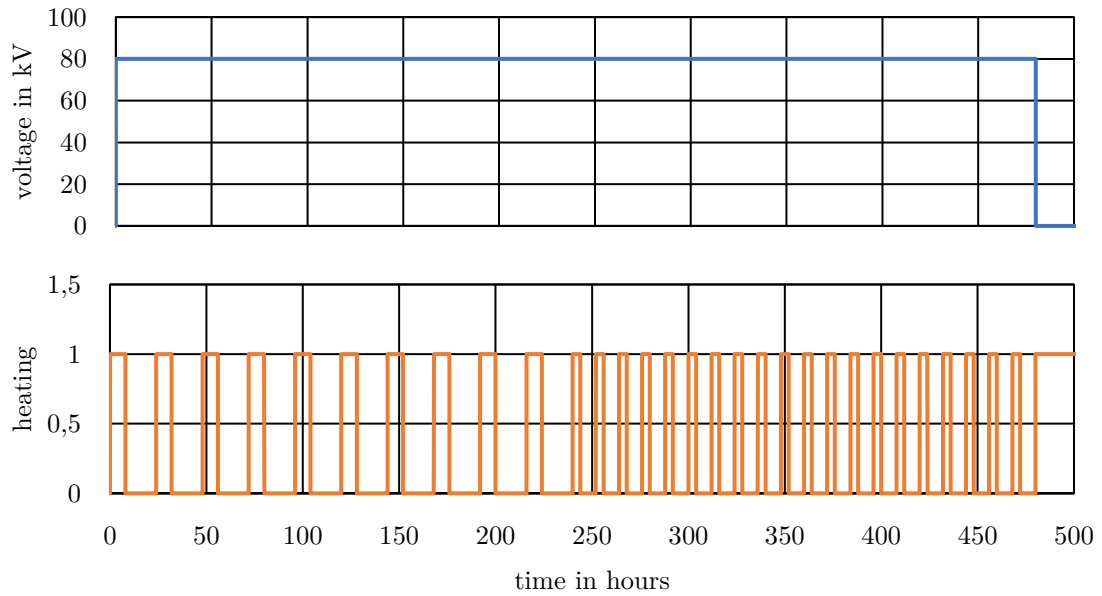


Figure 7-3: Voltage and current over time for load cycle with positive polarity (LC+)

After the 30 positive LC, 30 negative LC were completed in the same way (8/16 hours respectively 4/8 hours) as described above. In Figure 7-4 the voltage and the related current during the negative LC are shown.

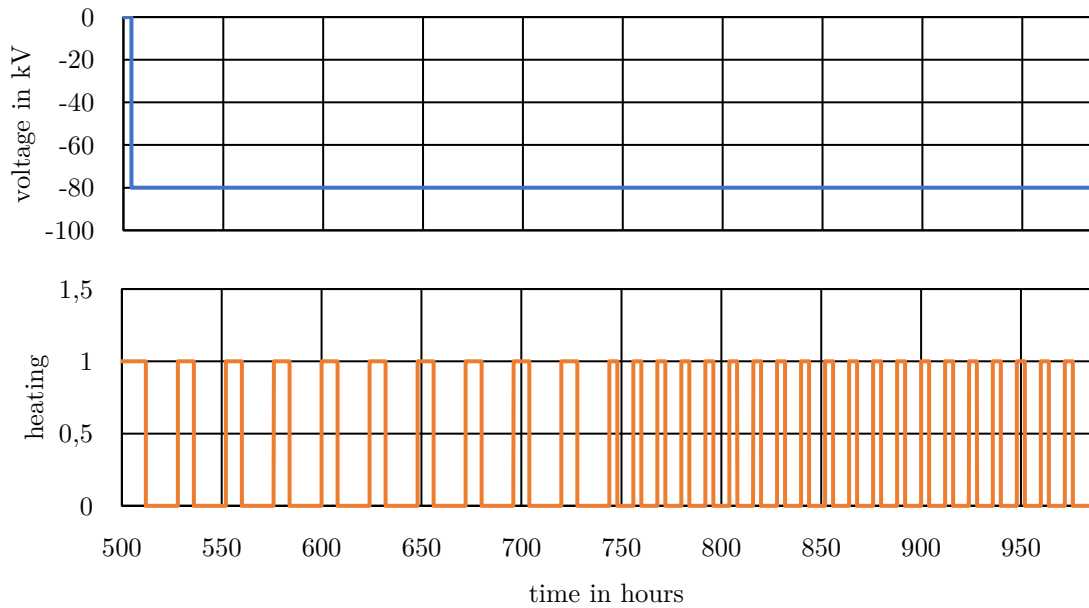


Figure 7-4: Voltage and current over time for load cycle with negative polarity (LC-)

To complete the long duration voltage test of the adapted PQ test, 20 load cycles with polarity reversal, in the style of the in 4.2.2 described LC + PR, were performed. Only the time parameters were changed as described above because of the small thermal time constant. This leads to the circumstance, that in one day one LC + PR and an additional LC were performed as shown in Figure 7-5. The voltage was set to $U_{TP2} = 69$ kV.

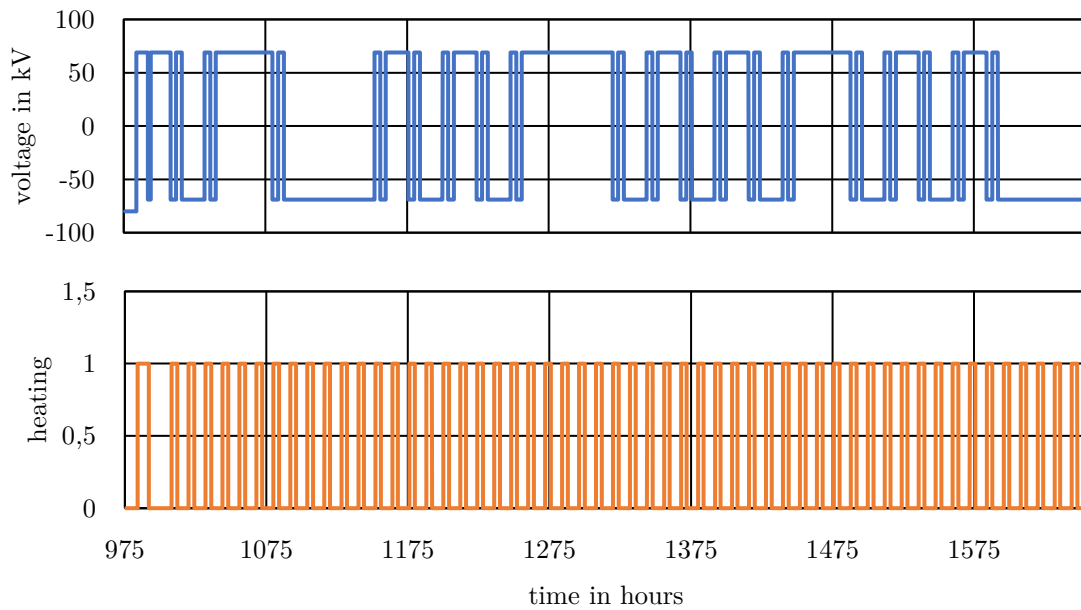


Figure 7-5: Voltage and current over time for load cycle with polarity reversal (LC + PR)

The partially long breaks in Figure 7-5 are owed to the manual PR, which were not performed on weekends.

These three tests were chosen as they were considered as the most challenging ones for a standard XLPE AC cable when using it as a DC cable. During all tests no anomalies occurred.

7.2 SUPERIMPOSED VOLTAGE TEST

At the end of the investigations for this thesis a superimposed voltage test was performed. To meet the parameters described in the TB 496, a positive voltage of + 55 kV DC in combination with an appropriate heating current was applied for at least 10 hours before the S/IMP test. After this conditioning phase 10 superimposed impulses with + 55 kV DC and - 66 kV SI were applied, as described in chapter 4.3. The according time parameters were $T_{CR} = 300 \mu\text{s}$ and $T_2 = 3500 \mu\text{s}$. An oscillogram of this superimposed voltage is shown in Figure 7-6. Between each impulse a break of two minutes was held.

After deenergising the system, a voltage of - 55 kV DC in combination with an appropriate heating current was applied for at least 10 hours to condition the cable system for the second S/IMP test. Subsequently, 10 superimposed impulses were applied with - 55 kV DC and + 66 kV SI as shown in Figure 7-7 with the according time parameters $T_{CR} = 300 \mu s$ and $T_2 = 3500 \mu s$. All 20 superimposed impulses were passed and no breakdown occurred.

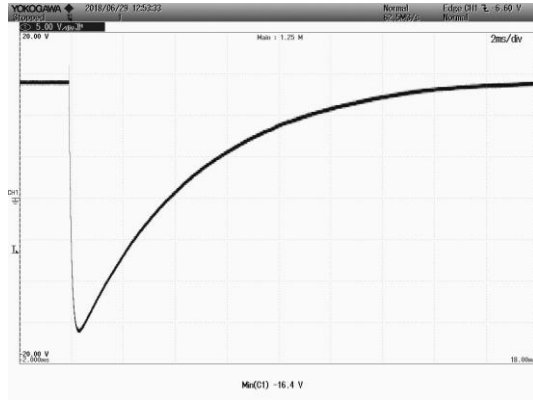


Figure 7-6: S/IMP with + 55 kV DC and - 65,6 kV SI

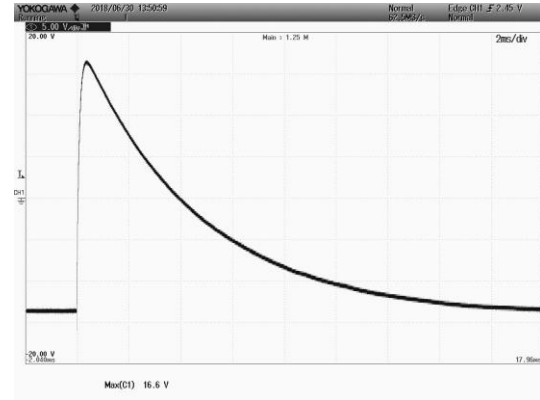


Figure 7-7: S/IMP with - 55 kV DC and + 66,4 kV SI

7.3 RESULTS

The described standard XLPE 12/20 kV AC cable system passed through 30 load cycles each polarity, 20 load cycles with polarity reversal and the final S/IMP voltage test as a 55 kV DC cable. Due to this stress, the cable system changed in a visible way. Especially at the end of the terminations this stress is observable, shown in Figure 7-8.



Figure 7-8: Visible stress at back end of termination

This is the result of different extension coefficients of all participating materials as well as different temperatures (conductor and sheath). Consequently, the conductor was stretched more by the temperature than the sheath. Therefore, the termination was pulled forward. However, this can be considered as normal.

Assuming an already built AC cable system, identical to the cable used in this thesis, with a nominal system voltage of $U_N = 20$ kV (phase to phase). The maximum current rating under AC can be seen in the corresponding datasheets and is here assumed with $I_{AC, \max} = 432$ A as described in chapter 6.4 to reach the maximum conductor temperature $T_{C, \max} = 90$ °C.

The maximum transmittable power under the assumption of pure active power transfer ($\cos(\varphi) = 1$) is $P_{AC, \max} = 14,9$ MW as shown in Equation 12.

$$P_{AC, \max} = 3 \cdot \frac{U_N}{\sqrt{3}} \cdot I_{AC, \max} = 14,9 \text{ MW} \quad (12)$$

$$\text{with } U_N = 20 \text{ kV}, I_{AC, \max} = 432 \text{ A}$$

If a cable system is changed to a DC system as shown in Figure 7-9, two cables can be used as poles (negative and positive) and the third cable is the common line (earth potential), which is called a bipolar MVDC system.

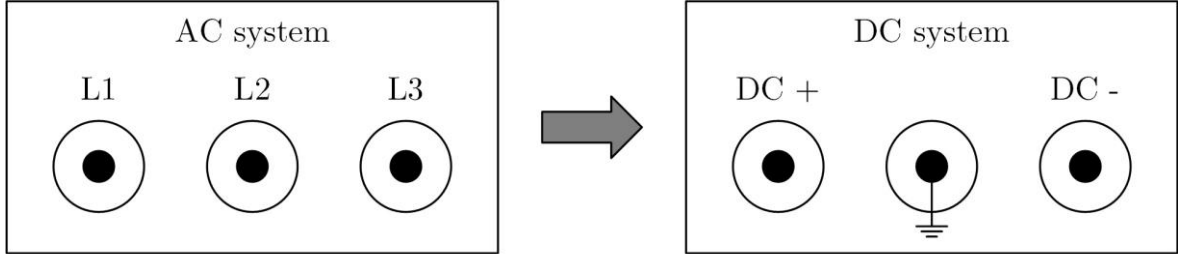


Figure 7-9: Cable system conversion

The nominal voltage of this system is set to $U_{DC} = 55 \text{ kV}$ with regard to the results of this thesis. Furthermore, the maximum current is defined by the maximum conductor temperature

$T_{C, \max} = 90 \text{ }^\circ\text{C}$, which results in a conductor current of $I_{DC, \max} = 500 \text{ A}$ as described in chapter 6.4.

With this configuration the maximum transmittable power is given by Equation 13 and is $P_{DC, \max} = 55 \text{ MW}$.

$$P_{DC, \max} = 2 \cdot U_{DC} \cdot I_{DC, \max} = 55 \text{ MW} \quad (13)$$

with $U_{DC} = 55 \text{ kV}$, $I_{DC, \max} = 500 \text{ A}$

Compared to the transmittable power of an identical AC cable system as shown above, the DC cable system would be capable of transmitting more than 360 % more power.

The main factors for the enormous improvement of the transmittable power are the rise of the nominal voltage and the higher allowed current, which is possible because of the lack of skin effect.

However, the performed tests do not qualify the cable system according to TB 496 to be used as DC cable due to the incompleteness of the long duration voltage test. The whole test sequence can be seen in Table 4-1 respectively Table 4-2, where the high load cycles are also considered as critical.

From the present point of view, a standard 12/20 kV AC XLPE cable can be used as 55 kV DC cable, but further investigations are necessary to prequalify this cable for DC use.

8 OUTLOOK

In the future, the described test setup will be improved further. First of all, an automatic test program will be set up and implemented to enable polarity reversals at night time and on weekends. Furthermore, it is intended to control the heating current by the sheath temperature to encounter environmental changes like air temperature drops. Due to the implementation of controlling the current, different temperatures can be kept constant. For this system, a current measurement device on the primary side of the current transformer, a proper temperature measurement system and a controllable variable transformer in combination with a control hard- respectively software is required.

To enable a PQ test for higher system voltages it is required to use a coupling capacitor capable of the desired voltages. The available DC generator (Figure 6-13) in combination with an appropriate coupling capacitor can be used for PQ tests at DC cables with nominal voltage of $U_0 = 360$ kV if only superimposed voltages with SI are required. If superimposed voltages with LI are required, the nominal voltage of the tested cable is limited to $U_0 = 260$ kV.

The design of the universal voltage divider will be assessed, in order to identify possible improvements regarding the design and the components. Furthermore, a way of how to adjust a universal divider to gain one single scale factor for all voltage forms will be found. After that, it is intended to manufacture three modules at the Institute of High Voltage Engineering and System Performance at Graz University of Technology.

All of the until now not performed parts of the test sequence for LCC (Table 4-1) will be carried out and another S/IMP voltage test will be performed. After this examination and some other tests (e.g. type test), a well-founded statement can be made whether a standard 12/20 kV AC cable system can be used as 55 kV DC cable or not.

9 SUMMARY

To use HVDC cables in the grid, several tests are necessary to verify the qualification and performance of the whole cable system. Tests are also required, if standard XLPE MVAC cables are used with DC. Throughout this thesis, the test environment to perform prequalification tests on HVDC cables according to the Cigré Technical Brochure 496 was established and tested. Therefore, a literature review about the test techniques required for the PQ test was done. Several preliminary tests were performed with a standard XLPE MVAC cable system, including standard cable terminations and joints, such as investigation of thermal behaviour or voltage limit tests to define a DC voltage for a 12/20 kV XLPE AC cable.

- At the end of the prequalification test, a superimposed voltage test is required to verify the integrity of the insulation system. Therefore, a setup according to IEC 60060-1 was established to generate superimposed voltages (DC + SI/LI). Both possibilities for coupling elements, coupling capacitor and spark gap, were investigated.
- To measure the voltage directly at the tested cable system, a prototype of a universal voltage divider (resistive - damped capacitive voltage divider) was designed and built. The calibration of the prototype according to IEC 60060-2 delivered measurement uncertainties for different voltage forms (DC₊: 1,66 %, DC₋: 2,90 %, AC₊: 1,29 %, AC₋: 1,24 %, LI₊: 1,76 %, LI₋: 1,60 %). Through the knowledge acquired during the prototype phase, a final design of a modular universal voltage divider was conceived and designed.
- A cable system, consisting of two 10 meter long standard 12/20 kV XLPE MVAC cables, one with two terminations, the other one with two terminations and a joint, was stressed with the in Cigré TB 496 described load cycle (positive and negative polarity) and load cycles with polarity reversal with a nominal voltage of $U_{DC} = 55$ kV for approximately 1650 hours.
- At the end of the adapted long duration voltage test a test with superimposed voltages was performed and successfully passed. A founded statement, that a standard XLPE MVAC cable can be used as DC cable, is only possible, if all tests described in TB 496 were performed and passed.

10 REFERENCES

- [1] IEA: "Key world energy statistics 2017",
<https://www.iea.org/publications/freepublications/publication/KeyWorld2017.pdf>,
accessed on Oktober 2018
- [2] Oeding, Oswald: "Elektrische Kraftwerke und Netze", Springer-Verlag, 2011
- [3] K uchler: "Hochspannungstechnik: Grundlagen - Technologie - Anwendung", Springer
Verlag, 2017
- [4] H aring et al.: "Development Process of Extruded HVDC Cable Systems", Jicable'15,
Report No. A6.6, 2015
- [5] Chen et al.: "Review of High Voltage Direct Current Cables", CSEE Journal of
Power and Energy Systems, Vol. 1, No. 2, pp. 9-21, June 2015
- [6] Deutsche Bundesregierung:
[https://www.bundesregierung.de/Webs/Breg/DE/Themen/Energiewende/Fragen-
Antworten/8_Kernkraft/_node.html](https://www.bundesregierung.de/Webs/Breg/DE/Themen/Energiewende/Fragen-Antworten/8_Kernkraft/_node.html), accessed on March 2018
- [7] European Commission: https://ec.europa.eu/clima/policies/strategies/2020_en,
accessed on June 2018
- [8] Deutsche Bundesregierung: Bundesbedarfsplangesetz - BBPlG, 2013, accessed on
March 2018
- [9] Amprion: www.amprion.net, accessed on March 2018
- [10] TenneT: www.tennet.eu, accessed on March 2018
- [11] Shekhar et al.: "Grid capacity and efficiency enhancement by operating medium
voltage AC cables as DC links with modular multilevel converters", International
Journal of Electrical Power and Energy Systems 93, pp. 479-493, 2017
- [12] Hampton: "Some of the Considerations for Materials Operating Under High-Voltage,
Direct-Current Stresses", IEEE Electrical Insulation Magazine, Vol. 24, No. 1, 2008
- [13] Mazzanti, Marzinotto.: "Extruded Cables for High-Voltage Direct Current
Transmission", IEEE Press, 2013
- [14] Eyerer et al.: "Polymer Engineering", Springer-Verlag, 2008
- [15] NKT: [https://www.nkt.com/about-us/innovation/640-kv-extruded-hvdc-cable-
systems](https://www.nkt.com/about-us/innovation/640-kv-extruded-hvdc-cable-systems), accessed on April 2018
- [16] Murata et al.: "Development of High Voltage DC-XLPE Cable System", J-Power
Systems Corporation: Sei Technical Review, Number 76, April 2013

- [17] Bergelin et al.: "640 kV extruded HVDC cable system", <https://www.nkt.com/about-us/innovation/640-kv-extruded-hvdc-cable-systems>, NKT, accessed on April 2018, 2017
- [18] Mazzanti: "Life Estimation of HVDC Cables Under the Time-Varying Electrothermal Stress Associated With Load Cycles", *IEEE Transactions on Power Delivery*, Vol. 30, No. 2, pp. 931-939, April 2015
- [19] Fabiani et al.: "Polymeric HVDC Cable Design and Space Charge Accumulation. Part 1: Insulation/Semicon Interface", *IEEE Dielectrics and Electrical Insulation Society*, Vol. 23, No. 6, pp. 11-19, November/December 2007
- [20] Lee et al.: "Development of the HVDC ± 80 kV XLPE Cable System and Construction of Test-bed in KOREA", Cigré Session, Paris, Report No. B1-304, 2012
- [21] Bodega: "Space Charge Accumulation in Polymeric High Voltage DC Cable Systems", PhD Thesis, Delft University of Technology, November 2006
- [22] Raja et al.: "Space Charge Measurement on XLPE Cable for HVDC Transmission using PEA Method", *International Conference on Electrical Engineering and Informatics 2013*
- [23] Saltzer et.al.: "A New Voltage Level for Extruded DC Cables", Cigré Session, Paris, Report No. B1-301, 2016
- [24] Crastan, Westermann: "Elektrische Energieversorgung 3", Springer Verlag, 2018
- [25] Cigré WG B1.32: "TB 496: Recommendations for Testing DC Extruded Cable Systems for Power Transmission at rated Voltages up to 500 kV", Cigré Technical Brochure 496, 2012
- [26] Cigré WG 21.02: "Recommendations for Tests of Power Transmission DC Cables for a rated Voltage up to 800 kV", *Électra* No. 189, pp. 39-55, April 2000
- [27] IEC 60060-1: "High-Voltage Test Techniques - Part 1: General Definitions and Test Requirements", October 2011
- [28] Prasser: "Hochspannungsprüfkreis für überlagerte Spannungen", Bachelor Thesis, Graz University of Technology, Institute of High Voltage Engineering and System Performance, 2016
- [29] Pischler, Schichler: "Challenges Resulting from the Use of Spark Gaps for Superimposed Voltage Tests", ICPADM, Xi'an, Report No. 54, 2018
- [30] Voß, Gamlin: "Superimposed impulse voltage testing on extruded DC-cables according to IEC CVD 62895", ISH, Buenos Aires, Report No. 195, 2017
- [31] Schwab: "Hochspannungsmesstechnik: Messgeräte und Messverfahren", Springer Verlag, 2011

- [32] Schon: "Stoßspannungs- und Stoßstrommesstechnik, Springer Verlag, 2010
- [33] Meisner et al.: "PTB's new standard impulse voltage divider for traceable calibrations up to 1 MV", ISH, Buenos Aires, Report No. 415, 2017
- [34] Passon et al.: "Modular Wideband High-Voltage Divider for Metrological Purposes", ISH, Buenos Aires, Report No. 414, 2017
- [35] Küpfmüller et al.: "Theoretische Elektrotechnik, Eine Einführung", Springer Vieweg, 2013
- [36] IEC 60060-2: "High-Voltage Test Techniques - Part 2: Measuring Systems", October 2011
- [37] Modrusan: "Hochspannungsteiler: Typen, Messeigenschaften und Einsatz", SEV/VSE 74(1983), pp. 1030 - 1037, September 1983
- [38] IEC 60287-1-1: "Current Rating Equations (100% Load Factor) and Calculation of Losses - General", December 2006
- [39] IEC 60287-2-1: "Thermal Resistance - Calculation of Thermal Resistance", May 2006
- [40] Pietsch et al.: "Tests with Superimposed Voltages", HIGHVOLT Kolloquium, 2015
- [41] Felk et al.: "Protection and Measuring Elements in the Test Setup of Superimposed Test Voltage", ISH, Buenos Aires, Report No. 182, 2017
- [42] Agreiter: "Festigkeit elektrischer Isoliersysteme bei Beanspruchung mit zusammengesetzter Spannung (DC+LI)", Bachelor Thesis, Graz University of Technology, Institute of High Voltage Engineering and System Performance, 2016

LIST OF ABBREVIATIONS

AC	<i>alternating current</i>
Cs'	<i>impulse capacity</i>
DC	<i>direct current</i>
DUT	<i>device under test</i>
FEM	<i>finite element method</i>
GRP	<i>glass-reinforced plastic</i>
HL	<i>high load</i>
HVDC	<i>high voltage direct current</i>
IGBT	<i>insulated-gate bipolar transistor</i>
LC	<i>load cycle</i>
LCC	<i>line commutated converter</i>
MV	<i>medium voltage</i>
PEA	<i>pulse electroacoustic method</i>
PPLP	<i>polypropylene laminated paper</i>
PQ	<i>prequalification</i>
PR	<i>polarity reversal</i>
PTB	<i>Physikalisch-Technische Bundesanstalt</i>
R _D '	<i>damping resistor</i>
R _E '	<i>discharging resistor</i>
S/IMP	<i>superimposed impulse</i>
T ₁	<i>time to crest as lightning impulse</i>
T ₂	<i>time to half value</i>
TB	<i>technical brochure</i>
T _C	<i>conductor temperature</i>
T _{C, max}	<i>maximum conductor temperature</i>
T _{CR}	<i>time to crest at switching impulse</i>
T _S	<i>sheath temperature</i>
U ₀	<i>rated DC voltage</i>
U _{TP1}	<i>voltage during LC test</i>
U _{TP2}	<i>voltage during PR test</i>
VSC	<i>voltage source converter</i>
XLPE	<i>cross-linked polyethylene</i>
ZL	<i>zero load</i>

LIST OF FIGURES

Figure 1-1: Transformation of AC system to DC system.....	2
Figure 2-1: Oil-filled HVDC cable [12]	3
Figure 2-2: Typical extruded MVAC cable [15].....	4
Figure 2-3: Schematic drawing of a triple extrusion [14].....	5
Figure 2-4: Electric field density E over the radius r	7
Figure 2-5: Electric field distribution [13] a) homocharge b) heterocharge.....	8
Figure 2-6: Typical signal of PEA space charge measurement without space charges [13] ..	9
Figure 2-7: Typical signal of PEA space charge measurement with space charges [13]	10
Figure 2-8: Block diagram of the pulsed electroacoustic (PEA) method [13]	10
Figure 2-9: Measurement setup for PEA with a cable [21]	10
Figure 2-10: Dynamic space charge distribution over time [21]	11
Figure 2-11: Electric field distribution over time due to space charges [21]	11
Figure 3-1: Line Commutated Converter versus Voltage Source Converter [24]	12
Figure 4-1: Example of a test loop according to TB 496 [25].....	14
Figure 4-2: Superimposed test voltages according to Cigré TB 496 [25]	18
Figure 4-3: Scheme of the test setup	19
Figure 5-1: Different types of high voltage dividers [3].....	20
Figure 5-2: Voltage divider with two impedances.....	21
Figure 5-3: Simplified circuit of a universal voltage divider.....	22
Figure 5-4: Simplified equivalent circuit of capacitive divider with concentrated earth capacity [32].....	23
Figure 5-5: Iterative equivalent circuit element of damped capacitive divider with earth capacity and inductivity [32].....	23
Figure 5-6: Overview and detail pictures of the prototype a) Prototype overview b) Geometry c) Components.....	25
Figure 5-7: Version A of low voltage part	26
Figure 5-8: Measured lightning impulse voltage with low voltage part A	26
Figure 5-9: Low voltage part B: outer view.....	27
Figure 5-10: Low voltage part B: inner view, top.....	27
Figure 5-11: Low voltage part B: inner view, front.....	27
Figure 5-12: Measured lightning impulse voltage with low voltage part B.....	29
Figure 5-13: Measured lightning impulse voltage (impulse from HILO).....	29
Figure 5-14: Step response of high voltage divider.....	29

Figure 5-15: Calibration setup DC 32

Figure 5-16: Calibration setup AC 32

Figure 5-17: Calibration setup LI..... 32

Figure 5-18: Relative change of scale factor over the voltage, DC 34

Figure 5-19: Relative change of scale factor over the voltage, AC 34

Figure 5-20: Relative change of scale factor over the voltage, LI..... 34

Figure 5-21: Magnetic flux situation by using double helix design..... 36

Figure 5-22: FEM simulation, outer coil under current 37

Figure 5-23: FEM simulation, inner coil under current 37

Figure 5-24: FEM simulation, both coils under current..... 37

Figure 5-25: Universal divider design 39

Figure 5-26: Sectional view of bottom of the universal divider 40

Figure 6-1: Cross-section of used cable..... 41

Figure 6-2: Electrical field distribution at end of a cable, uncontrolled [3]..... 42

Figure 6-3: Electrical field distribution at end of a cable with geometrical field control [3]
..... 42

Figure 6-4: Installed double standard 12/20 kV AC cable termination..... 43

Figure 6-5: Installed standard 12/20 kV AC cable joint..... 43

Figure 6-6: PQ test setup..... 45

Figure 6-7: Current circuit with safety circuit 46

Figure 6-8: Temperature development over the time, $I = 500$ A 46

Figure 6-9: Position of the thermal elements in the cable..... 47

Figure 6-10: Water resistor, conical shaped plug 49

Figure 6-11: Schematic drawing of impulse generator, electric elements as shown with
housing 50

Figure 6-12: Problem when using spark gap as coupling element (bottom: zoomed)..... 51

Figure 6-13: Overview of complete test setup..... 52

Figure 6-14: Schematic drawing of impulse generator, electric elements as shown with
housing, modified configuration..... 53

Figure 7-1: Temperature development over the time, $I = 425$ A 54

Figure 7-2: Temperature development over time during short Load Cycle (LC) 55

Figure 7-3: Voltage and current over time for load cycle with positive polarity (LC+) 56

Figure 7-4: Voltage and current over time for load cycle with negative polarity (LC-)..... 56

Figure 7-5: Voltage and current over time for load cycle with polarity reversal (LC + PR)
..... 57

Figure 7-6: S/IMP with + 55 kV DC and - 65,6 kV SI..... 58
Figure 7-7: S/IMP with - 55 kV DC and + 66,4 kV SI..... 58
Figure 7-8: Visible stress at back end of termination..... 59
Figure 7-9: Cable system conversion 60

LIST OF TABLES

Table 3-1: Basic information: LCC and VSC [24].....	13
Table 4-1: PQ test sequence for LCC [25]	15
Table 4-2: PQ test sequence for VSC [25]	15
Table 5-1: Specifications of universal high voltage divider.....	22
Table 5-2: Selected components for the universal voltage divider prototype.....	24
Table 5-3: Scale factors and measurement uncertainties of prototype voltage divider	32
Table 5-4: Scale factors and uncertainties for DC ₊	33
Table 5-5: Scale factors and uncertainties for DC ₋	33
Table 5-6: Scale factors and uncertainties for AC _{Peak,+}	33
Table 5-7: Scale factors and uncertainties for AC _{Peak,-}	33
Table 5-8: Scale factors and uncertainties for LI _{Peak,+}	33
Table 5-9: Scale factors and uncertainties for LI _{Peak,-}	33
Table 6-1: Preliminary tests.....	44
Table 6-2: Parameters for current calculation according to IEC 60287.....	48
Table 6-3: Calculated rated currents for different conductor temperatures T _C	48

Appendix A DATASHEETS

Appendix A.1 RESISTORS

Mini-Mox

Precision Thick Film Axial Terminal
High Voltage/High Resistance



FEATURES

- Wide resistance ranges
- Silicone or epoxy coating
- Metal oxide resistive element

APPLICATIONS

- Avionics
- Medical electronics
- High gain feedback applications
- Current pulse limiters
- Vacuum and space application

The Mini-Mox resistor is very versatile, covering a wide resistance range as well as a wide range of operating voltages. Provided with tolerances down to 0.5%, the Mini-Mox resistor works well in precision circuits.

SERIES SPECIFICATIONS

Ohmite Series	Resistance Range (Ohms)	Power	Voltage Rating	Available Tolerances*	Capacitance (pf)
• High-temperature (silicone coated)		@70°C			
MOX-400-22	500Ω to 300,000M	0.35W	2,500V	1% to 20%	1.00
MOX-750-22	750Ω to 600,000M	0.70W	5,000V	1% to 20%	0.75
MOX1125-22	1K to 1,000,000M	1.40W	7,500V	1% to 20%	0.25
• Standard (epoxy coated)		@25°C			
MOX-400-23	500Ω to 300,000M	0.75W	2,500V	0.5% to 20%	1.00
MOX-750-23	1K to 600,000M	1.00W	5,000V	0.5% to 20%	0.75
MOX1125-23	1K to 1,000,000M	1.50W	7,500V	0.5% to 20%	0.25

*Some tolerances are not available over the entire resistance range.

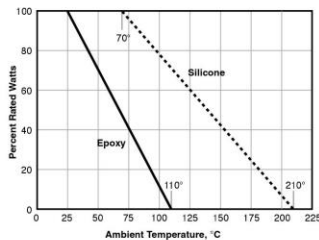
CHARACTERISTICS

Resistor	Metal Oxide
Coating	Silicone or Epoxy
Core	Alumina
Terminals	Solder-coated axial. RoHS solder composition is 96% Sn, 3.5% Ag, 0.5% Cu
Resistance Range	500Ω to 1 Teraohm
Power Rating	0.35W to 1.5W
Voltage Rating	2500V to 7.5KV
Tolerance	0.5% to 20%; not all tolerances available in all values
Operating Temperature	-55°C to +220°C
Temp. Coefficient	25ppm/°C 0° to 85°C available

Performance Data

Characteristic	Test Method	Specification
Humidity	MIL-STD-202, Method 103B, Condition B	±0.25%
Dielectric Withstanding Voltage	MIL-STD-202, Method 301, 750V	±0.25%
Insulation Resistance	MIL-STD-202, Method 302, Condition A or B	>10,000M or greater dry
Thermal Shock	MIL-STD-202, Method 107G, Condition B, B-1, or F	±0.20%
Load Life	MIL-STD-202, Method 108A, Condition D	±2.0%
Resistance to Solvents	MIL-STD-202, Method 215G	Acceptable for the Standard Series Only
Terminal Strength	MIL-STD-202, Method 211A, Condition A or B	±0.25%
Shock (Specified Pulse)	MIL-STD-202, Method 213B, Condition I	±0.25%
Vibration, High Frequency	MIL-STD-202, Method 204D, Condition D	±0.20%
Power Conditioning	MIL-R-49462A, Par 4.8	±0.50%
Solderability	MIL-STD-202, Method 208F	>95% Coverage

Derating



(continued)



Mini-Mox

Precision Thick Film Axial Terminal High Voltage/High Resistance

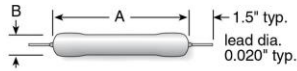
STANDARD TEMP./VOLTAGE COEFFICIENTS OF RESISTANCE

Resistor Series	Temp. Coeff. of Resistance		Voltage Coeff. of Resistance**		
	25 PPM/°C	50 PPM/°C	100 PPM/°C	< 2PPM/Volt	< 5PPM/Volt
MOX-400	1K-99M	100M-450M	451M-30,000M	1K-1,000M	1,001M-100,000M
MOX-750	1K-199M	200M-900M	901M-70,000M	1K-2,000M	2,001M-100,000M
MOX1125	1K-299M	300M-1,350M	1,351M-100,000M	1K-3,000M	3,001M-100,000M

*TCR of 25ppm for temperature range of 0°C-85°C. TCR of 50ppm and 100ppm for -55°C to 125°C. Consult factory for TCR values operating higher than 125°C
 **For tighter VCs please contact Ohmite.

DIMENSIONS

(in./mm)



Series	Power	A max.	B max.
• High-temperature (silicone coated)			
@70°C			
MOX-400-22	0.35W	0.510" / 12.95	0.140" / 3.56
MOX-750-22	0.70W	0.820" / 20.83	0.140" / 3.56
MOX1125-22	1.40W	1.210" / 30.73	0.140" / 3.56
• Standard (epoxy coated)			
@25°C			
MOX-400-23	0.75W	0.580" / 14.78	0.165" / 4.19
MOX-750-23	1.00W	0.880" / 22.35	0.165" / 4.19
MOX1125-23	1.50W	1.270" / 32.26	0.165" / 4.19

HOW TO ORDER

MOX 1125 23 1006 F E

Style 200, 300, 400, 750, 1125	Coating 2 = Black silicone 3 = Epoxy 6 = No coating	E = RoHS Compliant
Mini Mox Series	Terminal 0 = MOX-200 or 300; MOX-200 Z or 300 Z = 50ppm 2 = 0.020" 7 = 0.032"	Ohms First 3 digits are significant, 4th digit is multiplier (# of zeroes to follow). Examples: 10R2 = 10.2 ohms 1000 = 100 ohms 1503 = 150,000 ohms
		Tolerance D = 0.5% F = 1% G = 2% J = 5% K = 10% M = 15% P = 20%

Not all tolerances available in all values.

Appendix A.2 CAPACITORS

Type 940C, Polypropylene Capacitors, for Pulse, Snubber High dV/dt for Snubber Applications



Type 940 round, axial leaded film capacitors have polypropylene film and dual metallized electrodes for both self healing properties and high peak current carrying capability (dV/dt). This series features low ESR characteristics, excellent high frequency and high voltage capabilities.

Highlights

- High dV/dt
- High pulse current
- Low inductance
- Self healing

Specifications

Capacitance Range	0.01 to 4.7 μ F
Capacitance Tolerance	$\pm 10\%$ (K) Standard; $\pm 5\%$ (J) Optional
Rated Voltage	600 to 3000 Vdc (275 to 500 Vac, 60 Hz)
Operating Temperature Range	-55 $^{\circ}$ C to 105 $^{\circ}$ C* *Full rated voltage at 85 $^{\circ}$ C - derated linearly to 50% rated at 105 $^{\circ}$ C
Maximum rms Current	Check tables for values
Insulation Resistance	> 100,000 M Ω x μ F
Test Voltage between Terminals @ 25 $^{\circ}$ C	160% rated DC voltage for 60 s
Test Voltage between Terminals & Case @ 25 $^{\circ}$ C	3 kVac @ 50/60 Hz for 60 s
Life Test	2,000 h @ 85 $^{\circ}$ C, 125% rated DC voltage
Life Expectancy	60,000 h @ rated Vdc, 70 $^{\circ}$ C 30,000 h @ rated Vac, 70 $^{\circ}$ C
RoHS Compliant	

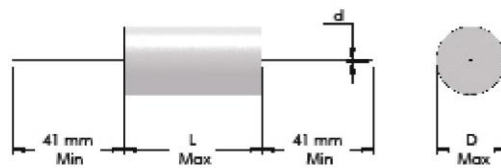
Dimensions

Construction Diagram



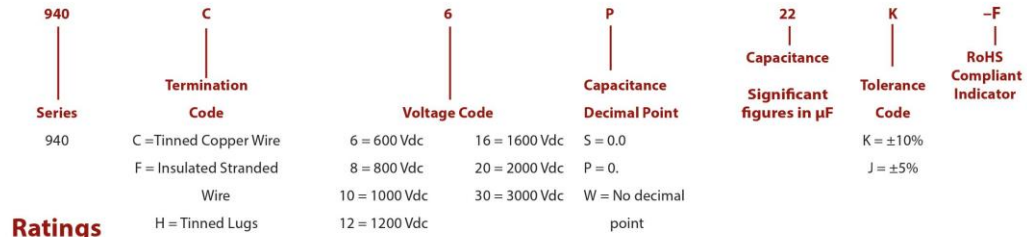
Construction Details

Case Material	UL510 Polyester Tape Wrap
Resin Material	UL94V-0 Epoxy Fill
Terminal Material	Tin Plated Copper



Type 940C, Polypropylene Capacitors, for Pulse, Snubber High dV/dt for Snubber Applications

Part Numbering System



Ratings

NOTE: Other ratings, sizes and performance specifications are available. Contact us.

Cap. (μF)	Catalog Part Number	D mm	L mm	d mm	Typical ESR (m Ω)	Typical ESL (nH)	dV/dt V/ μs	I peak (A)	I _{RMS} 100 kHz 70 °C (A)
600 Vdc (275 Vac)									
.10	940C6P1K-F	9.0	34.0	0.8	28	19	196	20	2.5
.15	940C6P15K-F	10.5	34.0	0.8	13	20	196	29	4.0
.22	940C6P22K-F	11.5	34.0	0.8	12	20	196	43	4.4
.33	940C6P33K-F	13.5	34.0	0.8	9	21	196	65	5.6
.47	940C6P47K-F	15.5	34.0	1.0	7	22	196	92	6.9
.68	940C6P68K-F	18.0	34.0	1.0	6	23	196	134	8.1
1.00	940C6W1K-F	21.0	34.0	1.0	6	24	196	196	8.9
1.50	940C6W1P5K-F	25.0	34.0	1.2	5	26	196	295	10.9
2.00	940C6W2K-F	23.5	46.0	1.2	5	31	128	255	11.8
3.30	940C6W3P3K-F	27.0	54.0	1.2	4	36	105	346	15.3
4.70	940C6W4P7K-F	31.5	54.0	1.2	4	38	105	492	16.8
850 Vdc (450 Vac)									
.15	940C8P15K-F	13.0	34.0	0.8	8	21	713	107	5.8
.22	940C8P22K-F	15.5	34.0	1.0	8	22	713	157	6.4
.33	940C8P33K-F	18.0	34.0	1.0	7	23	713	235	7.5
.47	940C8P47K-F	21.0	34.0	1.0	5	24	713	335	9.8
.68	940C8P68K-F	24.5	34.0	1.2	4	26	713	485	12.0
1.00	940C8W1K-F	22.5	46.0	1.2	5	30	400	400	11.5
1.50	940C8W1P5K-F	27.0	46.0	1.2	4	32	400	600	14.3
2.00	940C8W2K-F	30.5	46.0	1.2	3	34	400	800	17.9
2.20	940C8W2P2K-F	32.0	46.0	1.2	3	34	400	880	18.4
2.50	940C8W2P5K-F	34.0	46.0	1.2	3	35	400	1000	19.1
1000 Vdc (500 Vac)									
.15	940C10P15K-F	15.0	34.0	1.0	7	22	856	128	6.7
.22	940C10P22K-F	17.5	34.0	1.0	7	23	856	188	7.4
.33	940C10P33K-F	20.5	34.0	1.0	6	24	856	283	8.8
.47	940C10P47K-F	24.0	34.0	1.2	5	26	856	402	10.6
.68	940C10P68K-F	28.0	34.0	1.2	5	27	856	582	11.7
1.00	940C10W1K-F	26.0	46.0	1.2	5	32	480	480	12.5
1.50	940C10W1P5K-F	31.0	46.0	1.2	4	34	480	720	15.6
2.00	940C10W2K-F	35.5	46.0	1.2	3	36	480	960	19.6

CDE Cornell Dubilier • 1605 E. Rodney French Blvd. • New Bedford, MA 02744 • Phone: (508)996-8561 • Fax: (508)996-3830

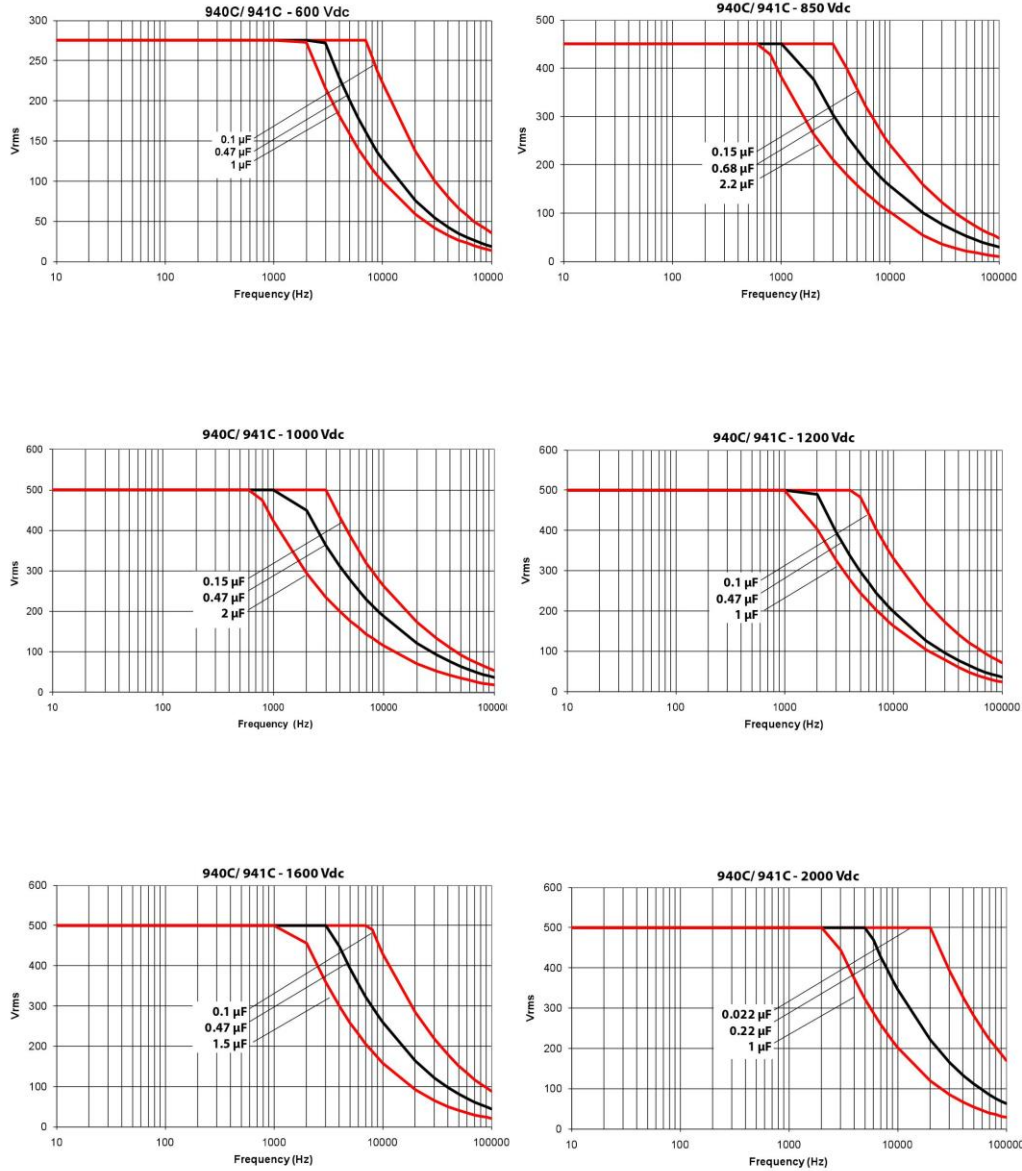
Type 940C, Polypropylene Capacitors, for Pulse, Snubber
High dV/dt for Snubber Applications

Cap. (μ F)	Catalog Part Number	D mm	L mm	d mm	Typical ESR (m Ω)	Typical ESL (nH)	dV/dt V/ μ s	I peak (A)	I _{RMS} 70 °C 100 kHz (A)
1200 Vdc (500 Vac)									
.10	940C12P1K-F	15.5	34.0	1.0	9	22	1142	114	6.1
.15	940C12P15K-F	18.5	34.0	1.0	7	23	1142	171	7.6
.22	940C12P22K-F	21.5	34.0	1.0	7	24	1142	251	8.4
.33	940C12P33K-F	20.0	46.0	1.0	7	29	640	211	9.0
.47	940C12P47K-F	23.0	46.0	1.2	7	30	640	301	9.8
.68	940C12P68K-F	27.0	46.0	1.2	6	32	640	435	11.7
1.00	940C12W1K-F	33.0	46.0	1.2	5	35	640	640	14.5
1.50	940C12W1P5K-F	35.0	54.0	1.2	4	39	502	754	17.9
1600 Vdc (500 Vac)									
.10	940C16P1K-F	18.0	34.0	1.0	7	23	1427	143	7.5
.15	940C16P15K-F	21.5	34.0	1.0	5	24	1427	214	9.9
.22	940C16P22K-F	25.5	34.0	1.2	7	26	1427	314	9.3
.33	940C16P33K-F	23.5	46.0	1.2	7	31	800	264	10.0
.47	940C16P47K-F	27.5	46.0	1.2	6	32	800	376	11.8
.68	940C16P68K-F	32.5	46.0	1.2	6	35	800	544	13.1
1.00	940C16W1K-F	39.0	46.0	1.2	5	37	800	800	16.2
1.50	940C16W1P5K-F	42.0	54.0	1.2	4	42	628	942	20.1
2000 Vdc (500 Vac)									
.022	940C20S22K-F	11.5	34.0	0.8	35	6	1712	38	2.6
.033	940C20S33K-F	13.5	34.0	0.8	20	21	1712	57	3.8
.047	940C20S47K-F	15.0	34.0	1.0	12	22	1712	80	5.2
.068	940C20S68K-F	17.5	34.0	1.0	8	23	1712	116	6.9
.100	940C20P1K-F	21.0	34.0	1.0	7	24	1712	171	8.3
.150	940C20P15K-F	19.5	46.0	1.0	7	29	960	144	8.9
.220	940C20P22K-F	22.0	46.0	1.0	8	30	960	211	9.0
.330	940C20P33K-F	27.0	46.0	1.2	8	32	960	317	10.1
.470	940C20P47K-F	32.0	46.0	1.2	6	34	960	451	13.0
.560	940C20P56K-F	31.0	54.0	1.2	7	37	754	422	12.6
.680	940C20P68K-F	34.0	54.0	1.2	6	39	754	513	14.3
1.00	940C20W1K-F	41.0	54.0	1.2	5	42	754	754	17.7
3000 Vdc (500 Vac)									
.010	940C30S1K-F	11.5	34.0	0.8	60	20	2568	26	2.0
.015	940C30S15K-F	13.5	34.0	0.8	40	21	2568	39	2.7
.022	940C30S22K-F	15.5	34.0	1.0	25	22	2568	57	3.6
.033	940C30S33K-F	18.0	34.0	1.0	14	23	2568	85	5.3
.047	940C30S47K-F	16.5	46.0	1.0	14	28	1440	68	5.7
.068	940C30S68K-F	19.0	46.0	1.0	12	29	1440	98	6.7
.100	940C30P1K-F	22.5	46.0	1.2	10	30	1440	144	8.1
.150	940C30P15K-F	27.0	46.0	1.2	8	32	1440	216	10.1

CDE Cornell Dubilier • 1605 E. Rodney French Blvd. • New Bedford, MA 02744 • Phone: (508)996-8561 • Fax: (508)996-3830

Type 940C, Polypropylene Capacitors, for Pulse, Snubber High dV/dt for Snubber Applications

RMS Voltage vs Frequency @ 25 °C

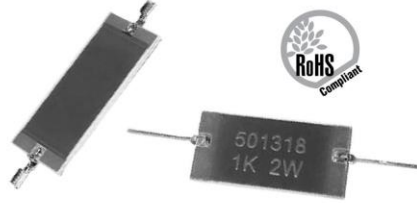


CDE Cornell Dubilier • 1605 E. Rodney French Blvd. • New Bedford, MA 02744 • Phone: (508)996-8561 • Fax: (508)996-3830

Appendix A.3 DAMPING RESISTORS

TFS Series

**Surge Capable
Thick Film Non Inductive**



FEATURES

- Appropriate for medical surge protection applications
- Ideal to replace standard carbon composition resistors
- Custom dimensions, values, tolerances and characteristics available

The TFS Series has been specifically developed to absorb large amounts of energy by efficient use of its compact mass. Ideal for medical surge protection applications, these thick film resistors offer non-inductive performance in an axial package.

Uses include power supply conversion, electron microscopes, X-ray systems, high-resolution CRT displays, and geophysical instrument related products.

SERIES SPECIFICATIONS

Type	U (KV)	Energy* (J)	Power (W)
TFSA	3	6	0.5
TFSB	3.5	9	0.5
TFSC	4	11	0.75
TFSD	7	33	1
TFSE	7	44	1.5
TFSF	11	55	2

*Published energy rating is for 10ms pulse. For shorter pulses energy rating has to be derated according to Max. Individual Pulse Rating chart and Single Pulse Energy Rating considerations.

CHARACTERISTICS

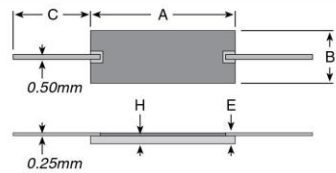
Resistive Element	Thick Film
Encapsulation	Screen Printed Glass
Resistance Value	100Ω up to 100KΩ
Temperature Coefficient	100ppm/°C
Tolerance	1%, 2%, 5%, 10%
Operating Temperature	-55°C to +200°C
Test	VDE 0750 (Pulse Duration 10 msec)

Notes

- Momentary overload capability is 5 times rated power for 1 second or 2 times rated power for 5 seconds. Always verify designs with pulse and surge conditions through thorough testing of the design at maximum operating temperature and maximum pulse loading (or some margin above maximum pulse loading).
- Damage to the resistor by excessive pulse loading is generally indicated by an increasing resistance of the resistor.
- Energy ratings are based on single pulses (at least 1 minute between pulses).
- For multiple pulse applications the energy pulse rating should be reduced and the average power should not exceed the nominal power rating of the selected model.
- See Single Pulse Energy section for more information

DIMENSIONS

mm



Type	Watts	A	B	C	H	E
TFSA	0.5	9	5.5	10	0.7	1.1
TFSB	0.5	11	5.5	10	0.7	1.1
TFSC	0.75	13	5.5	10	0.7	1.1
TFSD	1	21	8	10	0.9	1.3
TFSE	1.5	21	10.5	10	0.9	1.3
TFSF	2	26	10.5	10	0.9	1.3

(continued)

TFS Series

Surge Capable Thick Film Non Inductive

SINGLE PULSE ENERGY RATING

Although Ohmite's TFS Series resistors have been specially designed and developed to absorb much more energy than standard resistors, pulses and transients require special consideration since they cause an instantaneous temperature rise in the resistor film. This application note can guide you through these considerations.

For applications with transients, pulses or surges the following must be considered:

1. Do not exceed the normal rated operating voltage of the device.
2. Using the figure at right, estimate the energy (E_a) and the pulse duration (t_a) for a single pulse in your application.
3. Calculate the energy ratio in percent (E_r) between the nominal energy rating of the model you have chosen (see table) and the single pulse energy in your application (E_a from step 2) using the formula:

$$E_r = \frac{E_a}{E_{\text{nominal}}} \times 100$$

4. Refer to the Pulse Chart. On this chart find the point where the energy ratio (E_r), found at step 3, and time (t_a) coincide. Qualify that this point falls below the maximum pulse energy curve. If the point is above the curve a bigger model should be chosen.



$$E = \frac{V^2 t}{R}$$



$$E = \frac{1}{2} CV^2$$

$$t = RC$$



$$E = \frac{V^2 t}{3R}$$



$$E = \frac{V^2 t}{3R}$$

E = Energy (joules)
 t = Time (seconds)
 V = Voltage (volts)
 R = Resistance (ohms)
 C = Capacitance (farads)

Example

A $1\mu\text{F}$ capacitor is charged to 3.5kV and model TFSC, 1KOhm has been selected. Model TFSC is rated for 4kV, so the peak voltage of 3.5kV is acceptable.

$$E_a = \frac{1}{2} CV^2 = 6.1\text{J}$$

$$t_a = RC = 1\text{ms}$$

$$E_r = \frac{6.1\text{J}}{11\text{J}} \times 100 = 55\%$$

According to the pulse chart, an energy ratio of 55% for a pulse

width of 1ms falls well above the energy curve. The limit is actually located around 25-30%. Model TFSC cannot be used for this application.

A bigger model should be chosen, for example TFSD. Model TFSD, 1KOhm, can be used for this application because we have an energy ratio E_r of 18%, which is below the energy curve.

$$E_r = \frac{6.1\text{J}}{33\text{J}} \times 100 = 18\%$$

Maximum Individual Pulse Rating



ORDERING INFORMATION

RoHS Compliant

TFSA 100KJE

Series	Energy Rating (joules)	Ohm Value	Tolerance
A = 6	D = 33	Example: 100Ω	F = 1%
B = 9	E = 44	2k40 = 2400Ω	G = 2%
C = 11	F = 55		J = 5%
			K = 10%

Standard Part Numbers for TFS Series

Ohms	Tol.	6 Joules 0.5 Watts	9 Joules 0.5 Watts	11 Joules 0.75 Watts	33 Joules 1 Watts	44 Joules 1.5 Watts	55 Joules 2 Watts
100	1%	TFSA100RFE					
100	5%		TFSB100RJE		TFSD100RJE		TFSF100RJE
220	1%	TFSA220RFE					
270	5%	TFSA270RFE		TFSC270RJE	TFSD270RJE		TFSF270RJE
470	1%	TFSA470RFE					
470	5%	TFSA680RJE	TFSB470RJE			TFSE470RJE	
680	5%		TFSB750RJE	TFSC680RJE		TFSE680RJE	TFSF680RJE
750	5%				TFSD750RJE		TFSF750RJE
1,000	1%	TFSA1K00FE					
1,000	5%	TFSA1K00JE	TFSB1K00JE	TFSC1K00JE	TFSD1K00JE	TFSE1K00JE	TFSF1K00JE
1,500	5%	TFSA1K50JE		TFSC1K50JE	TFSD1K50JE		TFSF1K50JE
2,200	1%	TFSA2K20FE					
2,700	5%		TFSB2K70JE			TFSE2K70JE	
4,700	1%	TFSA4K70FE					
4,700	5%	TFSA4K70JE		TFSC4K70JE	TFSD4K70JE		
4,990	1%	TFSA4K99FE					
5,000	5%	TFSA75K0JE					
6,800	5%		TFSB6K80JE			TFSE6K80JE	
10,000	1%	TFSA10K0FE					
10,000	5%	TFSA10K0JE	TFSB10K0JE	TFSC10K0JE	TFSD10K0JE		TFSF10K0JE
16,000	5%						
20,000	1%	TFSA20K0FE					
20,000	5%		TFSB20K0JE		TFSD20K0JE		TFSF20K0JE
22,000	1%	TFSA22K0FE					
27,000	5%	TFSA27K0JE		TFSC27K0JE		TFSE27K0JE	
47,000	1%	TFSA47K0FE					
50,000	5%	TFSA50K0JE					
51,000	5%		TFSB51K0JE	TFSC51K0JE	TFSD51K0JE		TFSF51K0JE
75,000	5%					TFSE75K0JE	
100,000	1%	TFSA100KFE					
100,000	5%		TFSB100KJE	TFSC100KJE	TFSD100KJE		TFSF100KJE

Appendix B MEASUREMENTS

Appendix B.1 PROTOTYPE CALIBRATION DC₊

voltage observation	20 kV			40 kV			60 kV			80 kV			100 kV		
	U _{ref}	U _{div}	F _g	U _{ref}	U _{div}	F _g	U _{ref}	U _{div}	F _g	U _{ref}	U _{div}	F _g	U _{ref}	U _{div}	F _g
-	kV	V	-	kV	V	-	kV	V	-	kV	V	-	kV	V	-
1	20,05	5,00322	4007,42	39,63	9,87269	4014,10	59,43	14,7646	4025,17	79,41	19,6806	4034,94	99,93	24,8359	4023,61
2	19,98	4,99936	3996,51	39,67	9,89462	4009,25	59,65	14,8346	4021,00	78,29	19,4828	4018,42	99,92	24,8259	4024,83
3	20,08	5,00866	4009,06	39,83	9,96531	3996,87	59,63	14,8449	4016,87	79,10	19,6307	4029,40	100,9	25,0968	4020,43
4	20,02	5,00339	4001,29	39,61	9,90296	3999,81	59,40	14,7700	4021,67	79,40	19,7157	4027,25	99,85	24,8102	4024,55
5	20,00	5,00949	3992,42	39,63	9,91050	3998,79	59,74	14,8609	4019,94	79,35	19,6955	4028,84	100,4	24,9816	4018,96
6	19,97	4,99563	3997,49	39,96	9,97317	4006,75	59,36	14,7777	4016,86	79,17	19,6749	4023,91	99,67	24,7596	4025,51
7	19,96	4,98745	4002,05	39,97	10,01020	3992,93	59,37	14,7876	4014,85	78,62	19,5204	4027,58	100,9	25,0966	4020,46
8	20,00	4,99976	4000,19	40,05	10,01400	3999,40	60,15	14,9790	4015,62	78,87	19,5767	4028,77	100,2	24,8907	4025,60
9	19,89	4,97742	3996,05	39,50	9,85681	4007,38	59,93	14,9276	4014,71	78,73	19,5308	4031,07	100,1	24,8403	4029,74
10	20,02	5,00739	3998,09	40,00	9,98696	4005,22	59,84	14,8944	4017,62	79,58	19,7533	4028,69	100,2	24,9294	4019,35
	mean:	4000,06		mean:	4003,05		mean:	4018,43		mean:	4027,89		mean:	4023,31	

voltage observation	120 kV			140 kV			160 kV			180 kV			200 kV		
	U _{ref}	U _{div}	F _g	U _{ref}	U _{div}	F _g	U _{ref}	U _{div}	F _g	U _{ref}	U _{div}	F _g	U _{ref}	U _{div}	F _g
-	kV	V	-	kV	V	-	kV	V	-	kV	V	-	kV	V	-
1	122,0	30,2209	4036,94	140,5	34,7452	4043,72	160,3	39,5389	4054,24	180,1	44,1252	4081,57	199,5	49,1090	4062,39
2	120,9	29,9604	4035,33	140,7	34,7906	4044,20	159,6	39,4331	4047,36	179,1	43,8650	4082,98	201,1	49,5099	4061,81
3	121,5	30,0918	4037,64	139,8	34,5284	4048,84	159,0	39,2746	4048,42	179,9	44,3641	4055,08	199,0	48,9653	4064,10
4	121,4	30,0318	4042,38	141,0	34,8330	4047,89	160,9	39,7185	4051,01	181,9	44,8728	4053,68	199,9	49,1824	4064,46
5	119,7	29,6473	4037,47	141,0	34,8497	4045,95	159,0	39,2521	4050,74	180,5	44,5113	4055,15	198,1	48,7398	4064,44
6	119,7	29,6213	4041,01	139,6	34,4933	4047,16	160,2	39,5320	4052,41	179,7	44,2824	4058,05	198,6	48,8945	4061,81
7	119,4	29,5437	4041,47	140,3	34,6627	4047,58	160,8	39,6725	4053,19	181,7	44,8176	4054,21	196,9	48,4033	4067,90
8	120,2	29,7213	4044,24	141,5	35,0031	4042,50	161,0	39,7736	4047,91	180,8	44,5984	4053,96	198,5	48,7926	4068,24
9	120,0	29,6812	4042,96	140,7	34,8098	4041,97	160,2	39,5689	4048,63	180,2	44,4269	4056,10	199,6	49,1169	4063,77
10	120,4	29,7849	4042,32	140,2	34,5971	4052,36	159,4	39,3733	4048,43	181,3	44,7369	4052,58	197,8	48,6195	4068,33
	mean:	4040,18		mean:	4046,22		mean:	4050,23		mean:	4060,34		mean:	4064,73	

Appendix B.2 PROTOTYPE CALIBRATION DC.

voltage observation	20 kV			40 kV			60 kV			80 kV			100 kV		
	U _{ref}	U _{div}	F _g	U _{ref}	U _{div}	F _g	U _{ref}	U _{div}	F _g	U _{ref}	U _{div}	F _g	U _{ref}	U _{div}	F _g
-	kV	V	-	kV	V	-	kV	V	-	kV	V	-	kV	V	-
1	19,67	4,95010	3973,66	40,09	10,0631	3983,86	60,82	15,2104	3998,58	80,38	19,9675	4025,54	99,36	24,6575	4029,61
2	19,60	4,92462	3980,00	40,15	10,0555	3992,84	60,83	15,2272	3994,83	80,52	20,0337	4019,23	99,86	24,7995	4026,69
3	19,77	4,96065	3985,36	39,97	10,0651	3971,15	60,47	15,0987	4004,98	80,87	20,1228	4018,82	99,36	24,6926	4023,88
4	19,65	4,93563	3981,25	40,12	10,0838	3978,66	60,52	15,1439	3996,33	80,53	20,0280	4020,87	100,0	24,8679	4021,25
5	19,69	4,93388	3990,77	40,15	10,0820	3982,34	60,23	15,0479	4002,55	80,72	20,0637	4023,19	99,50	24,7298	4023,49
6	19,72	4,94584	3987,19	40,23	10,0782	3991,78	60,44	15,0811	4007,67	80,55	20,0355	4020,36	99,34	24,7121	4019,89
7	19,63	4,94803	3967,24	40,07	10,0803	3975,08	60,73	15,1685	4003,69	80,70	20,0594	4023,05	99,71	24,7514	4028,46
8	19,80	4,97077	3983,29	40,05	10,0565	3982,50	60,43	15,0838	4006,28	80,52	20,0143	4023,12	100,0	24,8043	4031,56
9	19,65	4,94063	3977,23	40,09	10,0557	3986,79	60,21	15,0416	4002,90	80,78	20,0849	4021,93	99,43	24,7019	4025,20
10	19,66	4,94666	3974,40	39,98	10,0409	3981,71	60,68	15,1572	4003,38	81,05	20,1677	4018,80	100,0	24,8409	4025,62
	mean: 3980,04			mean: 3982,67			mean: 4002,12			mean: 4021,49			mean: 4025,56		

voltage observation	120 kV			140 kV			160 kV			180 kV			200 kV		
	U _{ref}	U _{div}	F _g	U _{ref}	U _{div}	F _g	U _{ref}	U _{div}	F _g	U _{ref}	U _{div}	F _g	U _{ref}	U _{div}	F _g
-	kV	V	-	kV	V	-	kV	V	-	kV	V	-	kV	V	-
1	120,8	29,9804	4029,30	140,0	34,5338	4054,00	160,9	39,3190	4092,17	178,9	43,4631	4116,14	199,7	48,3561	4129,78
2	121,0	30,0207	4030,55	140,7	34,6824	4056,81	160,4	39,2919	4082,27	180,0	43,6367	4124,97	200,3	48,5272	4127,58
3	120,7	29,9221	4033,81	139,2	34,3071	4057,47	160,5	39,2390	4090,32	180,1	43,6276	4128,12	201,4	48,7891	4127,97
4	120,9	29,9693	4034,13	140,1	34,5665	4053,06	159,3	38,9779	4086,93	179,7	43,4907	4131,92	200,0	48,4585	4127,24
5	120,3	29,8138	4035,04	140,0	34,5204	4055,57	159,8	39,0075	4096,65	179,9	43,5541	4130,50	199,3	48,2301	4132,27
6	120,7	29,9090	4035,57	140,7	34,5827	4068,51	158,7	38,8346	4086,56	179,9	43,5391	4131,92	199,7	48,3489	4130,39
7	120,7	29,9148	4034,79	139,5	34,2750	4070,02	158,8	38,8217	4090,50	179,9	43,5467	4131,20	199,5	48,3005	4130,39
8	120,2	29,8174	4031,20	140,0	34,3770	4072,49	158,4	38,7056	4092,43	180,5	43,6763	4132,68	199,2	48,2212	4130,96
9	121,4	30,0747	4036,62	140,0	34,3868	4071,33	158,2	38,6477	4093,39	179,5	43,4193	4134,11	200,1	48,4225	4132,38
10	121,7	30,1604	4035,09	140,2	34,4710	4067,19	158,8	38,7913	4093,70	180,0	43,5658	4131,68	200,2	48,4581	4131,40
	mean: 4033,61			mean: 4062,64			mean: 4090,49			mean: 4129,32			mean: 4130,04		

Appendix B.3 PROTOTYPE CALIBRATION $AC_{PEAK,+}$

voltage observation	20 kV			40 kV			60 kV			80 kV			100 kV		
	U _{ref}	U _{div}	F _g	U _{ref}	U _{div}	F _g	U _{ref}	U _{div}	F _g	U _{ref}	U _{div}	F _g	U _{ref}	U _{div}	F _g
-	kV	V	-	kV	V	-	kV	V	-	kV	V	-	kV	V	-
1	27,91	7,055	3956,06	56,59	14,290	3960,11	85,78	21,750	3943,91	113,3	28,680	3950,49	143,5	36,400	3942,31
2	27,97	7,090	3944,99	56,56	14,305	3953,86	85,20	21,600	3944,44	113,4	28,750	3944,35	143,3	36,380	3938,98
3	27,93	7,095	3936,58	56,53	14,290	3955,91	85,34	21,630	3945,45	113,2	28,680	3947,00	143,3	36,350	3942,23
4	27,94	7,085	3943,54	56,49	14,275	3957,27	85,47	21,680	3942,34	113,1	28,680	3943,51	143,2	36,350	3939,48
5	27,94	7,095	3937,98	56,57	14,300	3955,94	85,47	21,690	3940,53	113,4	28,730	3947,09	143,5	36,420	3940,14
6	27,84	7,055	3946,14	56,57	14,290	3958,71	85,75	21,740	3944,34	113,4	28,750	3944,35	143,7	36,420	3945,63
7	27,89	7,100	3928,17	56,33	14,235	3957,15	85,53	21,690	3943,29	113,4	28,710	3949,84	143,9	36,480	3944,63
8	27,89	7,080	3939,27	56,38	14,250	3956,49	85,56	21,710	3941,04	113,2	28,700	3944,25	144,2	36,550	3945,28
9	27,91	7,080	3942,09	56,33	14,245	3954,37	85,47	21,680	3942,34	113,3	28,710	3946,36	144,0	36,550	3939,81
10	27,89	7,085	3936,49	56,22	14,205	3957,76	85,31	21,650	3940,42	113,3	28,730	3943,61	143,9	36,530	3939,23
	mean: 3941,13			mean: 3956,76			mean: 3942,81			mean: 3946,09			mean: 3941,77		

voltage observation	120 kV			140 kV			160 kV			180 kV			200 kV		
	U _{ref}	U _{div}	F _g	U _{ref}	U _{div}	F _g	U _{ref}	U _{div}	F _g	U _{ref}	U _{div}	F _g	U _{ref}	U _{div}	F _g
-	kV	V	-	kV	V	-	kV	V	-	kV	V	-	kV	V	-
1	172,0	43,500	3954,02	201,6	51,180	3939,04	230,9	58,480	3948,36	257,3	65,220	3945,11	286,0	72,200	3961,22
2	172,1	43,550	3951,78	200,8	50,950	3941,12	230,6	58,430	3946,60	256,3	64,930	3947,33	286,2	72,350	3955,77
3	172,0	43,580	3946,76	199,7	50,750	3934,98	230,3	58,350	3946,87	256,5	64,970	3947,98	286,0	72,300	3955,74
4	171,8	43,580	3942,18	200,7	50,950	3939,16	229,6	58,200	3945,02	256,5	65,050	3943,12	286,4	72,430	3954,16
5	172,2	43,580	3951,35	200,4	50,850	3941,00	229,4	58,150	3944,97	255,8	64,850	3944,49	286,1	72,280	3958,22
6	172,3	43,700	3942,79	200,7	50,950	3939,16	230,0	58,280	3946,47	255,8	64,780	3948,75	286,5	72,400	3957,18
7	172,7	43,780	3944,72	200,5	50,930	3936,78	229,8	58,250	3945,06	256,7	65,030	3947,41	287,0	72,550	3955,89
8	172,8	43,780	3947,01	200,4	50,880	3938,68	230,3	58,350	3946,87	255,9	64,930	3941,17	287,4	72,680	3954,32
9	171,6	43,480	3946,64	200,6	50,930	3938,74	230,3	58,530	3934,73	255,9	64,900	3942,99	287,0	72,550	3955,89
10	171,6	43,430	3951,19	200,0	50,780	3938,56	230,2	58,430	3939,76	256,9	65,080	3947,45	286,2	72,380	3954,13
	mean: 3947,84			mean: 3938,72			mean: 3944,47			mean: 3945,58			mean: 3956,25		

Appendix B.4 PROTOTYPE CALIBRATION $AC_{PEAK,-}$

voltage observation	20 kV			40 kV			60 kV			80 kV			100 kV		
	U _{ref}	U _{div}	F _g	U _{ref}	U _{div}	F _g	U _{ref}	U _{div}	F _g	U _{ref}	U _{div}	F _g	U _{ref}	U _{div}	F _g
-	kV	V	-	kV	V	-	kV	V	-	kV	V	-	kV	V	-
1	27,90	7,005	3982,87	56,73	14,230	3986,65	85,47	21,390	3995,79	114,5	28,760	3981,22	143,5	36,050	3980,58
2	27,95	7,020	3981,48	56,60	14,200	3985,92	85,42	21,390	3993,45	114,9	28,830	3985,43	143,7	36,030	3988,34
3	27,89	7,005	3981,44	56,59	14,235	3975,41	85,09	21,330	3989,22	113,7	28,560	3981,09	143,6	36,050	3983,36
4	27,71	6,970	3975,61	56,52	14,215	3976,08	85,53	21,430	3991,13	113,8	28,590	3980,41	143,7	36,030	3988,34
5	27,78	6,970	3985,65	56,53	14,205	3979,58	85,56	21,440	3990,67	113,6	28,540	3980,38	143,8	36,080	3985,59
6	27,76	6,965	3985,64	56,64	14,240	3977,53	85,45	21,400	3992,99	113,9	28,600	3982,52	143,3	36,050	3975,03
7	27,82	6,985	3982,82	56,59	14,220	3979,61	85,36	21,380	3992,52	113,4	28,450	3985,94	143,1	35,950	3980,53
8	27,90	7,010	3980,03	56,56	14,205	3981,70	85,47	21,410	3992,06	113,3	28,460	3981,03	143,7	36,050	3986,13
9	27,86	6,995	3982,84	56,53	14,205	3979,58	85,47	21,430	3988,33	113,5	28,530	3978,27	143,2	36,080	3968,96
10	27,84	7,000	3977,14	56,42	14,190	3976,04	85,34	21,380	3991,58	113,1	28,390	3983,80	143,2	35,920	3986,64
	mean: 3981,55			mean: 3979,81			mean: 3991,78			mean: 3982,01			mean: 3982,35		

voltage observation	120 kV			140 kV			160 kV			180 kV			200 kV		
	U _{ref}	U _{div}	F _g	U _{ref}	U _{div}	F _g	U _{ref}	U _{div}	F _g	U _{ref}	U _{div}	F _g	U _{ref}	U _{div}	F _g
-	kV	V	-	kV	V	-	kV	V	-	kV	V	-	kV	V	-
1	171,7	43,130	3980,99	200,0	50,180	3985,65	229,5	57,650	3980,92	257,0	64,470	3986,35	287,1	71,950	3990,27
2	172,7	43,280	3990,30	200,8	50,430	3981,76	229,8	57,700	3982,67	256,4	64,280	3988,80	287,0	72,000	3986,11
3	171,9	43,200	3979,17	200,7	50,350	3986,10	230,4	57,980	3973,78	256,6	64,430	3982,62	286,0	71,700	3988,84
4	171,8	43,080	3987,93	200,7	50,400	3982,14	229,3	57,630	3978,83	257,1	64,470	3987,90	286,2	71,720	3990,52
5	172,5	43,250	3988,44	200,7	50,450	3978,20	229,4	57,700	3975,74	255,8	64,280	3979,46	286,7	71,900	3987,48
6	172,2	43,280	3978,74	201,1	50,500	3982,18	229,8	57,830	3973,72	256,6	64,430	3982,62	286,7	71,850	3990,26
7	172,5	43,280	3985,67	201,1	50,500	3982,18	229,6	57,750	3975,76	257,1	64,530	3984,19	287,2	71,970	3990,55
8	173,0	43,330	3992,61	200,3	50,430	3971,84	229,8	57,830	3973,72	256,1	64,400	3976,71	287,3	72,050	3987,51
9	172,1	43,250	3979,19	200,2	50,430	3969,86	230,1	57,880	3975,47	256,9	64,470	3984,80	287,0	71,950	3988,88
10	172,6	43,130	4001,85	200,7	50,450	3978,20	230,1	58,000	3967,24	256,6	64,430	3982,62	287,0	71,950	3988,88
	mean: 3986,49			mean: 3979,81			mean: 3975,78			mean: 3983,61			mean: 3988,93		

Appendix B.5 PROTOTYPE CALIBRATION $LI_{PEAK,+}$

voltage observation	50 kV			100 kV			150 kV			200 kV			250 kV			300 kV		
	U_{ref}	U_{div}	M_g															
-	kV	V	-	kV	V	-	kV	V	-	kV	V	-	kV	V	-	kV	V	-
1	49,23	12,2757	4010,54	98,94	24,7354	3999,77	150,15	37,2061	4035,63	199,96	49,3681	4050,39	248,95	61,8485	4025,16	297,33	73,8045	4028,61
2	48,81	12,1683	4011,01	99,00	24,6482	4016,31	149,55	37,1975	4020,43	199,33	49,3233	4041,30	250,11	61,8331	4044,92	299,48	74,4768	4021,12
3	48,56	12,0801	4019,50	100,03	24,8893	4019,00	149,46	37,0765	4031,12	200,17	49,6263	4033,55	248,96	61,8562	4024,82	301,18	74,5056	4042,38
4	48,49	12,0505	4023,49	99,81	24,9570	3999,44	149,57	37,0863	4033,03	200,02	49,6319	4030,07	250,21	61,8684	4044,23	300,94	74,4181	4043,91
5	48,36	12,0661	4007,85	99,76	24,8507	4014,41	149,43	37,0715	4030,86	200,14	49,6165	4033,73	249,95	61,7652	4046,77	300,84	74,4555	4040,53
6	48,30	12,0755	3999,76	100,27	24,9734	4015,06	150,09	37,1302	4042,26	200,07	49,5940	4034,16	248,93	61,8421	4025,25	300,83	74,3981	4043,52
7	48,25	12,0367	4008,74	99,59	24,9327	3994,23	149,45	37,1195	4026,19	200,35	49,6639	4034,12	250,07	61,8759	4041,48	300,62	74,4086	4040,12
8	48,42	12,0617	4014,28	99,64	24,9140	3999,16	149,64	37,1680	4026,05	200,43	49,7112	4031,89	249,98	61,7811	4046,22	299,29	74,4324	4020,96
9	48,27	12,0559	4003,76	99,78	24,9496	3999,43	149,54	37,1981	4020,09	200,14	49,7022	4026,78	249,54	61,7030	4044,21	299,17	74,3664	4022,92
10	48,46	12,0718	4013,90	100,03	24,9662	4006,61	149,67	37,1304	4030,93	201,00	49,6682	4046,86	249,66	61,7110	4045,63	300,76	74,4622	4039,10
	mean: 4011,28			mean: 4006,34			mean: 4029,66			mean: 4036,29			mean: 4038,87			mean: 4034,32		

Appendix B.6 PROTOTYPE CALIBRATION $LI_{PEAK,-}$

voltage observation	50 kV			100 kV			150 kV			200 kV			250 kV			300 kV		
	U_{ref}	U_{div}	M_g															
-	kV	V	-	kV	V	-	kV	V	-	kV	V	-	kV	V	-	kV	V	-
1	49,43	12,3653	3997,41	98,94	24,6673	4010,82	148,37	36,7950	4032,34	197,27	49,0150	4024,69	246,24	61,3265	4015,23	294,86	73,4191	4016,12
2	49,38	12,3740	3990,70	98,37	24,5967	3999,48	147,77	36,8555	4009,45	198,03	48,9755	4043,45	246,25	61,3333	4014,95	294,73	73,3165	4019,97
3	49,42	12,3698	3994,99	98,97	24,6263	4018,95	147,78	36,8111	4014,55	197,99	48,9876	4041,64	247,09	61,3514	4027,46	295,19	73,5330	4014,39
4	49,33	12,3442	3995,96	98,94	24,6265	4017,46	148,37	36,8377	4027,66	197,13	48,9922	4023,70	246,93	61,3030	4028,02	297,29	73,7240	4032,47
5	49,36	12,3662	3991,29	98,99	24,6736	4011,99	147,92	36,8705	4011,88	197,34	48,9701	4029,81	247,09	61,2798	4032,16	298,09	73,7961	4039,38
6	49,54	12,3766	4002,95	98,98	24,6495	4015,66	148,38	36,8471	4026,91	198,16	49,0688	4038,41	245,83	61,2631	4012,69	297,19	74,0690	4012,34
7	49,75	12,3767	4019,80	98,85	24,6636	4008,01	147,81	36,7310	4024,13	198,34	49,0923	4040,15	245,98	61,3355	4010,40	298,29	73,9006	4036,37
8	49,48	12,3875	3994,60	99,01	24,6745	4012,52	147,75	36,8005	4014,89	197,42	49,0679	4023,41	247,58	61,3570	4035,08	297,24	73,9477	4019,60
9	49,49	12,3589	4004,33	98,91	24,6358	4014,73	148,38	36,8402	4027,66	198,21	49,0050	4044,69	247,43	61,3619	4032,31	297,25	73,9637	4018,87
10	49,78	12,3968	4015,24	98,85	24,6384	4012,10	147,67	36,8335	4009,12	197,36	49,1109	4018,66	247,50	61,3884	4031,71	297,31	73,9765	4018,98
	mean: 4000,73			mean: 4012,17			mean: 4019,86			mean: 4032,86			mean: 4024,00			mean: 4022,85		

Appendix B.7 PROTOTYPE CALIBRATION LI_{TIMECOMP}

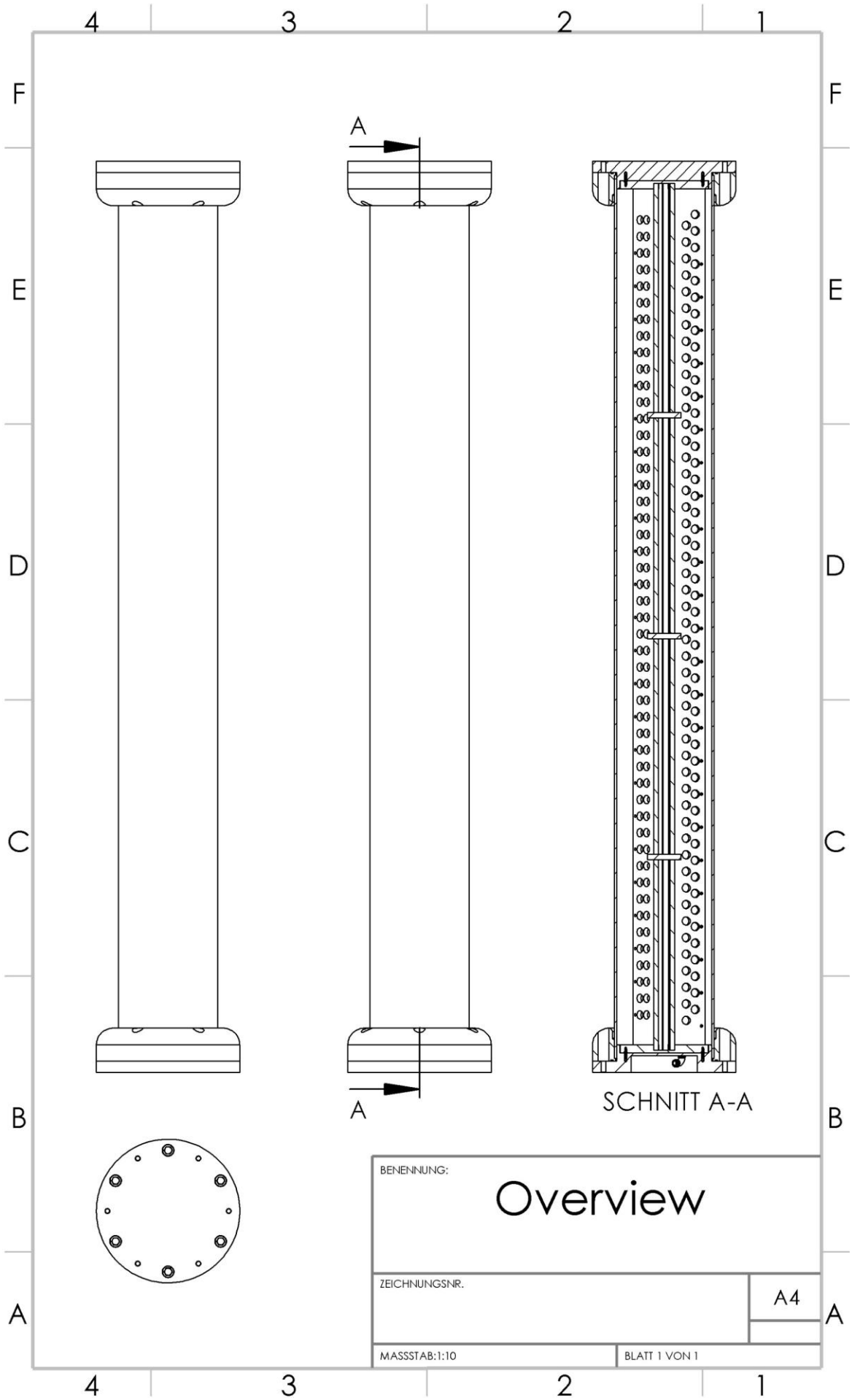
0,7/43 μ s:

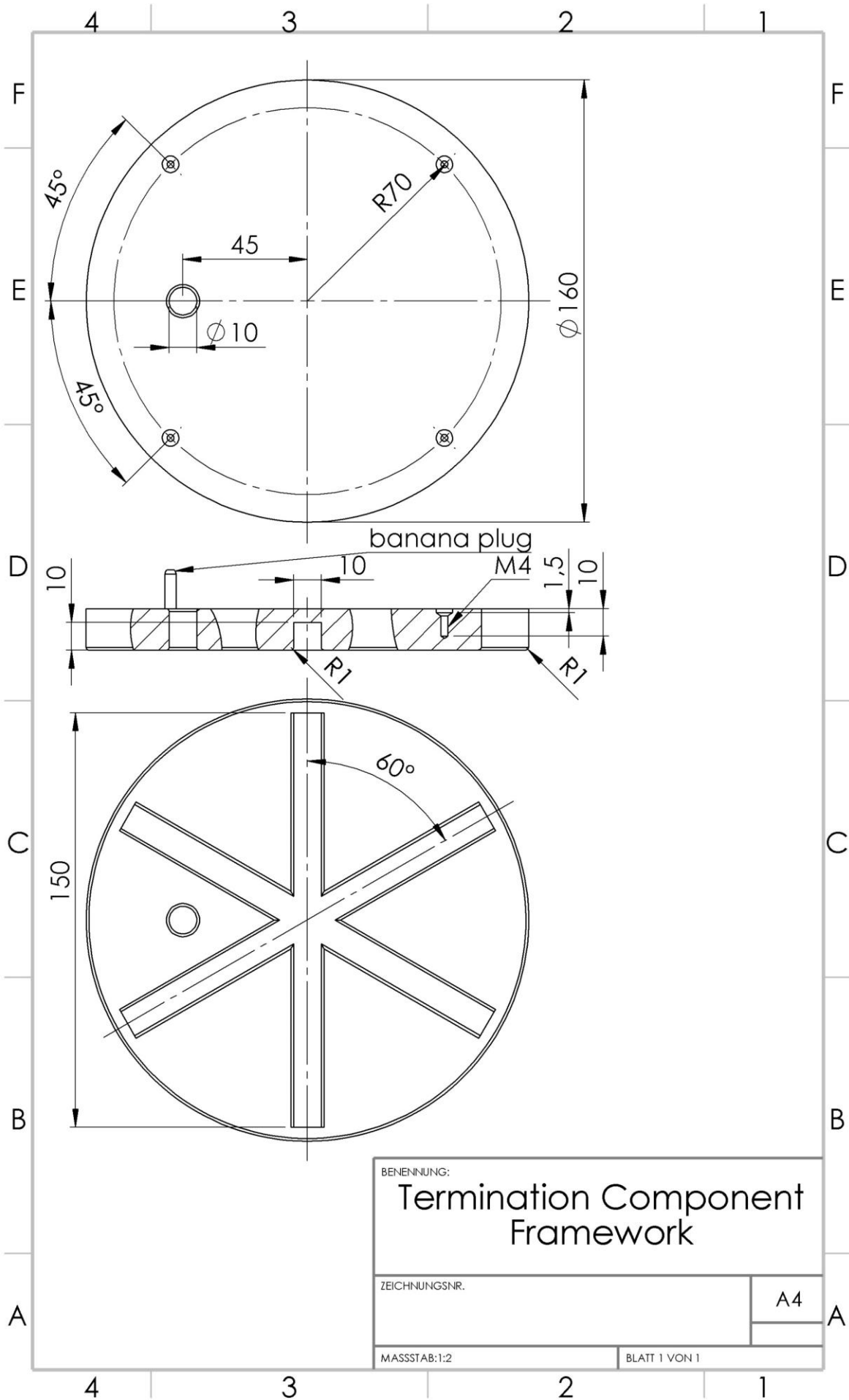
polarity observation	positive						negative					
	U _{ref}	T _{1,ref}	T _{2,ref}	U _{div}	T _{1,div}	T _{2,div}	U _{ref}	T _{1,ref}	T _{2,ref}	U _{div}	T _{1,div}	T _{2,div}
-	kV	μ s	μ s	V	μ s	μ s	kV	μ s	μ s	V	μ s	μ s
1	297,33	0,708	43,05	73,805	0,610	43,50	294,86	0,716	42,99	73,419	0,617	43,24
2	299,48	0,710	43,04	74,477	0,620	43,44	294,73	0,716	43,01	73,316	0,621	43,34
3	301,18	0,727	42,69	74,506	0,621	43,37	295,19	0,716	43,02	73,533	0,621	43,27
4	300,94	0,723	42,73	74,418	0,617	43,34	297,29	0,730	42,69	73,724	0,624	43,25
5	300,84	0,722	42,76	74,456	0,619	43,40	298,09	0,720	42,72	73,796	0,617	43,36
6	300,83	0,723	42,75	74,398	0,619	43,45	297,19	0,715	43,03	74,069	0,621	43,29
7	300,62	0,725	42,78	74,409	0,621	43,34	298,29	0,728	42,75	73,901	0,623	43,40
8	299,29	0,707	43,04	74,432	0,620	43,36	297,24	0,717	43,00	73,948	0,622	43,31
9	299,17	0,708	43,00	74,366	0,618	43,27	297,25	0,715	43,01	73,964	0,621	43,30
10	300,76	0,721	42,73	74,462	0,621	43,36	297,31	0,717	43,00	73,977	0,625	43,25

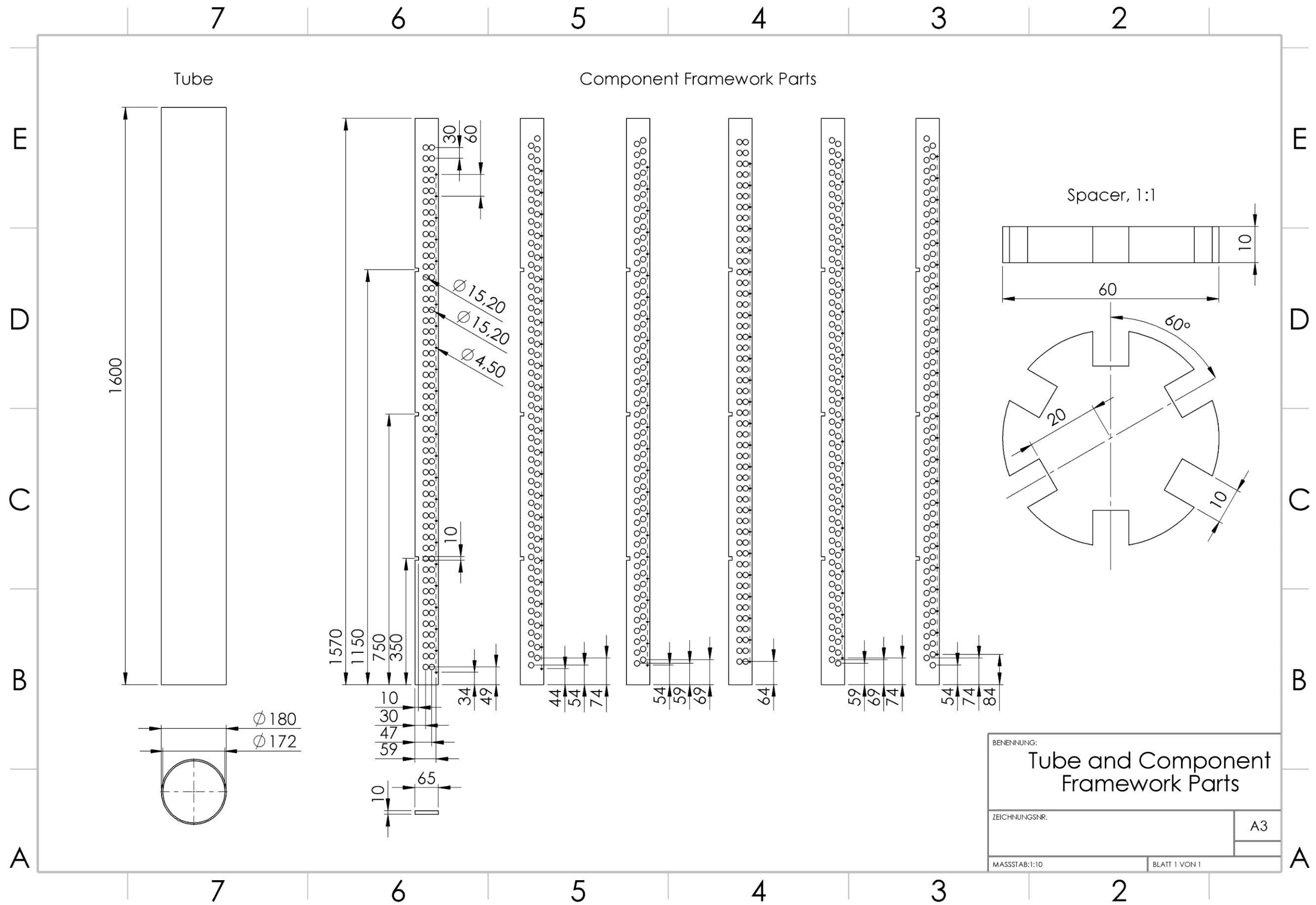
1,5/45 μ s:

polarity observation	positive						negative					
	U _{ref}	T _{1,ref}	T _{2,ref}	U _{div}	T _{1,div}	T _{2,div}	U _{ref}	T _{1,ref}	T _{2,ref}	U _{div}	T _{1,div}	T _{2,div}
-	kV	μ s	μ s	V	μ s	μ s	kV	μ s	μ s	V	μ s	μ s
1	295,50	1,581	44,50	73,164	1,594	45,10	294,68	1,572	44,50	73,229	1,564	44,78
2	297,47	1,582	44,52	73,669	1,602	45,10	305,50	1,563	44,55	75,759	1,492	45,06
3	298,70	1,581	44,54	73,935	1,594	45,08	299,40	1,568	44,55	74,310	1,573	44,90
4	300,06	1,578	44,51	74,299	1,587	45,08	302,05	1,568	44,55	75,016	1,528	45,03
5	300,32	1,575	44,50	74,374	1,586	45,07	304,40	1,569	44,55	75,535	1,500	45,12
6	300,22	1,578	44,52	74,327	1,593	45,03	310,30	1,570	44,58	76,904	1,500	45,16
7	300,39	1,569	44,52	74,384	1,569	45,05	292,26	1,568	44,49	72,675	1,600	44,77
8	300,18	1,577	44,51	74,290	1,585	45,04	296,05	1,568	44,51	73,487	1,549	45,00
9	300,35	1,575	44,53	74,290	1,589	45,23	297,34	1,567	44,49	73,816	1,515	44,96
10	300,38	1,572	44,53	74,387	1,587	44,97	299,47	1,568	44,49	74,367	1,510	44,95

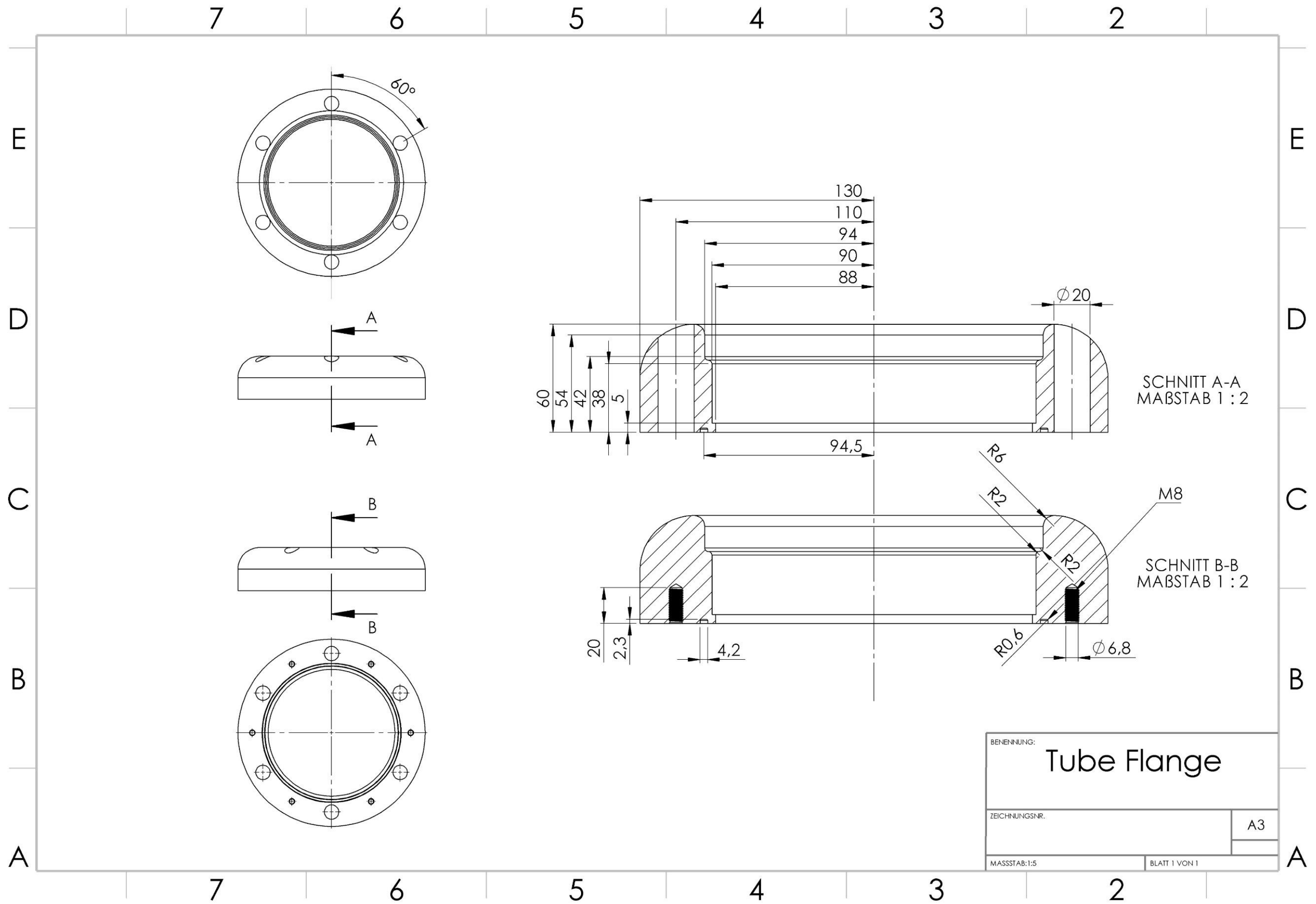
Appendix C CONSTRUCTION DRAWINGS







BENENNUNG:	
Tube and Component Framework Parts	
ZEICHNUNGSNR.	A3
MASSTAB:1:10	BLATT 1 VON 1



BENENNUNG:		Tube Flange	
ZEICHNUNGSNR.		A3	
MASSSTAB: 1:5		BLATT 1 VON 1	

